Developing non-viral vector formulations for the delivery of synthetic self-amplifying RNA

Dylan Matthew Kairuz

A Dissertation submitted to the Faculty of Health Sciences, University of the Witwatersrand, in fulfilment of the requirements for the degree of Master of Science in Medicine.

Johannesburg, 2024

Declaration

I, Dylan Matthew Kairuz, declare that this Dissertation is my own, unaided work. It is being submitted for the Degree of Master of Science in Medicine at the University of the Witwatersrand, Johannesburg. It has not been submitted before for any degree or examination at any other University.

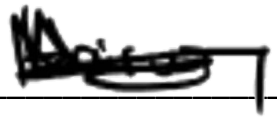

Signature

05/03/2024

Date

Dedication

To my family

Christine, Peter, and Leigh Kairuz

Publications

1. Singh P, Kairuz D, Arbuthnot P, Bloom K. Silencing hepatitis B virus covalently closed circular DNA: The potential of an epigenetic therapy approach. *World J Gastroenterol*. 2021;27(23):3182-3207. Impact Factor: 5.374
2. Kairuz D, Singh P, Smith T, Arbuthnot P, Ely A, Bloom K. "Synthetic mRNA Gene Therapies and Hepatotropic Non-viral Vectors for the Treatment of Chronic HBV Infections.," In: Jurga S, Barciszewski J, editors. Cham: Springer International Publishing (2022). p. 157–179 doi: 10.1007/978-3-031-08415-7_8.
3. Kairuz D, Samudh N, Ely A, Arbuthnot P, Bloom K. Advancing mRNA technologies for therapies and vaccines: An African context. *Front Immunol* (2022) 0:6452. doi: 10.3389/FIMMU.2022.1018961. Impact Factor: 8.787
4. Kairuz D, Samudh N, Ely A, Arbuthnot P, Bloom K. Production, Characterization, and Assessment of Permanently Cationic and Ionizable Lipid Nanoparticles for Use in the Delivery of Self-Amplifying RNA Vaccines. *Pharmaceutics* (2023) 15: doi: 10.3390/pharmaceutics15041173. Impact Factor: 6.321

Conference Presentations

1. IXth Conference of the South African Immunology Society (SAIS). 2-4 October 2022. Poster presentation: Kairuz, D., Samudh, N., Ely, A., Arbuthnot, P., Bloom, K. Optimising Lipid Nanoparticles for The Delivery of Self-Amplifying RNA for Vaccines and Therapies.
2. Molecular Biosciences research Thrust (MBRT) Postgraduate Research Day 2022. 1 December 2022. Poster presentation: Kairuz, D., Samudh, N., Ely, A., Arbuthnot, P., Bloom, K. Optimising Lipid Nanoparticles for The Delivery of Self-Amplifying RNA for Vaccines and Therapies.

Abstract

Conventional vaccines have been instrumental in reducing worldwide morbidity and mortality of infectious diseases. However, some diseases require improvements to their vaccines or do not have an effective vaccine. This has led to the development of next generation vaccines including messenger ribonucleic acid (mRNA) vaccines, a versatile platform allowing simple exchange of encoded antigen sequences for different pathogens in the mRNA. Alternatively, self-amplifying mRNA (saRNA) presents a vaccine platform which replicates *in situ* using Alphavirus-derived non-structural proteins, mimicking viral replication and prolonging antigen expression. This has the potential to improve immune responses and significantly lower mRNA vaccine doses. Although this is a promising platform, a vector is essential to protect saRNA from ribonuclease degradation and deliver saRNA into cells. Lipid nanoparticles (LNPs) are a safe, highly efficient delivery system, with multiple approved mRNA vaccines. However, saRNA is significantly larger than mRNA, and hence LNPs need to be optimised to achieve efficient delivery. Two main categories of LNPs have been denoted, ionisable (iLNPs) and permanently cationic LNPs (cLNPs). cLNP lipids are less expensive to synthesise and have recently been used successfully to deliver saRNA vaccines. Hence, these were predominantly examined in this study. A library of empty cLNPs were successfully produced using lipid film hydration (LFH) with sizes <150 nanometres (nm). When saRNA was complexed exteriorly to cLNPs (saRNA-Ext-cLNPs) varying sizes were observed depending on the N:P used. N:P ratio is the molar ratio of nitrogen and phosphate on the lipids and RNA respectively, hence larger sizes are expected at a lower N:P. saRNA formulated on the interior of cLNPs (saRNA-Int-cLNPs) were produced by microfluidics or a modified solvent injection (SI) method. Microfluidics formulated saRNA-Int-cLNPs had small sizes and lower polydispersity indices (PDIs) compared to the larger sizes and PDIs of SI formulated cLNPs. The library of saRNA-cLNPs were optimised by transfecting mammalian cells with saRNA encoding reporter genes at a variety of N:P ratios. Generally, the size of the LNPs did not influence the delivery efficiency and the main contributor was N:P ratio for both saRNA-Ext- and saRNA-Int-cLNPs. DOTAP (1,2-dioleoyl-3-trimethylammonium-propane) and DOTMA (1,2-di-O-octadecenyl-3-trimethylammonium propane) performed the best, particularly the F1 cLNPs. Although dimethyldioctadecylammonium (DDA) cLNPs showed poorer delivery efficacy at 24 hours post-transfection, interesting effects on saRNA expression kinetics were observed. A remarkable boost in expression was observed from 24

to 48 hours, and saRNA-Int DDA-cLNPs outperformed DOTAP and DOTMA cLNPs at 48 hours. High encapsulation efficiencies of >90% were observed for all cLNP candidates and the top saRNA-Ext-cLNPs candidates were not toxic. Even though unfavourable results were obtained upon intramuscular injection of saRNA-Ext-cLNPs into mice, this could be as a result of lipid film hydration (LFH) production and could be solved by microfluidics formulation. Although setbacks related to purification of saRNA-Int-cLNPs limited *in vivo* examination, these showed a strong potential for saRNA delivery for delivery of saRNA vaccines in the future. Overall, the work in this dissertation has developed the protocols for production and characterisation of LNPs. A library of potential cLNP candidates for saRNA vaccine delivery have been optimised in cell culture, with many showing highly efficient saRNA delivery. This will facilitate saRNA vaccine development and examination in a pre-clinical setting in South Africa, reducing reliance on the global North for equitable access of RNA vaccines and improving preparedness for potential future pandemics.

Acknowledgements

- I would like to thank my supervisors, Dr Kristie Bloom and Prof. Patrick Arbuthnot for their support and guidance throughout my research and write up.
- I would also like to thank Prof. Abdullah Ely for his assistance with *in vivo* experiments and guidance during my write up, as well as Ms. Ridhwaanah Jacobs for her guidance during the write-up of my dissertation.
- I appreciate the assistance, support and encouragement of the students and staff of the Antiviral Gene Therapy Research Unit (AGTRU). Especially to Mrs. Nazia Samudh for our brainstorming sessions and perseverance through scientific difficulties.
- I would like to thank my parents, Christine and Peter, and my sister Leigh. Their love, encouragement, laughter, and emotional support throughout my university career have helped me persist and work hard.
- I would also like to thank my funding bodies for their financial support: the University of the Witwatersrand Postgraduate Merit Award, Poliomyelitis Research fund and the Antiviral Gene Therapy Research Unit.

Table of Contents

List of Abbreviations

ApoE – Apolipoprotein E

ARCA – Anti-Reverse Cap Analogue

CCAU – CleanCap® Reagent AU

cLNP – Permanently cationic Lipid Nanoparticle

CDS – Coding Sequence

CNE – Cationic Nanoemulsion

CSEs – Conserved Sequence Elements

DCs – Dendritic Cells

DDA – Dimethyldioctadecylammonium

DLinDMA - 1,2-dilinoleyloxy-3-dimethylaminopropane

DMG-PEG2000 – 1,2-dimyristoyl-sn-glycero-3-phosphoethanolamine-N-[methoxy(polyethylene glycol)-2000]

DNA – Deoxyribonucleic Acid

DOE – Design of Experiments

DOPE – 1,2-dioleoyl-sn-glycero-3-phosphoethanolamine

DOTAP – 1,2-dioleoyl-3-trimethylammonium propane

DOTMA – 1,2-di-O-octadecenyl-3-trimethylammonium propane

DSPC – 1,2-diastearoyl-sn-glycero-3-phosphocholine

dsRNA – Double Stranded RNA

E. coli – Escherichia coli

EE – Encapsulation Efficiency

eIF – Eukaryotic Initiation Factor

eGFP – Enhanced Green Fluorescent Protein

FBS – Foetal Bovine Serum

FDA – Food and Drug Administration

Fluc – Firefly Luciferase

FRR – Flow Rate Ratio

GMP – Good Manufacturing Practice

HBS – HEPES Buffered Saline

HIV – Human Immunodeficiency Virus

i.d. – Intradermal

IgG – Immunoglobin G

IFN – Interferon

iLNP – Ionisable Lipid Nanoparticle

i.m. – Intramuscular

i.n. – Intranasal

IRES – Internal Ribosomal Entry Site

IVT – *In Vitro* Transcription

LDLR – Low Density Lipoprotein Receptor

LFH – Lipid Film Hydration

LiCl – Lithium Chloride

LNP – Lipid Nanoparticle

m1Ψ – N1-methylpseudouridine

MDA5 – Melanoma Differentiation-Associated Protein 5

MERS-CoV – Middle East Respiratory Syndrome Coronavirus

$MgOAc_2$ – Magnesium Acetate

MHC I – Major Histocompatibility Complex I

MHC II – Major Histocompatibility Complex II

MLV – Multilamellar Vesicle

mRNA – Messenger Ribonucleic Acid

MTT – [3-(4, 5-dimethylthiazol-z-yl)-2, 5-diphenyltetrazolium bromide]

NF-κB – Nuclear Factor Kappa Light Chain Enhancer of Activated B Cells

NLRP3 – NOD-like receptor family pyrin domain containing 3

nm – Nanometres

N:P – Nitrogen to Phosphate

nsP – Non-Structural Protein

OAS – 2′,5′-Oligoadenylate Synthetase

PBS – Phosphate-Buffered Saline

PDI – Polydispersity Index

pDNA – Plasmid Deoxyribonucleic Acid

PEG – Polyethylene Glycol

PKR – Protein Kinase R

RdRP – RNA- dependent RNA Polymerase

RIG-1 – Retinoic Acid Inducible Gene 1

RNA – Ribonucleic Acid

RNase – Ribonuclease

rNTPs – Ribonucleotide Triphosphates

RSV – Respiratory Syncytial Virus

saRNA – Self-Amplifying Ribonucleic Acid

SARS-CoV-2 – Severe Acute Respiratory Syndrome Coronavirus 2

SI – Solvent Injection

STING – Stimulator of Interferon Genes

SUV – Small Unilamellar Vesicles

TLR – Toll-like Receptor

Ψ – Pseudouridine

µm – Micrometres

UTRs – Untranslated Regions

VEE – Venezuelan Equine Encephalitis

List of Figures

List of Tables

Chapter 1

Introduction

From variolation as early as 1000 A.D. and the development of the smallpox vaccine to conventional and now nucleic acid vaccines, improvements in immunisation strategies have continuously been made. Throughout history conventional vaccines have had an immense global impact on health and the economy through the prevention of infectious disease spread and mortality (1,2).

Variolation generally involved exposing the patient to scab material from an infected individual, which led to symptoms of the illness (1). There was however, marked improvement in survival compared to natural infection. Eventually, Edward Jenner developed a smallpox vaccine by using the less virulent cowpox virus to vaccinate individuals, leading to the eradication of smallpox (2). Louis Pasteur's discovery of attenuation resulted in rabies and anthrax vaccines, and the development of modern conventional vaccines followed. Conventional vaccines utilise the complete or parts of the infectious agent. These include inactivated vaccines, which use infectious particles killed by heat or chemicals, and attenuated vaccines where the pathogen is weakened, but still able to replicate. Subunit vaccines administer part of the organism as a purified protein or a polysaccharide (3). Polysaccharides can also be covalently bound to proteins in the form of conjugate vaccines (4). Finally, toxoid vaccines use inactivated microbe toxin (5).

These vaccines have had an immense global impact by preventing infectious disease spread and mortality (6,7). However, effective vaccines are not yet available for many detrimental diseases such as human immunodeficiency virus (HIV), and dependency on more costly and complex egg or mammalian cell culture methods to manufacture vaccines can limit clinical development. These shortcomings have led to the development of next-generation vaccine platforms including nucleic acid (NA) vaccines. This provides the opportunity to improve the immune response to vaccines by mediating cellular CD8+ T-cell immunity alongside CD4+ T-cell, humoral and B-cell immunity produced by the conventional vaccines. These will also provide a platform to rapidly respond to microbe variants and disease outbreaks. Together with these NA vaccines are their delivery and adjuvant systems. For synthetic NAs, non-viral

vectors have played a pivotal role in the success of RNA vaccines, such as with the COVID-19 pandemic. Among these, lipid nanoparticles (LNPs) have shown the most clinical success, however constant improvements of these vectors and adaptation for emerging NA technologies is crucial for future success of this promising platform.

1.1. Utilising Nucleic Acids for Next-Generation Vaccines

Nucleic acid-based vaccines involve the delivery of genetic material in the form of nucleic acids (DNA or RNA) encoding antigenic sequences. Genetic vaccines differ from most conventional vaccines, as they stimulate both B-cells and CD4+ and CD8+ T-cells. B-cells are stimulated by proteins translated from the nucleic acid. These proteins are also processed and modified by cellular machinery resulting in T-cell stimulation through peptide presentation to T-cells on major histocompatibility complexes I and II (MHC class I and II, Figure 1.1.1) (8). NA vaccines circumvent the risk of occasional viral reactivation caused by attenuated vaccines. Although attenuated polio vaccines are very effective, they can cause outbreaks of vaccine-derived poliovirus, which differ from the wild-type virus (9). The versatility of these platforms allows rapid antigen design by conventional cloning techniques, while maintaining the ability to add or remove antigen modifications, such as glycosylation motifs all of which may improve vaccine efficacy (10).

DNA-based nucleic acid vaccines encompass the use of viral vectors encapsulating viral DNA, and delivery of plasmid DNA (pDNA) to express antigenic proteins in cells. Use of viral vectors, such as adenoviral vectors, to deliver their nucleic acids encoding antigens, have shortcomings such as pre-exposure anti-vector neutralising antibodies which may limit prime and boost vaccine efficacy by vector clearance (11). Two major hurdles limit use of pDNA vaccines: the risk of genomic integration, and potential expression of unwanted genes encoded in the DNA vector, such as antibiotic resistance. To express the vaccine antigens, the DNA has to be delivered into the nucleus (Figure 1.1.1B), a process which is not very efficient using non-viral vectors, as endosomal escape releases nucleic acids into the cytoplasm. Hence, historically these have not performed well in clinical trials (12). Nevertheless, both viral vector and pDNA vaccines have still shown promise such as in their use in Severe Acute Respiratory Syndrome Coronavirus 2 (SARS-CoV-2) vaccines (13,14).

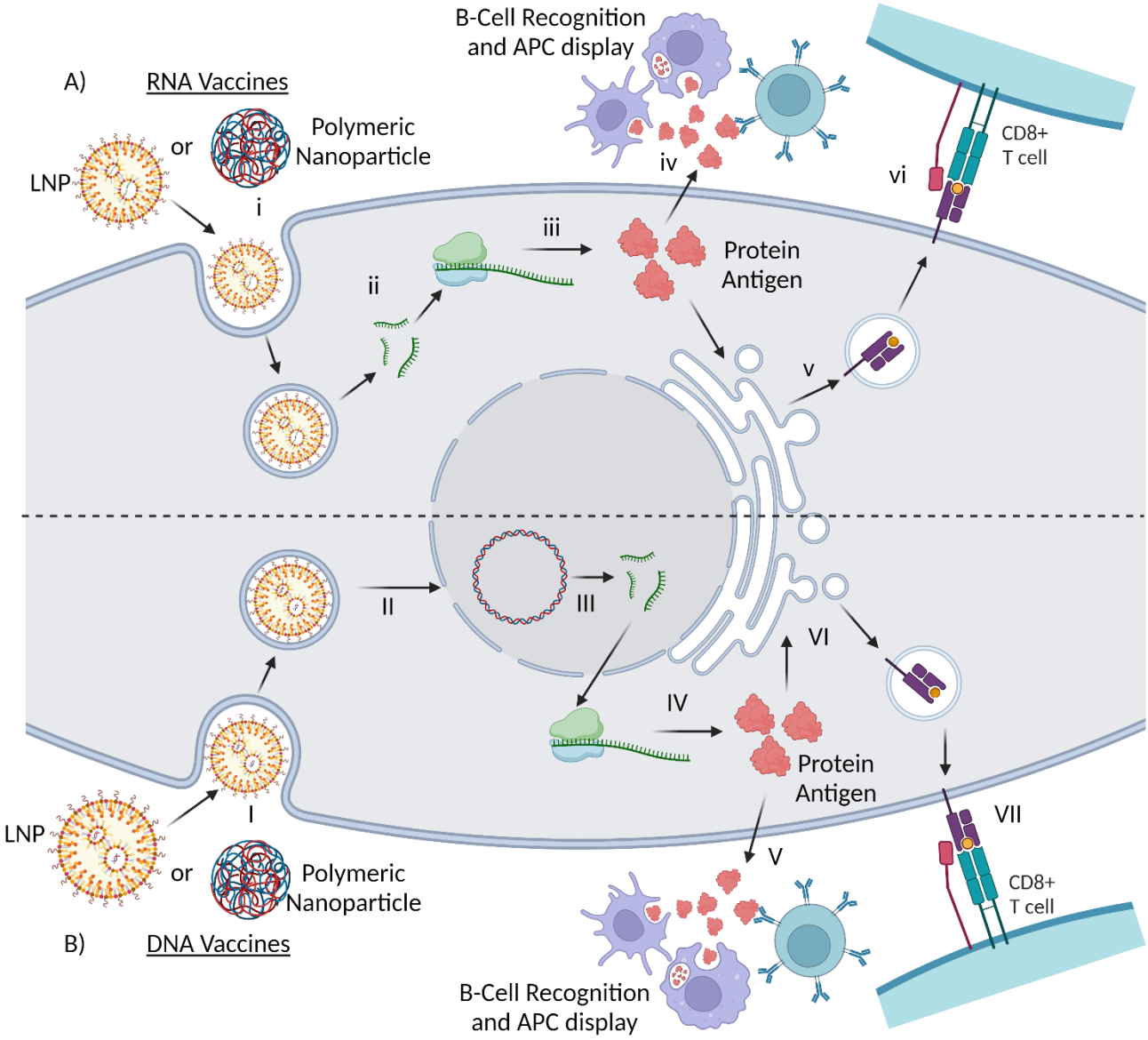

Figure 1.1.1. Mechanism of action of nucleic acid vaccines delivered using non-viral vectors. Nucleic acids can be packaged into non-viral vectors including LNPs and polymeric nanoparticles. A) RNA vaccines: i) RNA-Nanoparticle vaccines enter the cell by endocytosis and are released from the endosome into the cytoplasm (ii). iii) Protein antigens are translated from the RNA which can be secreted if a signal peptide is present (iv) resulting in B cell and T helper cell responses. Translated antigen is also processed by the Golgi into MHCI (v) where it can be displayed on the cell surface and presented to CD8+ T cells (vi). B) DNA vaccines: I) DNA-Nanoparticle vaccines enter the cells by endocytosis, however unlike RNA vaccines they must be delivered into the nucleus (II) to be transcribed into mRNA (III) and proteins are then translated (IV). After translation, the process of antigen secretion and MHC presentation is identical to that of RNA vaccines (V-VII).

In the current light of the two Food and Drug Administration (FDA) approved COVID-19 vaccines, mRNA vaccines have been propelled into the spotlight as a platform for pandemic preparedness, and safe for human use following worldwide administration (15–17).

1.2. Synthetic RNA as a Platform for Vaccines

The first glimpse into the potential for the use of *in vitro* transcribed (IVT) RNA for vaccines and therapies in 1990 showed expression of reporter genes after injection of messenger RNA (mRNA) in mice (18). However, therapeutics and vaccines initially avoided RNA due to instability, poor delivery efficiency, and poor immune stimulation. Upon development of technologies and further understanding of IVT RNA, these short-comings were either overcome, or used to the advantage of therapies (19), and are continuously being improved (20).

RNA vaccines encompass many types of synthetic or non-synthetic RNA including mRNA, self-amplifying RNA (saRNA) and circular RNA. Synthetic RNA is produced enzymatically through IVT, while non-synthetic RNA can be derived from organisms such as yeast. The work in this dissertation will focus on synthetic RNA, specifically mRNA and saRNA. RNA vaccines hold some significant advantages over DNA and conventional vaccines. Firstly, they can be delivered and directly translated in the cell cytosol (Figure 1.1.1A). This eliminates the challenge of crossing the nuclear membrane and the risk of genomic integration and expression of undesired genes found in pDNA (21). Unlike inactivated and live attenuated vaccines, there is no risk of reactivation and infection of the pathogen. The short half-life of RNA allows for easier dosage calculation as it is not functional for long periods of time. Improvements have also been made in the production of RNA to reduce immune system recognition of the RNA, resulting in improved antigen translation. IVT is a simple, cost-effective method of RNA production, and can be scaled to large scale Good Manufacturing Practice (GMP)-compliant manufacturing. Formulation of the RNA in non-viral vectors allows for streamlined GMP production of different vaccines, with simple quality control analysis as the non-viral vector systems are very similar or the same. This removes optimisation of purification of different mRNA vaccines, unlike for subunit vaccines, where purification changes based on the vaccine as proteins may have vastly different characteristics.

The consistent molecular structure of different RNA vaccine candidates allows this streamlined production. Conventional mRNA comprises a 5’ cap, 5’ untranslated region (UTR),

coding sequence (CDS), 3' UTR and a poly A tail (Figure 1.2.1A). The 5' cap is comprised of a 7'-methylguanosine cap, which is a guanosine nucleotide modified with a methyl group (CH_3), joined to the 5' end of the first nucleotide by a triphosphate bond. The cap is recognised by eukaryotic initiation factors (eIFs) and is essential for translation of the CDS (22). UTRs have been shown to be essential for efficient translation of mRNA and regulation thereof, and improved duration of RNA expression (23–27). These can be derived from natural eukaryotic mRNA, viruses, or are completely synthetic. The poly A tail is important for RNA stability and enhancing translation (28,29).

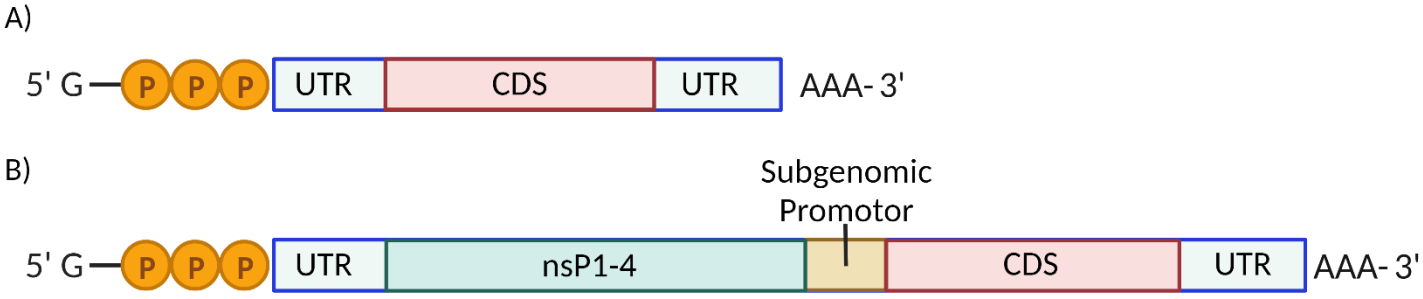

Figure 1.2.1. Comparison of components of conventional messenger RNA (mRNA) and self-amplifying RNA (saRNA). A) mRNA consists of a 5' Cap 1, Untranslated Region (UTR), Coding Sequence (CDS), 3' UTR and poly-A tail. B) saRNA contains similar aspects however, they contain a subgenomic promotor upstream of the CDS and their UTRs are adapted from Alphavirus conserved sequence elements (CSEs) preventing immune suppression of translation. They also contain genes encoding the non-structural replication proteins (nsP1-4), allowing for replication *in situ*.

1.2.1. *In Vitro* Transcription Methodology of RNA

The process of synthesising mRNA/saRNA involves the incorporation of these components into a DNA sequence, most commonly a pDNA backbone, downstream of a bacteriophage promoter. This is then used as a template for IVT of the synthetic RNA. IVT is an enzymatic reaction that does not require cells for production. When pDNA is utilised, the pDNA vector must be completely linearised at the end of the poly A sequence by restriction digestion prior to IVT so that the RNA polymerase "falls off" the template after transcription of the complete RNA sequence. Other important components of the reaction include ribonucleotide triphosphate (rNTP) monomers, which are incorporated into the growing RNA sequence by the RNA polymerase. Magnesium ions are an important component in this interaction

between the rNTPs and the enzyme (30,31). After synthesis, the DNA is degraded, and the RNA is purified to remove all reaction components prior to capping or formulation.

Initially, commercially available cap analogues, which mimic the first capped NTP were incorporated at the start of the RNA during IVT, however this resulted in inefficient translation due to reversed or inefficient capping (32,33). Newer technologies including vaccinia virus-based enzymatic capping with 2'-O-methyltransferases (34–36), the anti-reverse cap analogue (ARCA) and the highly efficient co-transcriptional CleanCap® analogue system from TriLink BioTechnologies (37) provide alternative, efficient and scalable capping methods. The use of the Vaccinia Capping and CleanCap® systems in the Moderna (16) and Pfizer/BioNTech (38) SARS-CoV-2 mRNA vaccines respectively emphasise the clinical relevance of these technologies. The poly A tail can be added through enzymatic methods or by incorporating the sequence into the pDNA vector. The size of naturally occurring mRNA poly A tails are variable, while optimal IVT mRNA poly A tails have been shown to be 100-120 bp (24,39). Enzymatic addition is limited by requirement of an additional purification step and inconsistent poly A tail length (24,40). Although, alteration of the long, repeating DNA-incorporated poly A tail during propagation of pDNA in *E. coli* can also be problematic (40,41). A possible solution to this problem involves using a split poly A sequence in the pDNA, with each 40-60 base pair sequence joined by a linker sequence as used in the BioNTech COVID mRNA vaccine (42). The synthesised synthetic RNA can then be used as a drug substance in RNA vaccines and therapeutics.

1.2.2. Applications of Conventional mRNA Vaccines

Since RNA design and production is a streamlined process, RNA can be applied to a broad spectrum of vaccines and therapeutics. mRNA has been extensively applied to cancer and infectious diseases through active and passive vaccination (20,43). Two mRNA vaccines against SARS-CoV-2 (Spikevax and Comirnaty) have been fully approved by the FDA. Passive vaccination by delivering antibodies to prevent infection has been achieved in pre-clinical studies against hepatitis B virus (44), HIV (45), and respiratory syncytial virus (RSV) (46). Although these have shown great promise for vaccines, they are limited by factors such as high production costs due to the requirement of modified nucleotides, and higher doses. Self-amplifying RNA (saRNA) vaccines are a technology that may be able to overcome some of these shortcomings and improve immune responses to RNA vaccines.

1.2.3. Mimicking Viral Amplification Using Self-amplifying mRNA Vaccines

Although mRNA vaccines simply result in translation of the desired antigen, saRNAs additionally code for a positive-sense alphavirus-derived RNA-dependent RNA polymerase complex (RdRP), comprised of non-structural proteins 1-4 (nsP1-4; Figure 1.2.1B). This allows *in situ* mRNA amplification following recognition of the 5′ and 3′ conserved sequence elements (CSEs) found in the viral UTRs (8). These UTRs regulate replication of the RNA and recruitment of host proteins important during replication as a result of their secondary structures, thermodynamics and motifs (47). nsP1 is involved in association and sequestration of nsP1-4 and saRNA with the plasma membrane resulting in saRNA immune escape (48). nsP2 acts as a protease and RNA helicase, regulating the expression of the other nsPs by breaking down excess protein and changing secondary RNA structures, which alters RNA-protein interactions. nsP3 mediates host-viral protein interactions important for RNA replication, and nsP4 is an RNA-dependent RNA polymerase, which is responsible for transcription of the RNA, resulting in replication. saRNA is a positive-sense RNA, meaning that proteins can be translated directly from the viral RNA. Upon transcription of a negative strand by nsP4, double stranded intermediates form, after which the positive-sense strand and subgenomic mRNA can be synthesised from the negative-sense strand resulting in the translation of proteins.

nsP1 and nsP2 are also important in RNA capping, which is performed differently to conventional eukaryotic capping. In eukaryotic mRNA capping, after RNA triphosphatase activity removes one of the three phosphate groups from the first NTP at the 5′ end of the RNA, guanosine monophosphate is added by guanyltransferase to form the GpppN triphosphate linkage. This is followed by addition of a 7′-methyl (CH_3) group on the guanosine added to the RNA, forming a cap 0 structure. Finally, a methyl group is added onto the second oxygen of the ribose of the first nucleotide, forming a cap 1 structure. In Alphaviruses, although there is cap-dependent translation, only a cap 0 structure is produced. This occurs by removal of one phosphate from the 5′ end of the RNA by nsP2. nsP1 then methylates guanosine monophosphate, this 7′-methyl guanosine monophosphate is then added to the diphosphate 5′ end of the RNA, which is catalysed by the 7′-methyl guanyltransferase activity of nsP1, forming the required cap 0 structure (47,48).

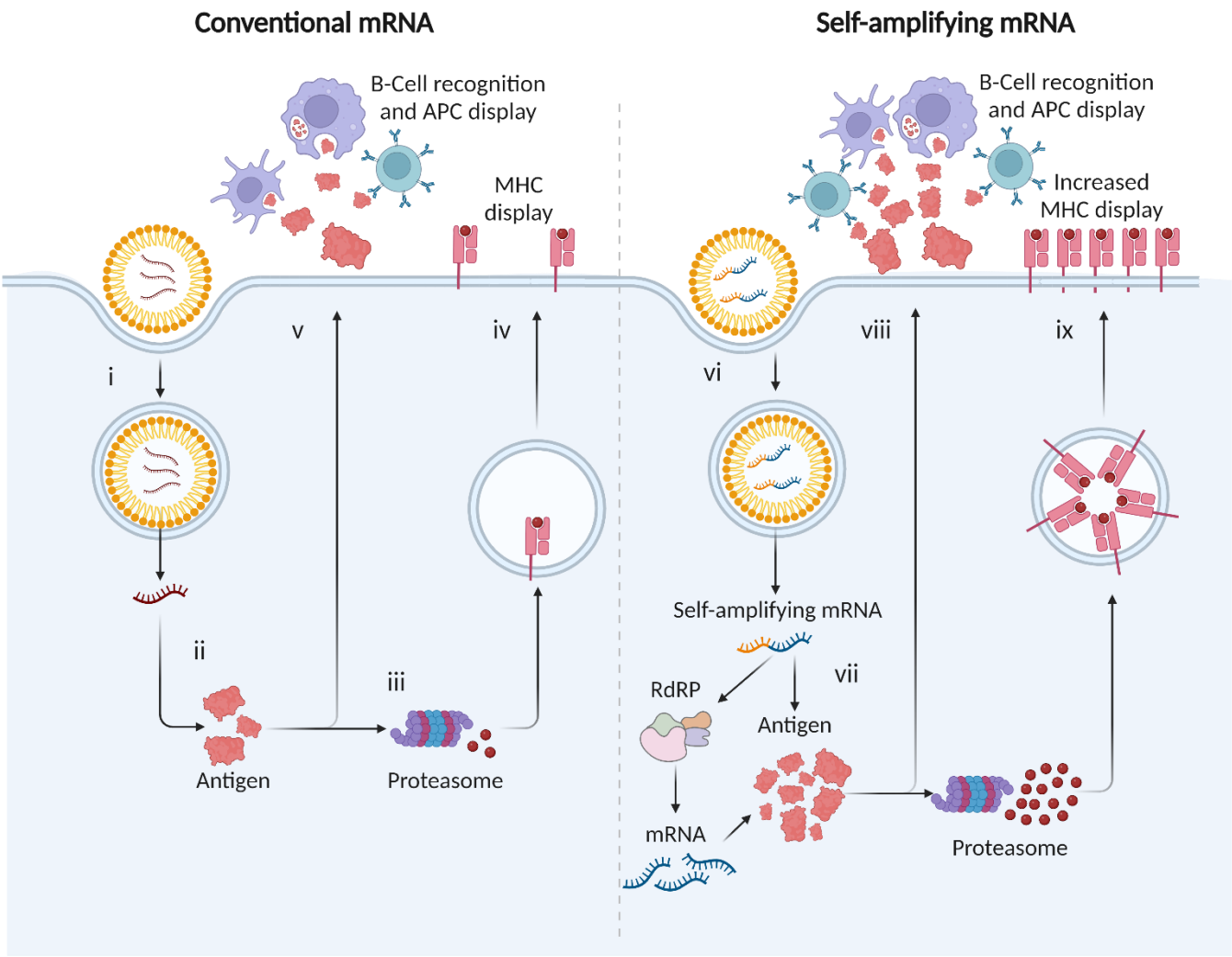

Figure 1.2.2. Translation of conventional versus self-amplifying RNA vaccines *in situ*. mRNA (left) enters the cell (i) is simply used to translate the antigen (ii), which can then be processed in the Golgi onto MHC (iii + iv) and/or secreted (v), and presented to the immune system, stimulating B- and T-cell responses. After cell transfection (vi; Right) saRNA is additionally used to translate nsP1-4, triggering *in situ* RNA replication (vii). This results in prolonged and amplified antigen expression and presentation to the immune system (viii + ix), improving cellular and humoral immune responses at significantly lower doses. Adapted from "Conventional vs. Self-Amplifying mRNA Vaccines," by BioRender.com (2023). Retrieved from https://app.biorender.com/biorender-templates.

Although nsP1 causes immune escape of the saRNA, the double stranded RNA (dsRNA) intermediates can still be recognised by pattern recognition receptors, resulting in a self-adjuvating, innate immune response. Similar to conventional mRNA, single stranded RNA (ssRNA) stimulates toll-like receptors and cellular receptors. However, the combination of the two intermediates mimics an acute viral infection improving stimulation of anti-pathogenic T- and B-cell immunity (49,50). An innate interferon response is also stimulated in resident cells at the site of injection such as myocytes for intramuscular injection (50). Adaptive immune responses are then stimulated by antigen presenting cells, such as dendritic cells [DCs; (51)].

Amplification of the antigen-encoding mRNA and the addition of a subgenomic promoter on the 5' end of the CDS coding region significantly boosts antigen expression (52), and results in prolonged antigen expression at lower RNA doses than conventional mRNA vaccines (Figure 1.2.2; (53)). Vogel *et al.* compared an mRNA and saRNA influenza vaccine encoding the haemagglutinin (HA) antigen (53). Equal protection against influenza virus could be achieved with 80 µg and 1.25 µg doses of mRNA and saRNA respectively, which is a 64-fold reduction in required dosage of saRNA. However, unlike conventional mRNA, saRNA is considerably longer (~9-12 kb), making it more sensitive to degradation and physical shear stress during handling, which may complicate synthesis, purification, and formulation.

saRNA was first described in literature for vaccination as early as 1994, where Zhou et al. (54) used naked intramuscular injection of Semliki Forest virus-based saRNA to immunise mice against influenza virus nucleoprotein. They obtained detectable antibody levels for a single and boost vaccination. Since then, many vaccination studies have been conducted against infectious diseases and cancer [reviewed in (8,55,56)]. A variety of saRNA vaccines have been examined for infectious diseases such as viruses including HIV-1 and rabies virus; bacteria such as *Streptococci*; and parasites such as *Toxoplasma gondii*. saRNA encoding multiple pathogen epitopes have also shown promise when used in pre-clinical influenza vaccines encoding multiple influenza antigens (57), and a *Toxoplasma gondii* hexaplex saRNA (58). Passive vaccinology against Zika virus using an saRNA encoding the neutralising monoclonal antibody (mAb) ZIKV-117 has also shown promise (59). An alternative use of saRNA in cancer therapeutics involving the delivery of saRNA encoding cytokines to stimulate immune responses and cause immunogenic cancer cell death shows encouraging flexibility of the platform (60,61). Although these synthetic RNA platforms allow broad applicability depending

on the desired application, if the RNA is unable to enter the cell, the vaccine is unlikely to have a high efficacy. It is unfavourable for naked RNA to naturally enter cells due to the negative charge of both the RNA and the cell membrane. It is also susceptible to ribonucleases (RNases) and hence needs to be protected from degradation (62). Hence, an efficient system needs to be optimised to deliver and protect RNAs and provide an adjuvant response for vaccines. Non-viral vectors satisfy this need efficiently; however, these vectors may still need optimisation for much longer saRNA vaccines.

1.3. Delivery of saRNA Vaccines, an Essential Factor in Vaccine Efficacy

A plethora of approaches have been used to deliver RNA vaccines, including physical methods such as gene guns, electroporation, and viral and non-viral vectors. Physical approaches are limited by equipment size, and viral vectors are cannot be produced synthetically, but rather are produced by more complex cell culture techniques (63). Non-viral vectors combine the advantages of cell-independent formulation and simple administration for efficacious RNA vaccines. Many different non-viral vectors including cationic nanoemulsions (CNE), polymers and lipid nanoparticles (LNPs) have been used extensively with success (64). LNPs have been studied for decades and are being continuously improved for use with RNA. Many drugs and vaccines utilising RNA-LNPs have reached FDA approval including Onpattro (65), Spikevax (16) and Comirnaty (38). LNPs have also been utilised in a plethora of non-RNA FDA approved therapeutics, such as Doxil® which is used in combination with doxorubicin, a small molecule chemotherapeutic (66). The plethora of data showing pre-clinical and clinical safety and efficacy of this platform prompted its assessment as a saRNA delivery platform in this project.

1.3.1. Overview, Composition, and Adjuvant Effects of Lipid Nanoparticles

LNPs are essentially spheres made up of lipids (fats). The lipids are comprised of two ends, a hydrophilic and hydrophobic end, hence they are soluble in alcohols such as ethanol, but when they are mixed with an aqueous solution such as water, they shield their hydrophobic region and expose their hydrophilic region. This is a spontaneous process and results in the formation of vesicles (spheres). While the structures of these LNPs differ based on the lipids used, they are all generally similar and can be used to encapsulate small molecule drugs, DNA, RNAs and proteins.

Generally, LNPs are formulated using an ionisable or permanently cationic lipid, a helper or neutral phospholipid, cholesterol, and a lipid conjugated to polyethylene glycol (PEGylated

lipid). Table 1 shows the chemical structures of the different lipids in each subdivision. The ionisable/cationic lipid is responsible for drug substance (RNA, DNA, protein) complexation using its positive nitrogen group. Phospholipids assists in endosomal escape by altering its physical structure, and cholesterol improves LNP structural stability [reviewed in (67)]. The PEGylated lipid can reduce the size of the LNPs and is important for storage and *in vivo* structural stability, and preventing immune clearance (68). An important characteristic of RNA-LNPs is the ratio of the positively charged nitrogen of the lipid to the negatively charged RNA phosphate known as the N:P ratio, which determines how much of each is added. Two main LNP subsets have been defined, ionisable (iLNPs) and cationic LNPs (cLNPs, also known as lipoplexes). iLNPs (Figure 1.3.1A) consist of lipid monolayers, the NAs are surrounded by inverted micelles in the "electron-dense" core (69), while cLNPs (Figure 1.3.1B) consist of lipid bilayers (70). Ionisable lipids used in iLNPs remain relatively neutral at a physiological, neutral pH. At an acidic pH such as in endosomes, the ionisable nitrogen group of the lipid adopts a positive charge. This allows the lipids to interact, and fuse with the negatively charged endosomal membrane, resulting in endosomal escape and release of the RNA payload into the cytosol (71). Hence, formulation of RNA is also performed at an acidic pH. RNA is diluted in an acidic buffer, and when mixed with lipids that are dissolved in alcohol, the lipid's ionisable nitrogen group becomes cationic. The anionic RNA forms a complex with the lipids, and LNPs spontaneously form, resulting in the RNAs being encapsulated within the LNPs. These LNPs naturally mediate cellular uptake using low density lipoprotein receptor (LDLR)-based endocytosis facilitated by Apolipoprotein E (ApoE) LNP surface adsorption [Figure 1.3.1C, (72)].

cLNPs are similar in composition to iLNPs, however they use lipids that have permanently cationic nitrogen groups, regardless of the pH of their environment. This allows high percentages of RNA encapsulation, and delivery to cells as a result of the opposing charges of both components (73). The main cellular uptake mechanism of cLNPs is thought to be clathrin-mediated endocytosis [Figure 1.3.1D; (74)], however caveolae-mediated endocytosis, and macropinocytosis independent of this mechanism are also thought to mediate cLNP entry (75–79).

Table 1. Structures, Chemical Names and Molecular Weights of Lipids used in LNPs.

Common Lipid Name and Chemical Structure	Chemical Lipid Name and MW
Ionizable Lipids	
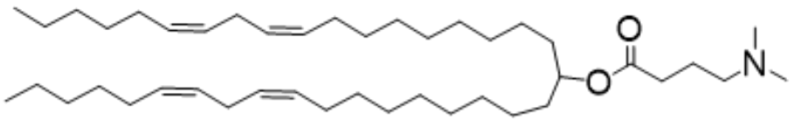 Dlin-DMA-MC3	O-(Z,Z,Z,Z-heptatriaconta-6,9,26,29-tetraen-19-yl)-4-(N,N-dimethylamino) ($C_{43}H_{79}NO_2$) MW=641.61 g/mol
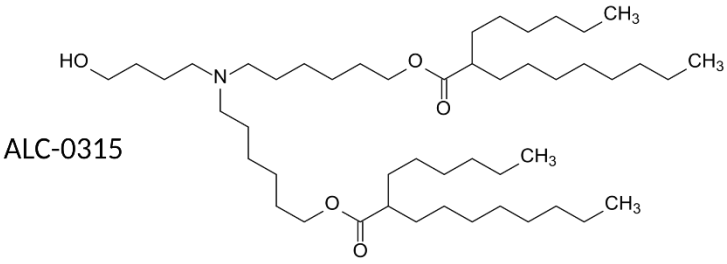 ALC-0315	[(4-hydroxybutyl)azanediyl] di(hexane-6,1-diyl) bis(2-hexyldecanoate) ($C_{48}H_{95}NO_5$) MW=766.29 g/mol
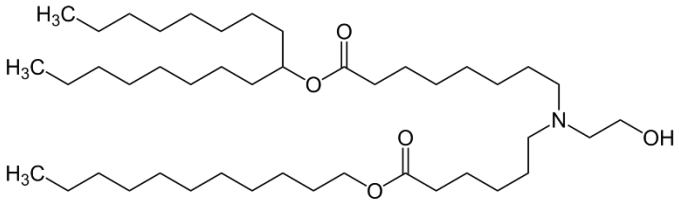 SM-102	8-[(2-hydroxyethyl)[6-oxo-6-(undecyloxy)hexyl]amino]-octanoic acid, 1-octylnonyl ester ($C_{44}H_{87}NO_5$) MW=710.17 g/mol
Lipidoids	
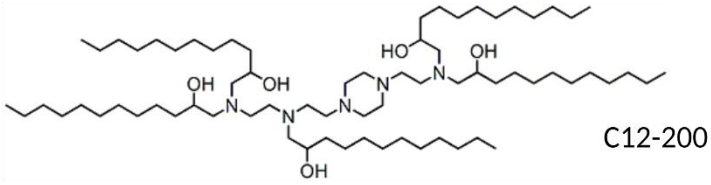 C12-200	1-[2-[bis(2-hydroxydodecyl) amino] ethyl-[2-[4-[2-[bis(2-hydroxydodecyl)amino]ethyl] piperazin-1-yl]ethyl]amino] dodecan-2-ol ($C_{70}N_5O_5H_{145}$) MW=1136.93 g/mol
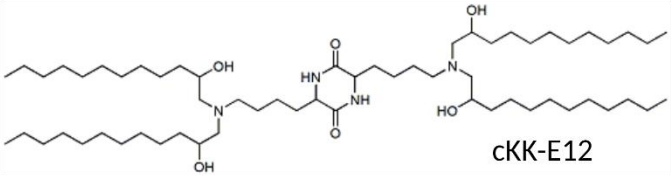 cKK-E12	3,6-bis({4-[bis(2-hydroxydodecyl) amino] butyl})piperazine-2,5-dione ($C_{60}H_{120}N_4O_6$) MW=993.62 g/mol
Permanently Cationic Lipids	
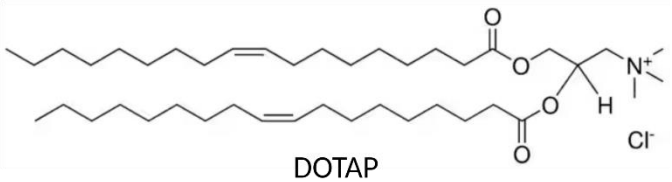 DOTAP	1,2-Dioleoyl-3-trimethylammonium-propane ($C_{42}H_{80}NO_4^+$) MW=698.54 g/mol
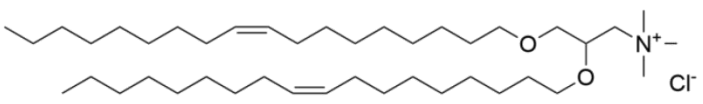 DOTMA	1,2-di-O-octadecenyl-3-trimethylammonium propane ($C_{42}H_{84}ClNO_2$) MW=670.58 g/mol

Table 1. cont.

Common Lipid Name and Chemical Structure	Chemical Lipid Name and MW
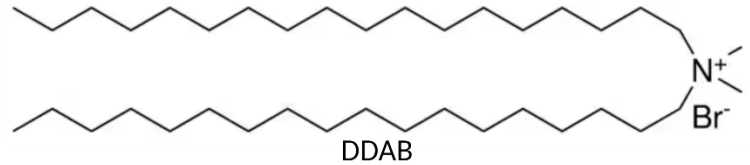 DDAB	Dimethyldioctadecylammonium (Bromide Salt) ($C_{38}H_{80}NBr$) MW=630.95 g/mol
Cholesterol and Phospholipids	
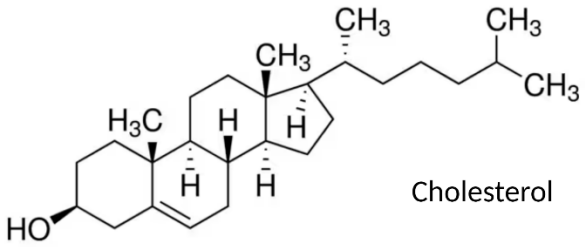 Cholesterol	(3β)-cholest-5-en-3-ol ($C_{27}H_{46}O$) MW=386.654 g/mol
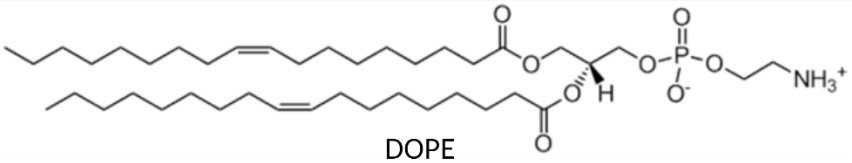 DOPE	1,2-dioleoyl-sn-glycero-3-phosphoethanolamine ($C_{41}H_{78}NO_8P$) MW=744.03 g/mol
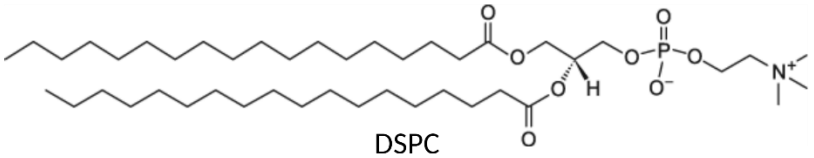 DSPC	1,2-distearoyl-sn-glycero-3-phosphocholine ($C_{44}H_{88}NO_8P$) MW=790.15 g/mol
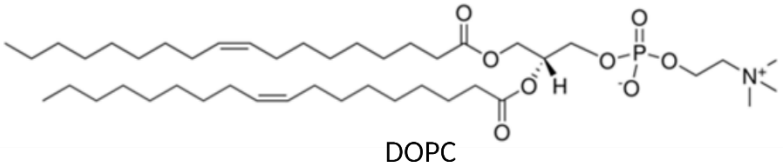 DOPC	1,2-dioleoyl-sn-glycero-3-phosphocholine ($C_{44}H_{84}NO_8P$) MW=786.11 g/mol
PEGylated Lipids	
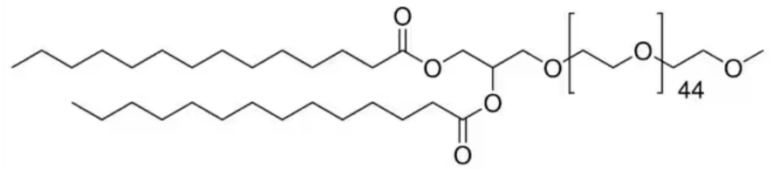 DMG-PEG2000	1,2-dimyristoyl-rac-glycero-3-methoxypolyethylene glycol-2000 ($C_{122}H_{242}O_{50}$) MW=2509.2 g/mol
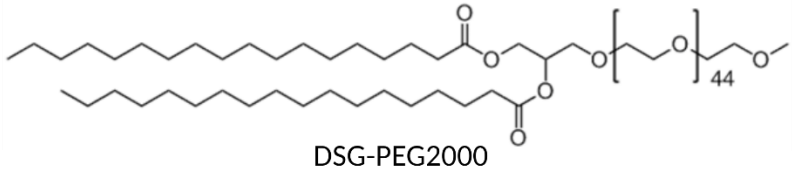 DSG-PEG2000	1,2-Distearoyl-*rac*–glycero-3-methoxypolyethylene glycol-2000 ($C_{130}H_{258}O_{50}$) MW=2621.4 g/mol

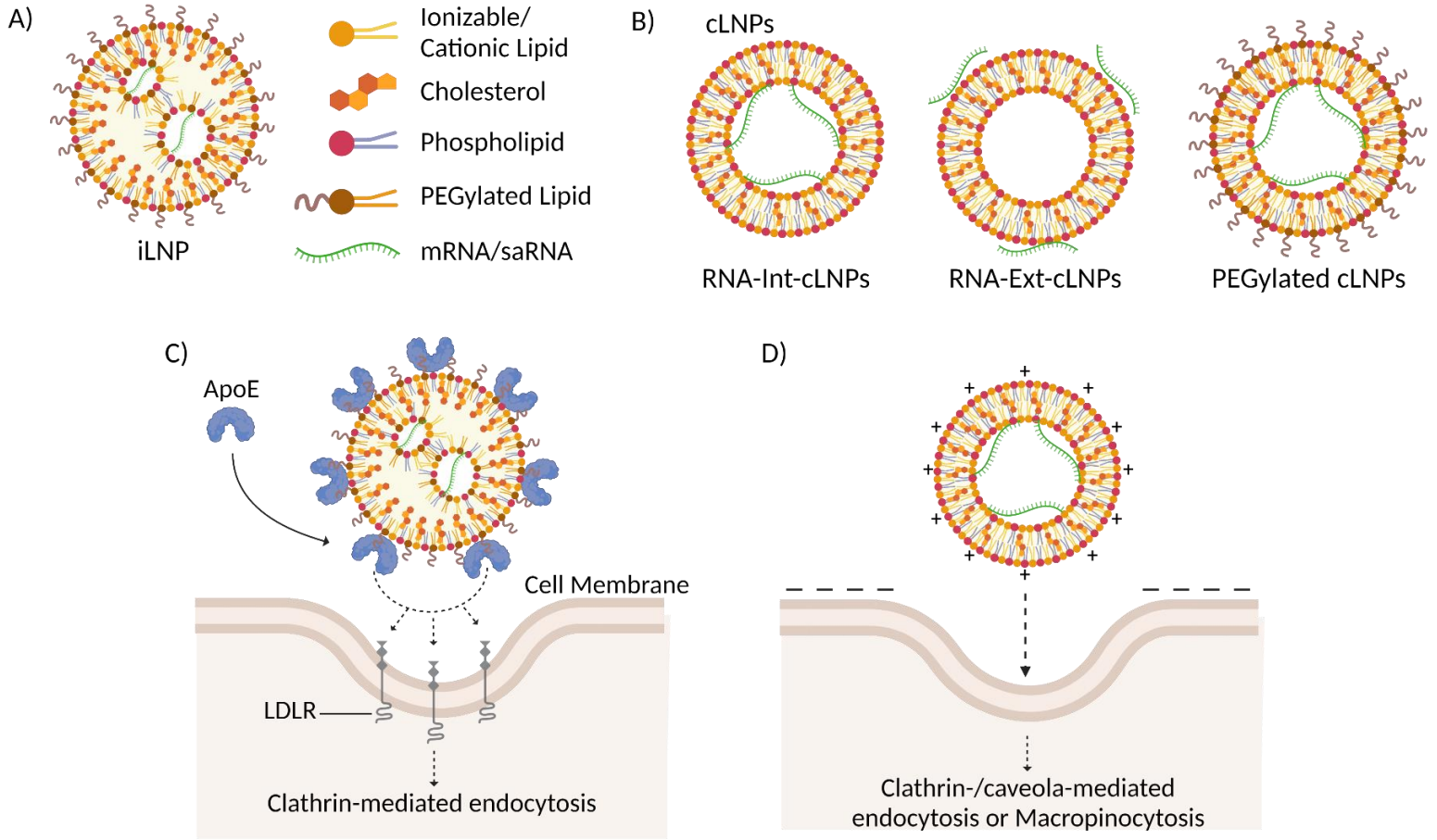

Figure 1.3.1. Structure and mechanism of RNA delivery using Lipid Nanoparticles (LNPs). Generally, LNPs consist of a cationic/ionisable lipid, cholesterol, a phospholipid, and a PEGylated lipid. A) Ionisable LNPs (iLNPs) consist of a single lipid layer surrounding an electron-dense core comprising of RNA surrounded by inverted micelles. B) Cationic LNPs (cLNPs) consist of lipid bilayer surrounding an aqueous core. RNA can either be complexed internally (left and right) or externally (middle). These LNPs can also be un-PEGylated (left and middle) or PEGylated (right). C) iLNPs adsorb ApoE onto the surface of the LNP, resulting in LDLR-mediated cellular entry. D) cLNPs are permanently positively charged, facilitating entry into negatively charged cells. This occurs predominantly by clathrin-mediated endocytosis. Adapted from Kairuz *et al.* (20).

Although LNPs are both effective at delivery of RNA and protection from RNases, they also provide an adjuvant effect, improving vaccine efficacy. Although the exact mechanism is not fully understood yet, many different lipids have been shown to activate different arms of the immune response. The immunogenicity is also important to note, as high protein expression may not be the sole contributor to vaccine efficacy. Blakney and colleagues found that although the polymer pABOL [poly(CBA-co-4-amino-1-butanol)] showed high luciferase expression from saRNA, immunogenicity of a SARS-CoV-2 saRNA-polymer vaccine was lower than that of LNP-based vaccines (80).

Different lipids are known to activate different cell types and alter innate immune responses (81,82). For example, DOTAP does not induce production of pro-inflammatory cytokines in DCs (83). However in monocytes, T-cells and B-cells, type 1 interferon responses and T helper cell type 1-related cytokine release was observed as a result of toll-like receptor 4 (TLR4) recognition of DOTAP (84). Cellular signalling pathways activated downstream of recognition by pattern recognition receptors is dependent on the lipid structure (85), which is important to consider when designing LNPs for vaccine use.

LNP size has shown to have an effect on cytokine production (86), and surface modification by protein adsorption resulting in formation of a protein corona on the LNP surface increases macrophage uptake (87). However, this corona may be detrimental to RNA delivery, and hence to prevent opsonisation, many LNPs use a PEGylated lipid to create a steric barrier.

1.3.2. Production Methods Used for LNP Formulation

Since characteristics such as size is important in vaccine efficacy, production methodology is an important consideration. Acceptable sizes of the LNPs for RNA vaccines are generally below 100 nm (88), however larger particle sizes have been used with success (62). The polydispersity index (PDI) of the LNPs is especially important to measure, this indicates the LNP size distribution within the single LNP population. This is calculated by dividing the square root of the standard deviation by the mean particle size (89). A value of 0.3 is generally accepted as the cut-off, with lower PDI values indicating a more homogeneous size distribution of the single LNP population. The method of formulation also needs to ensure that there is a high percentage of RNA that is complexed to the lipid, known as the encapsulation efficiency. The scale of production is an important consideration, as methods

used in a small-scale research laboratory may not be scalable to a large scale GMP setting or may need different equipment or optimisation.

Originally, lipid film hydration (LFH) was predominately used for LNP production (Figure 1.3.2A). This method, developed by Bangham *et al.* (90), is performed by evaporating the solvent the lipids are dissolved in using an inert gas, forming a multilamellar lipid film. The film is then hydrated with a buffer of choice, allowing the spontaneous formation of large multilamellar vesicles [MLVs; (91)]. This buffer can contain the drug or RNA of interest, allowing encapsulation of the drug substance interiorly. However, these MLVs are limited in use by their larger size and heterogeneity. Size reduction methods such as extrusion, homogenisation, and sonication (Figure 1.3.2B) can be performed to reduce size and heterogeneity, forming small unilamellar vesicles (SUVs). Extrusion involves pressurised movement of MLVs through polycarbonate membranes with defined pore sizes (92). While scale-up of extrusion is difficult, it is not impossible, as Doxil® currently uses LFH, freeze thaw cycles, and extrusion for cLNP production (93). Sonication involves using sound waves at ultrasonic frequencies to homogenise or break up the MLVs, allowing them to form small unilamellar vesicles (SUVs). Probe sonication may cause contamination from the probe, and damage to lipids and RNA. Bath sonication is a more feasible method as there is not breakdown of the lipids, however RNA is sensitive to physical disruption and may be degraded by the shearing force. Other homogenisation methods using high-pressure pumps to force LNPs through an interaction chamber at a high pressure to homogenize, may be a much better option for scale up. However, this method still poses issues related to high shear, which may be difficult for internal formulation of RNA.

Many of the limitations of these traditional “top-down” approaches can be overcome by using “bottom-up” methodologies. Batch production or solvent injection was an earlier method of production prior to microfluidics, this involves injecting lipids dissolved in solvent into an aqueous solution while stirring (94). Modern microfluidics (Figure 1.3.3) is currently a very efficient, scalable method of RNA-LNP production. Microfluidics involves controlled mixing of an aqueous solution containing RNA and an organic phase containing the lipids of interest. This method allows for precise control over parameters such as flow rate, flow rate ratio, shear force and mixing, especially when using modern technologies such as Precision NanoSystems microfluidics and Knauer impingement systems.

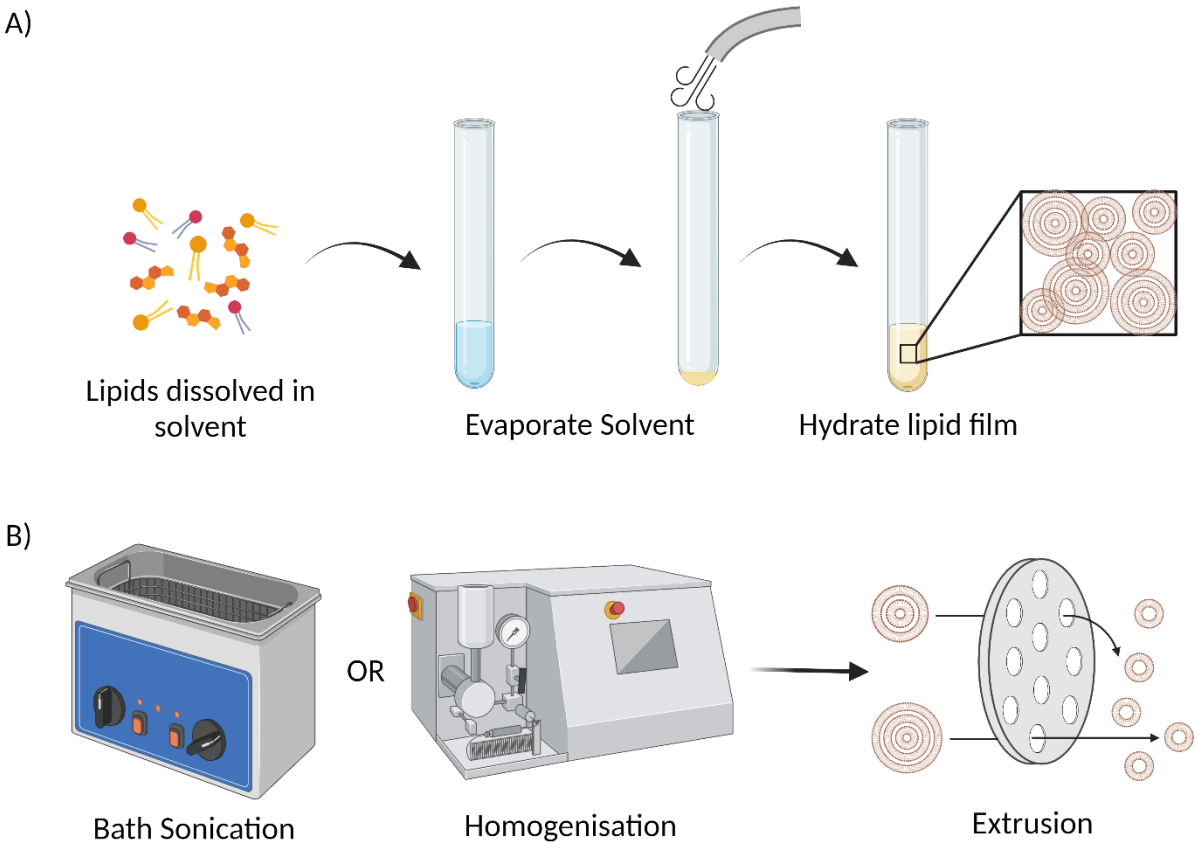

Figure 1.3.2. Formulation of LNPs using lipid film hydration (LFH). A) LFH involves evaporating the organic solvent off of the lipids, forming a dry lipid film. This film is then hydrated with buffer (which can contain the drug of interest), resulting in large multi-lamellar vesicles (MLVs) being formed. B) Large MLVs can be converted into small uni-lamellar vesicles (SUVs) using methods such as bath sonication and homogenisation followed by extrusion. These methods involve breaking the LNPs apart, either through sonic or physical force, after which the LNPs will spontaneously re-form as SUVs.

Asymmetrical microfluidics tubing geometry and impingement used in the respective systems results in chaotropic advection, resulting in efficient RNA encapsulation (95). The downside of this technology is cost, as many of the large-scale systems and their consumables are expensive, often using single use consumables. Impingement systems, which do not use consumables such as microfluidics cassettes, while maintaining the ability to scale up production, may be a more affordable form of microfluidic production.

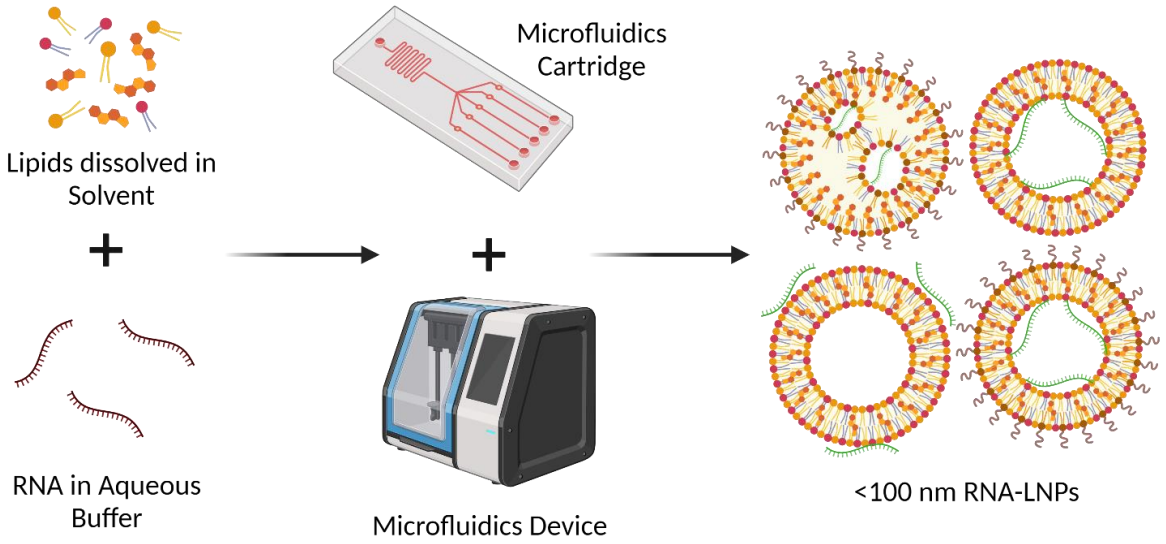

Figure 1.3.3. Microfluidics, a modernised method of LNP formulation. Lipids dissolved in alcohol and RNA dissolved in a buffer are mixed by a microfluidics device through a microfluidics cartridge. This formulates RNA-LNPs with diameters generally <100 nm. The example shown is utilising the Precision NanoSystems® Ignite™, however impingement systems are an alternative, efficient microfluidics system.

1.3.3. Application of Lipid Nanoparticles for Efficient Delivery of saRNA Vaccines

LNPs have been widely used in the delivery of mRNA and saRNA vaccines, in pre-clinical and clinical trial studies (8,96). Geall *et al*. were the first to use non-viral vectors for saRNA vaccine delivery through the use of iLNPs comprised of an ionisable lipid, phospholipid, cholesterol, and PEGylated lipid, to deliver saRNA encoding a RSV fusion glycoprotein (97). Following this, many other saRNA vaccines have utilised iLNPs for successful saRNA vaccine delivery (50,57,62,98–103). Although they have been more extensively used than cLNPs in saRNA

vaccine delivery, they are limited by their increased production costs, hence cLNPs still present a potential alternative delivery system. saRNA delivered using the cLNP platform have shown potential using both RNA internally formulated (saRNA-Int-cLNPs; Figure 1.3.1A and B), or when added to “empty” cLNPs, resulting in external formulation (saRNA-Ext-cLNPs, Figure 1.3.1B). Although some studies show inferiority to iLNPs, further optimisation of saRNA-cLNPs and use of a larger variety and more novel lipids may improve the applicability. Blakney and colleagues have recently studied the efficacy of cLNPs lacking a PEGylated lipid, allowing a comparison of saRNA-Int- and saRNA-Ext-cLNPs (62). Although variability was observed in RNase protection for saRNA-Int versus saRNA-Ext DOTAP and DDA cLNPs, and *in vivo* expression of DDA cLNPs, both formulations resulted in antigen-specific immunogenicity. saRNA-Ext-cLNPs induced stronger HIV-1 Immunoglobin G (IgG) titres after the first (prime) dose than saRNA-Int-cLNPs. Although saRNA-Ext-cLNPs showed a reduction or minimal boost IgG in titres after the boost dosage, saRNA-Int-cLNPs had a large boost in IgG titres. In another study a design of experiments (DOE) approach was utilised to examine cLNPs in skin explants to observe cellular distribution of saRNA expression after intradermal injection (104). Fifty percent of GFP+ cells were identified as immune cells despite being a low percentage of the total skin cells, presenting the potential feasibility of these cLNPs as intradermal injection vaccine candidates. With the importance of different cell populations in an effective immune response, this highlights the advantages of examining alternative routes of RNA-LNP vaccine administration. Intradermal and intranasal administration are simpler and less invasive to perform and may prove beneficial based on the mode of pathogen infection and required immune response. This translates to a sociological impact, as fear of needles may increase the hesitancy of patients to receive an RNA-LNP vaccine administered intramuscularly. These studies on saRNA-cLNPs highlight the importance of identifying and examining a library of cLNPs *in vivo*.

In an important study comparing different non-viral formulations, Lou *et al.* compared DOTAP and DDA cLNPs comprising cationic lipid, DOPE, and a PEGylated lipid, to benchmark iLNPs, and DOTAP CNEs using a rabies saRNA vaccine (103). cLNPs were able to produce a strong antibody response comparable to iLNPs at a higher dose, however at the lower dose tested, iLNPs outperformed cLNPs. Cellular responses similar to the commercial Rabies vaccine were observed for cLNPs and CNEs, however iLNPs had significantly improved CD8+ T cell responses

and CD4+ responses. Anderluzzi performed similar experiments, where polymeric nanoparticles and a proprietary CNE (CNE56) induced superior humoral and cellular immune responses (105). cLNPs were less potent, however this could be due to the formulation lacking cholesterol or a PEGylated lipid, which differs to that of the formulations used by Blakney and Lou. Therefore, the composition of the cLNPs is especially important, and multiple candidates should be evaluated to achieve a better comparison.

RNA-LNPs represent an efficacious, scalable technology for application to RNA vaccines. Self-amplifying RNA presents advantages over conventional mRNA as it can be administered at lower doses, mimics viral replication for enhanced antigen expression, and does not require expensive modified nucleotides for synthesis. However, delivery of these RNAs, which are significantly longer than conventional mRNA, still requires optimisation. While iLNPs are more commonly used for saRNA delivery, permanently cationic lipids are cheaper, and have a longer history of safe use in the pharmaceutical industry. cLNPs have recently been explored for delivery of saRNA vaccines with success, showing potential to be utilised for human use. Since cLNPs are permanently cationic, they allow for high encapsulation efficiencies, RNase protection, and delivery to cells in a receptor-independent manner.

This research conducted in this dissertation involved designing and evaluating the saRNA-cLNP platform for use in saRNA vaccines. Plasmid DNA templates were cloned to improve saRNA transgene expression. The *in vitro* transcription of saRNA was optimised to accommodate the larger size of these RNAs compared to conventional mRNAs. Different methods of LNP production were explored including lipid film hydration, modified solvent injection, and microfluidics. This is advantageous to produce consistent, high quality and homogenous LNPs. External and internal saRNA formulation, and alteration of N:P and LNP size was explored to examine their effects on saRNA delivery, expression, and expression kinetics of different saRNA-cLNP candidates. This impacts delivery and vaccine efficacy, as well as production methodology, and hence is important to study. The investigation of different lipids and lipid combinations with different immunological and pharmacological profiles could aid in improving immune responses for the requirements of different vaccines. cLNPs were examined in cell culture and *in vivo* to obtain important data on expression, biodistribution and toxicity. While DOTAP and DDA have been examined in previous studies, this was the first known study to examine DOTMA as a cationic lipid for saRNA delivery.

Overall, a saRNA vaccine pipeline for cloning and production of future vaccine candidates in South Africa has been developed. A library of saRNA-cLNPs has been examined, with potential to be examined *in vivo* and for future saRNA vaccine candidates. These technologies could improve vaccine efficacy in lower middle-income countries such as South Africa by lowering production costs and dosage.

1.4. Aim and Objectives

This dissertation aimed to investigate the design, production, optimisation, and characterisation of saRNA-cLNPs for use in vaccines.

Objectives:

- To clone saRNAs encoding reporter genes using conventional cloning methodology.
- To *in vitro* transcribe large saRNAs by optimising the reaction based on current available kits and literature.
- To produce lipid nanoparticles and formulate saRNA-LNPs by examining and optimising a variety of formulation techniques.
- To characterise saRNA-cLNP size, zeta potential and encapsulation efficiency using dynamic and electrophoretic light scattering, and RiboGreen assays respectively.
- To examine the delivery efficiency and expression kinetics of saRNA-cLNP candidates using fluorescence microscopy and firefly luciferase assays.
- To evaluate cell culture toxicity of *in vivo* saRNA-cLNP candidates using an MTT assay.
- To examine delivery efficacy of saRNA-cLNPs *in vivo* after intramuscular injection in NMRI mice.

Chapter 2

Methods

2.1. Generation of reporter gene self-amplifying RNA vectors

To generate a vector that produces saRNA that encodes for the reporter genes enhanced green fluorescent protein (eGFP) or Firefly luciferase (Fluc), basic bacterial cloning was performed using T7-VEE-eGFP as the backbone plasmid (cloning strategy schematics in Figures 2.1.1 and 2.1.2).

pUC57-saRNA-MCS-polyA(60) (saRNA-MCS; Supplementary Figure 1A) and pGL4.50[luc2; CMV; Hygro] (pGL4.50 Luc2; Supplementary Figure 1B; Promega, WI, USA) were propagated in NEB Turbo *E. coli* (New England Biolabs, NJ, USA; Appendix 5.1.4 and 5.1.5) and purified using the Qiagen Plasmid Maxi Kit (Qiagen, MD, USA; Appendix 5.2.7). These were screened using restriction digestion and agarose gel electrophoresis (Supplementary Figure 2A). To insert the Luc2 gene into the subcloning vector, saRNA-MCS was digested with *Hin*d III and *Nhe* I (Figure 2.1.1). The pGL4.50[luc2; CMV; Hygro] plasmid was digested with *Hin*d III and *Xba* I, which allowed for the removal of Luc2 (Supplementary Figure 2B). Digests were electrophoresed on a 1% Tris-Acetate EDTA (TAE) agarose gel in a TAE running buffer. DNA was stained with ethidium bromide and examined using the Omega Fluor gel documentation system (aplegen, CA, USA) under ultraviolet light. The desired bands of 2697 bp and 1692 bp for saRNA-MCS and pGL4.50 Luc2 respectively, were extracted and purified using the QIAquick Gel Extraction Kit according to the manufacturer's instructions (Qiagen, MD, USA; Appendix 5.3.1). A ligation was performed using T4 DNA ligase (ThermoFisher Scientific, MA, USA) at a 1:3 and 1:5 vector:insert ratio (1:0 control included) at room temperature for 10 minutes to generate saRNA-MCS-Luc2-polyA(60) (Supplementary Figure 3). NEB® Turbo Competent *E. coli* cells (New England Biolabs, NJ, USA) were transformed with the ligation reaction by heat shock at 42 °C followed by an overnight incubation on ampicillin selection agar plates. Colonies were picked and cultured, and pDNA was extracted by alkaline lysis (Appendix 5.2.8). Restriction analysis of saRNA-MCS-Luc2-polyA(60) was performed with restriction enzymes *Lgu* I and *Apa* I, which yielded band sizes of 2268, 1278, 484 and 359 bp (Supplementary Figure 4A).

To remove the eGFP, puromycin resistance genes, internal ribosomal entry site (IRES), 3' UTR and 25 bp poly A sequence from the T7-VEE-eGFP plasmid (Supplementary Figure 7A) and replace it with the Luc2 gene, 3' UTR and 60 bp poly A sequence from T7-MCS-Luc2-polyA(60) both plasmids were digested with *Nde* I and *Mlu* I (Figure 2.1.1.). The 9394 bp and 1902 bp bands of interest from T7-VEE-eGFP and saRNA-MCS-Luc2 were gel extracted (Supplementary Figure 4B; Appendix 5.3.1). Ligation of T7-VEE-eGFP and saRNA-MCS-Luc2 generated T7-saRNA-VEE-Luc2-polyA(60) (Figure 2.1.1, Supplementary Figure 8A). Restriction analysis of T7-saRNA-VEE-Luc2-polyA(60) using *Bsp*1407 I and *Lgu* I yielded band sizes of 7010 and 4286 bp (Supplementary Figure 6).

Table 2. Description and Source of Plasmids Utilised and Generated in the Study

Plasmid Name	Description	Generated/Reference
T7-VEE-eGFP	saRNA-eGFP reporter RNA production plasmid containing a 25 bp poly A sequence	Steven Dowdy (Addgene plasmid # 58977)
T7-VEE-Fluc-IRES-mCherry	saRNA-Fluc-mCherry reporter RNA production plasmid containing a 25 bp poly A sequence	Unpublished
pUC57-saRNA-MCS-polyA(60)	Subcloning plasmid containing VEE 3' UTR and a 60 bp poly A sequence. For subcloning reporter genes/vaccine antigens into the T7-VEE-eGFP plasmid backbone.	Generated by GeneScript (NJ, USA)
pGL4.50[luc2; CMV; Hygro]	Commercial plasmid containing a codon optimised Fluc gene, Luc2 under the control of a cytomegalovirus promoter. For cloning Luc2 into the saRNA plasmid	Purchased from Promega (WI, USA)
saRNA-MCS-Luc2-polyA(60)	Subcloning vector containing Luc2 gene	This study
T7-saRNA-VEE-Luc2-polyA(60)	saRNA-Luc2 reporter RNA production plasmid containing a 60 bp poly A sequence	This study
T7-saRNA-VEE-eGFP-polyA(60)	saRNA-eGFP reporter RNA production plasmid containing a 60 bp poly A sequence	This study

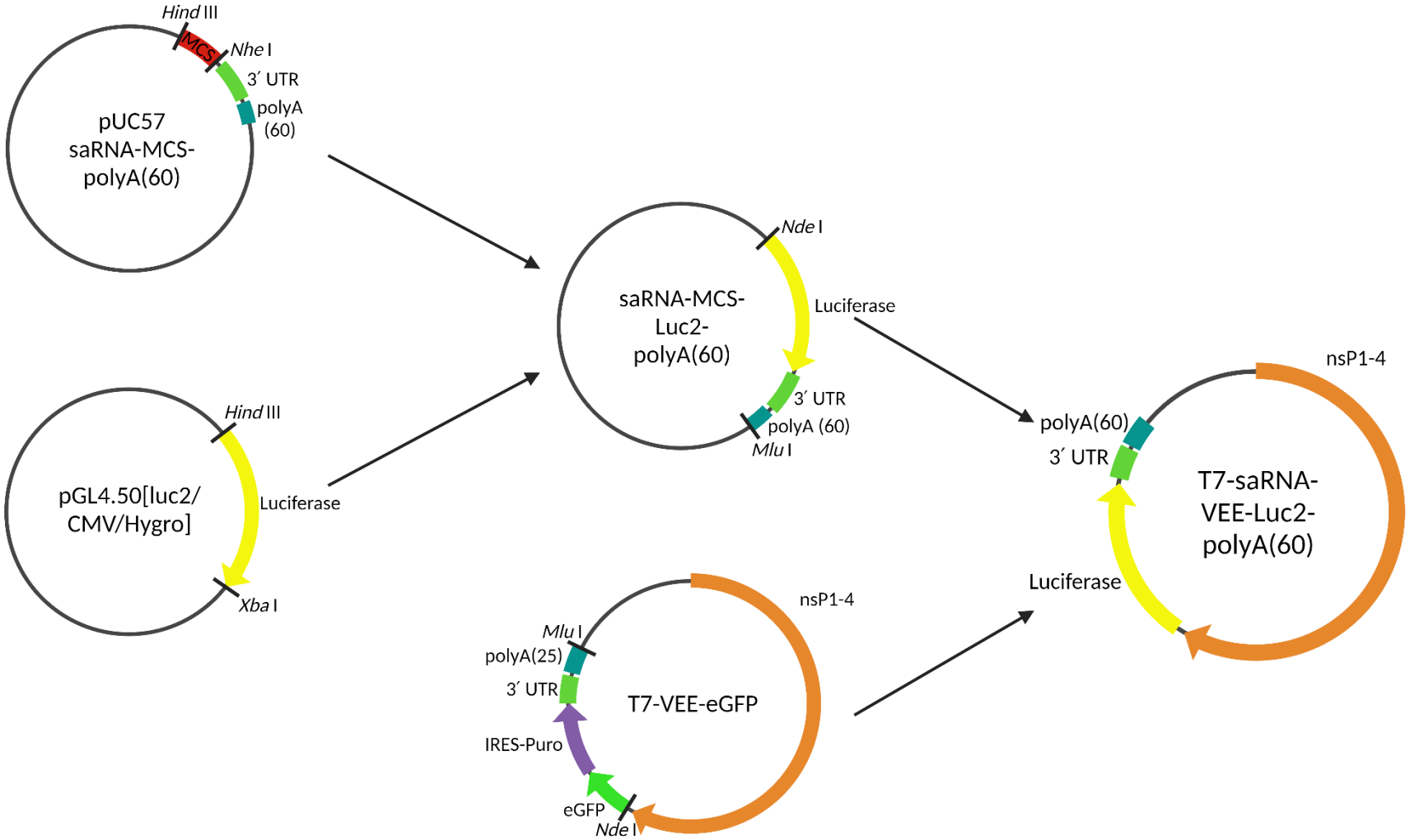

Figure 2.1.1. Schematic of cloning strategy of T7-saRNA-VEE-Luc2-polyA(60). From left to right, the Luc2 gene was removed from pGL4.50[luc2/CMV/Hygro] and cloned into pUC57 saRNA-MCS-polyA(60) to generate saRNA-MCS-Luc2-polyA(60). The Luc2 gene, 3' UTR and poly A sequence were removed from saRNA-MCS-Luc2 and cloned into T7-VEE-eGFP, replacing the eGFP-IRES-Puro genes, and 3' UTR and poly A sequence of the original plasmid. This generated T7-saRNA-VEE-Luc2-polyA(60).

To generate an alternative saRNA-eGFP production plasmid, the IRES, puromycin resistance selection gene, 25 bp poly A sequence of T7-VEE-eGFP were removed and replaced with the VEE 3' UTR and a 60 bp poly A sequence from saRNA-MCS (Figure 2.1.2). Both plasmids were digested with *Not* I and *Mlu* I (Supplementary Figure 5A and B). Fragment sizes of 10 169 bp and 174 bp were gel extracted for T7-VEE-eGFP and saRNA MCS (Appendix 5.3.1). Ligation of T7-VEE-eGFP and saRNA-MCS generated T7-saRNA-VEE-eGFP-polyA(60) (Supplementary Figure 8B). Restriction analysis of T7-saRNA-VEE-eGFP-polyA (60) using *Kpn* I and *Xba* I yielded band sizes of 4967, 3972 and 1404 bp (Supplementary Figure 6). T7-VEE-GFP was a gift from Steven Dowdy (Addgene plasmid # 58977; http://n2t.net/addgene:58977; RRID:Addgene_58977)

2.2. *In vitro* transcription of self-amplifying RNA

To prepare pDNA vectors for *in vitro* transcription, linearisation was performed. T7-saRNA-VEE-eGFP-polyA(60) and T7-saRNA-VEE-Luc2-polyA(60) vectors were linearised by restriction digestion with *Mlu* I (ThermoFisher Scientific, MA, USA) for 2 hours at 37°C. The linearised product was purified by sodium acetate precipitation; 1/10 volume sodium acetate and 2.5× volumes 100% ethanol were added to the reaction followed by a precipitation incubation at -80°C for 15 minutes. The pDNA was pelleted by centrifugation at 14 000 ×g for 15 minutes at 4°C, followed by a 70% ethanol wash. Purified linearised pDNA was resuspended in nuclease-free water to a concentration above 1 µg/µl. Linearisation was confirmed by electrophoresis on a 1% TAE agarose gel in a TAE running buffer. DNA was stained with ethidium bromide and examined using the Omega Fluor gel documentation system (aplegen, CA, USA) under ultraviolet light.

Initial IVTs were performed using either the AmpliScribe T7-Flash Transcription Kit (Epicentre Biotechnologies, WI, USA), TranscriptAid T7 High Yield Transcription Kit (ThermoFisher Scientific, MA, USA), and the RiboMAX™ Large Scale RNA Production System (Promega, WI, USA). The final optimised IVT was performed using an in-house reaction based on a design of experiments (DOE) journal article (106), increasing the T7 Polymerase from 100 units (U) to 800 U. The reaction was set up as in Table 3 using a HEPES-based buffer (Table 4, Appendix Table 4). The IVT reaction was incubated at 37°C for 2 hours, followed by DNase treatment to remove the pDNA template for 15 minutes at 37°C.

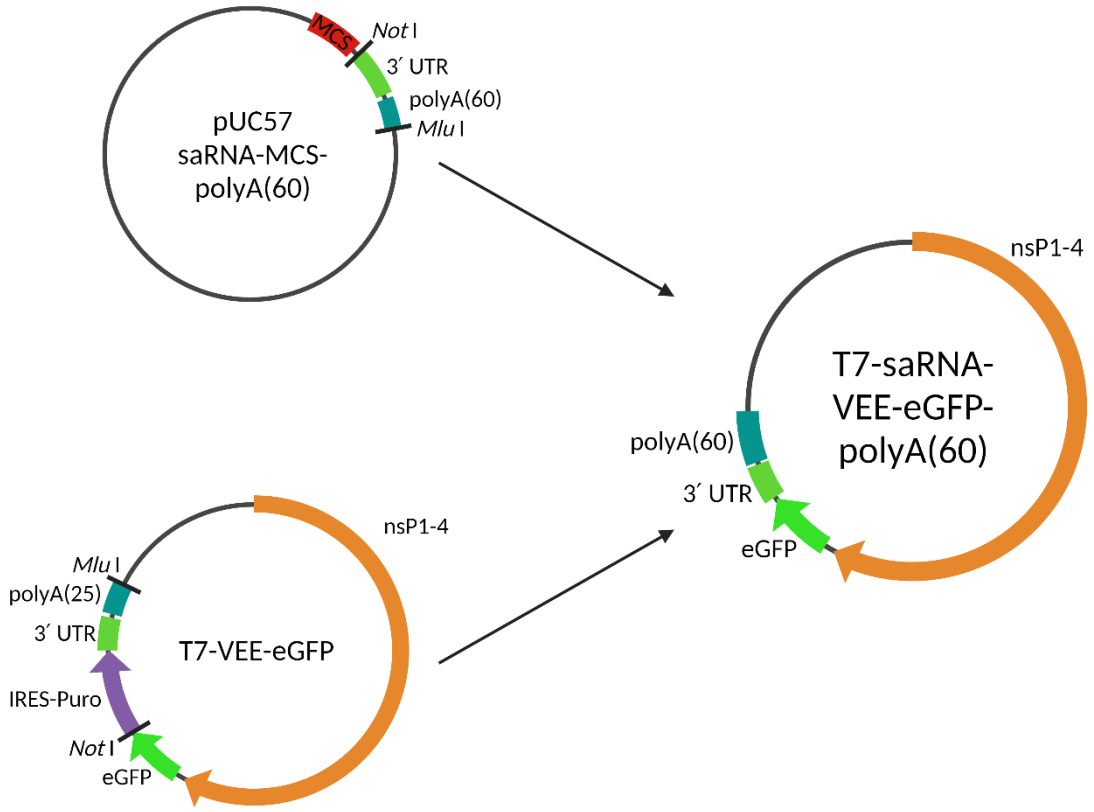

Figure 2.1.2. Schematic of cloning strategy of T7-saRNA-VEE-eGFP-polyA(60). From left to right, the 3′ UTR and poly A sequence of pUC57 saRNA-MCS-polyA(60) were cloned into the original VEE-eGFP plasmid to replace the IRES-Puro, 3′ UTR, and poly A sequence. This generated T7-saRNA-VEE-eGFP-polyA(60).

RNA purification was performed by Lithium Chloride (LiCl) precipitation. A LiCl precipitation solution (7.5 M LiCl, 50 mM EDTA) was added to a final concentration of 2.5 M LiCl and incubated at -20°C for a minimum of 30 minutes to precipitate RNA. This was then pelleted by centrifugation at 14 000 ×g for 15 minutes at 4°C. The supernatant was discarded, and the RNA pellet was washed with ice-cold 70% v/v ethanol followed by a 10-minute centrifugation step (14 000 ×g, 4°C). The ethanol was completely discarded, and the RNA pellet was resuspended in nuclease-free water and stored in aliquots at -80°C to maintain integrity. Quantification of RNA was performed by spectrophotometry using a NanoPhotometer® (Implen, CA, USA). RNA integrity was assessed using a denaturing formaldehyde-agarose gel (Appendix 5.4.3). The RNA (1 µg) was mixed with an equal volume of 2× loading dye buffer containing formamide, SDS and ethidium bromide (ThermoFisher Scientific, MA, USA). To denature the RNA, the dilution was incubated at 70°C for 10 minutes followed by incubation on ice for 5 minutes before adding the mixture to the gel. The gel was electrophoresed for 45 minutes at 80 V in a 3-(N-morpholino)propanesulfonic acid (MOPS)-formaldehyde-based buffer. RNA size was measured using either the ssRNA ladder (New England Biolabs, NJ, USA) or the RiboRuler HR (ThermoFisher Scientific, MA, USA).

Table 3. DOE *In Vitro* Transcription Reaction Setup.

Component	Final Concentration
Nuclease-Free Water	(To Final Volume)
rNTPs (ATP, CTP, GTP, UTP)	10 mM each
Cap Analogue	10 mM (8 mM for CleanCap AU)
Transcription Buffer	1×
Linearised Template	100 ng/µl
RNase Inhibitor	0.04 U/µl
T7 RNA Polymerase	8 U/µl

Table 4. Components of 1× DOE Transcription Buffer.

Component	Concentration (mM)
HEPES	40
Magnesium acetate	75
DTT	40
Spermidine	0.2
Sodium acetate	10

The saRNA was co-transcriptionally capped using the Anti-Reverse-Cap-Analogue (ARCA, Cap 0; New England, NJ, USA), for *in vitro*/cell culture experiments and CleanCap® AU (Cap 1; TriLink Biotechnologies, CA, USA) for *in vivo* experiments. Enzymatic capping was performed using the Vaccinia Capping system and 2´-O-Methyltransferase (Cap 1; New England Biolabs, NJ, USA). Integrity of enzymatically capped RNA was confirmed again by denaturing formaldehyde-agarose gel electrophoresis (Appendix 5.4.3).

Vaccinia capping was performed by diluting 10 µg of RNA in 13.5 µl of nuclease-free water. This was denatured at 65°C for 5 minutes, followed by incubation on ice for 5 minutes. The reaction was then set up according to Table 5, incubated for 1 hour at 37°C, and purified using LiCl precipitation (Appendix 5.4.1).

Table 5. Vaccinia Capping System Reaction Setup

	Initial Concentration	Volume (µl)
Denatured uncapped RNA	-----	13.5
10× Capping Buffer	10×	2
GTP	10 mM	1
SAM	4 mM	1
Vaccinia Capping Enzyme	50 U/µl	1
mRNA Cap 2´-O-Methyltransferase	50 U/µl	1
Murine RNase Inhibitor	40 U/µl	0.5
Total volume		**20**

2.3. Lipid Nanoparticle Production

DOTAP, DOTMA, DDA, DSPC, DOPE and DMG-PEG 2000 were obtained from Avanti Polar Lipids, Inc (AL, USA). Cholesterol was obtained from Sigma-Aldrich (MO, USA).

LNPs were produced using three different methods: LFH, microfluidics and modified solvent injection (SI). LFH was used to produce saRNA-Ext-cLNPs; and microfluidics or modified SI were used to produce saRNA-Int-cLNPs. Lipid stocks were dissolved in ethanol at a concentration of 20 mg/ml and stored under a nitrogen gas layer. Multi-component LNP lipid formulation stocks (20 mg/ml) were pre-mixed and stored at -20°C (Appendix Table 5).

2.3.1. Production of LNPs using LFH and external formulation of RNA

Multi-component LNP lipid stocks were diluted to 4-10 mg/ml in ethanol to a final volume of 0.5-1 ml in a glass Poly Top vial. Lipid films were produced by evaporating the ethanol using nitrogen under spiral flow using the Smart Evaporator C1 (BioChromato, Inc.; JP) for 15-20 minutes. This spiral flow allowed for a more evenly distributed lipid film. The vial was placed in a desiccator containing silica gel beads to absorb moisture, and the lipid film was vacuum desiccated for 2 hours to remove any residual ethanol. Lipid films were then hydrated with HEPES buffered saline (HBS; Appendix 5.5.1) for 30 minutes with occasional vortexing. HBS was pre-warmed at a temperature above the lipid's phase transition temperature. The hydrated film was incubated overnight at 4°C to ensure sufficient hydration. To create unilamellar vesicles and reduce LNP size, bath sonication and extrusion were performed. Bath sonication was performed for 12-15 minutes using the Bandelin Sonorex (Bandelin, BE, DE). LNPs were then sized using the ZetaSizer Pro Blue (Malvern Panalytical, UK) to determine the extrusion membranes needed.

Extrusion was accomplished using the Avanti® Mini Extruder (Avanti Polar Lipids, Inc, AL, USA) according to manufacturer's instructions. The appropriate porous polycarbonate membrane was chosen based on unilamellar vesicle particle size, choosing the first membrane with a slightly smaller pore size than the LNPs. Two membrane supports and the chosen polycarbonate membrane were pre-wet in HBS. The extruder components were washed thoroughly with detergent and rinsed with injection-grade water. The extruder was then assembled in the order of extruder outer casing, internal membrane support with O-ring, 1 filter support, polycarbonate membrane, 1 filter support, internal membrane support with O-ring, Teflon bearing, retainer nut (Figure 2.3.1A). The assembled extruder was placed into the heating block and pre-wet with 1 ml of HBS to avoid sample loss. LNPs were loaded into one of the 1 ml Hamilton syringes and assembled with the extruder (Figure 2.3.1B). The heating block was then heated to a temperature above the LNPs phase transition temperature. LNPs were then extruded by passing the LNPs from one syringe to the other through the membrane a minimum of 11 times to ensure a uniform size distribution. This was performed an odd number of times so that the final LNP solution was in the opposite syringe, this guarantees that no debris was brought over from the original solution. This was performed sequentially from higher to lower pore sizes ranging from 400 nm – 100 nm, cleaning and assembling the

extruder between every membrane. LNPs were sized post-extrusion and Zeta Potential was measured using the ZetaSizer Pro Blue (Malvern Panalytical, Malvern, United Kingdom). saRNAs were complexed externally by mixing with LNPs at different N:P ratios (Positive nitrogen on the cationic lipid:Negative phosphate on the RNA) and incubating the mixture at room temperature for 30 – 45 minutes before use. Size and zeta potential measurements were then performed as before.

A)

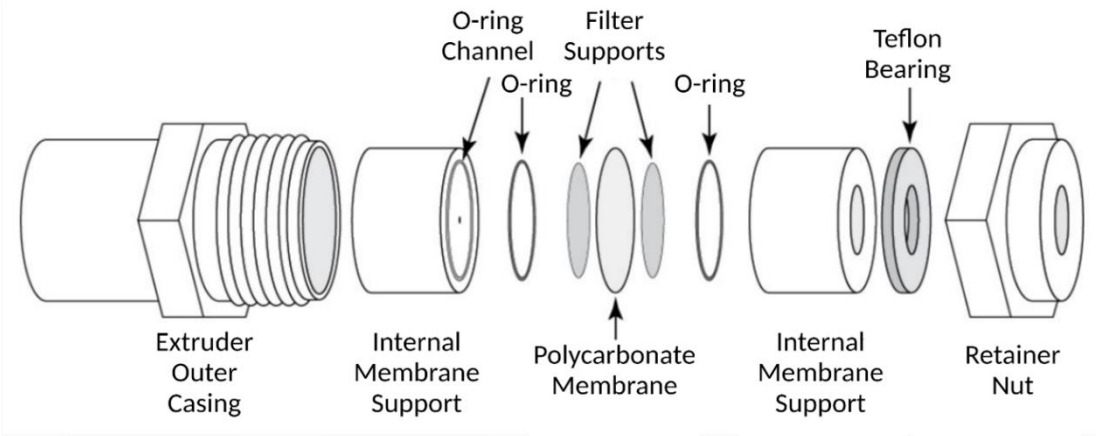

B)

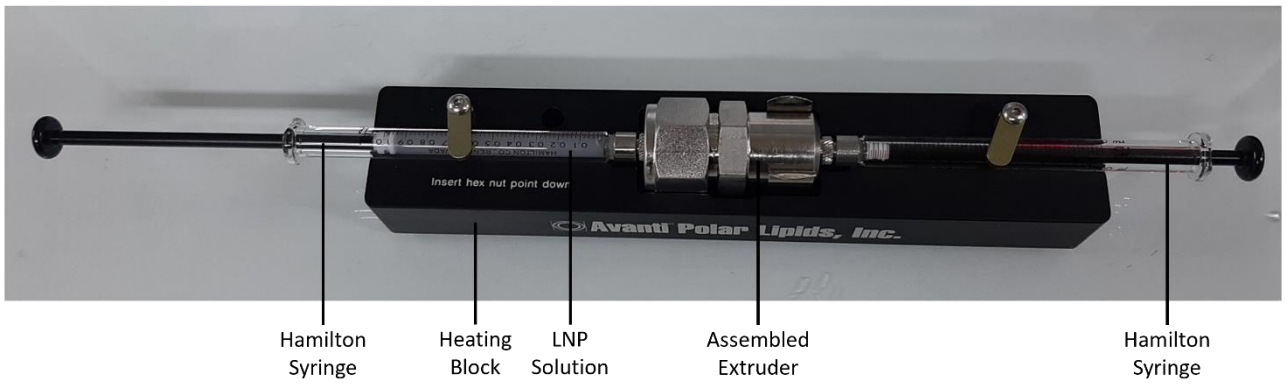

<u>Figure 2.3.1. Set-up of the Avanti® Mini Extruder for reducing LNP size.</u> A) Set up of the assembly of the extruder using pre-wet filter supports and polycarbonate membrane. B) After pre-wetting the extruder with HBS, bath sonicated LNPs were loaded onto one side of the extruder in the black heating block, preheated above the lipids' phase transition temperatures, and extruded by passing the solution from one syringe to the other through the membrane a minimum of 11×, with the final extrusion pushing the LNPs into the syringe on the right.

For size and zeta potential measurements, 40 µl (usually 40 µl, but dependant on the concentration on the LNP solution) of LNPs were diluted to 1 ml with nuclease-free water. For sizing, this was added to a clear rectangular cuvette, placed in the ZetaSizer, and run under default conditions (n=3 technical replicates). For zeta potential the dilution was placed in a

cuvette with gold-plated electrodes using a 1 ml syringe, and any bubbles were removed. This was placed in the ZetaSizer and run under default conditions (n=3 technical replicates).

N:P was calculated by calculating the moles of RNA to be used (RNA Molecular Weight=333.8 g/mol), dividing this by the desired ratio (e.g. 6:1 N:P – divide by 6) to determine the number of moles of cationic lipid to be used. From this, the weight of cationic lipid component required can be calculated.

2.3.2. Internal RNA-LNP formulation using microfluidics

For microfluidics, LNPs were produced using the NanoAssemblr® Ignite™ (Precision NanoSystems, Canada) using NxGen cartridges. Lipids were dissolved in ethanol at a final total lipid concentration of 4-20 mg/ml and RNA was dissolved in 100 mM Tris buffer (pH 7; ThermoFisher Scientific, MA, USA) or 6.25 mM Sodium Acetate buffer (pH 5; Appendix 5.5.2) for cLNPs and iLNPs, respectively. The diluted lipids and RNA were drawn into separate syringes and attached to the NxGen cartridge in the NanoAssemblr Ignite machine. Solvent and aqueous phases were mixed simultaneously at a 3:1 flow rate ratio (FRR) and a total flow rate of 5-15 ml/min. Ethanol was removed either by buffer exchange and concentration, or dialysis. For buffer exchange and concentration, the final LNP formulation was diluted approximately with 40× the volume of 10 mM Tris Buffer (pH 7) or PBS (pH 7.4) or for cLNPs and iLNPs, respectively. This was then concentrated using Amicon® Ultra-15 Centrifugal filters (10 kDa MWCO; Sigma-Aldrich, MO, USA) by centrifugation in a swing bucket rotor at 2000 ×g for 30 minutes with washing of the membrane between centrifugation steps. This was repeated until the solution was at the desired final volume, followed by filter sterilisation using Acrodisc® Supor® membrane syringe filters (Pall Corporation, NY, USA). cLNP dialysis was performed against 10 mM Tris buffer for cLNPs for 2 hours with mixing using Pur-A-Lyzer™ Midi dialysis kit (3.5 kDa MWCO, Sigma-Aldrich, MO, USA). Size and zeta potential measurements were then performed as mentioned previously.

2.3.3. Modified solvent injection formulation of RNA-LNPs

Modified solvent injection method was performed for internal formulation of RNA-LNPs. RNA was diluted in 100 mM Tris buffer (pH 7, ThermoFisher Scientific, MA, USA) or 6.25 mM Sodium Acetate buffer (pH 5; Appendix 5.5.2) for cLNPs and iLNPs, respectively. Ten and twenty micrograms were used for final formulation volumes of 100 and 200 µl, respectively. The dilution volume was equal to that of the required lipid volume. The appropriate volume

of a 20 mg/ml lipid mix, dependent on the N:P ratio, was added by pipetting, followed by addition of 100 mM Tris buffer (pH 7) up to the final formulation volume. The mixture was then vortexed for 5 seconds. Particle size measurements were then performed as before. These were roughly produced RNA-cLNPs, and hence were used solely for cell culture transfection experiments.

2.4. RNA quantification and Encapsulation Efficiency assessment

To quantify RNA in formulated RNA-LNPs (effective dose) and assess encapsulation efficiency of RNA-Int- and RNA-Ext-LNPs, the Quant-iT RiboGreen RNA Kit (ThermoFisher Scientific, MA, USA) was used. This assay allows quantification of unformulated RNA in the absence of a detergent, and total RNA after lysis of LNPs with a detergent (Triton X-100). The encapsulation efficiency and effective dose (encapsulated RNA) can subsequently be calculated using this information.

The assay was set up in a black 96-well plate (ThermoFisher Scientific, MA, USA) as in Figure 2.4.1. An appropriate amount of RNA-LNP sample was diluted in 250 µl total volume of 1× TE buffer, pH 7.5 (Figure 2.4.1, Row A). An appropriate concentration was calculated as that required to achieve a final concentration in a range of 1-1.5 ng/µl after addition of the RiboGreen dye. A background control was included to exclude background interference of Triton X-100. Fifty microlitres of the diluted sample were further diluted in 50 µl of either TE buffer (pH 7.5), or in Triton buffer (2% Triton X-100 in TE buffer; Appendix 4.6.4). This was performed in duplicate. A standard curve was set up as in Table 6. These included Triton buffer to mitigate background interference from Triton X-100, allowing accurate quantification of total RNA in the sample after LNP lysis (Figure 2.4.2). Samples were then incubated at 37°C for 10 minutes to lyse LNPs in the presence of the Triton X-100 detergent. Ribogreen reagent was then added to each well (100 µl of a 1:100 dilution of Ribogreen reagent). Fluorescence was measured using the GloMax® Explorer (Ex: 475 nm; Em: 500-550 nm; Promega, WI, USA). Encapsulation efficiencies and effective saRNA concentrations were calculated using the following equations where total RNA (µg/ml) was calculated using the standard curve:

Encapsulation Efficiency (%) =

$$\left(1 - \frac{Fluorescence\ Value\ of\ RNA\ LNPs\ in\ the\ Absence\ of\ Lysis}{Fluorescence\ Value\ of\ RNA\ LNPs\ Lysed\ with\ Triton\ Buffer}\right) \times 100$$

Effective Concentration (µg/ml)=

$$Total\ RNA\ Concentration\ (\mu g/ml) \times Encapsulation\ Efficiency\ (\%)$$

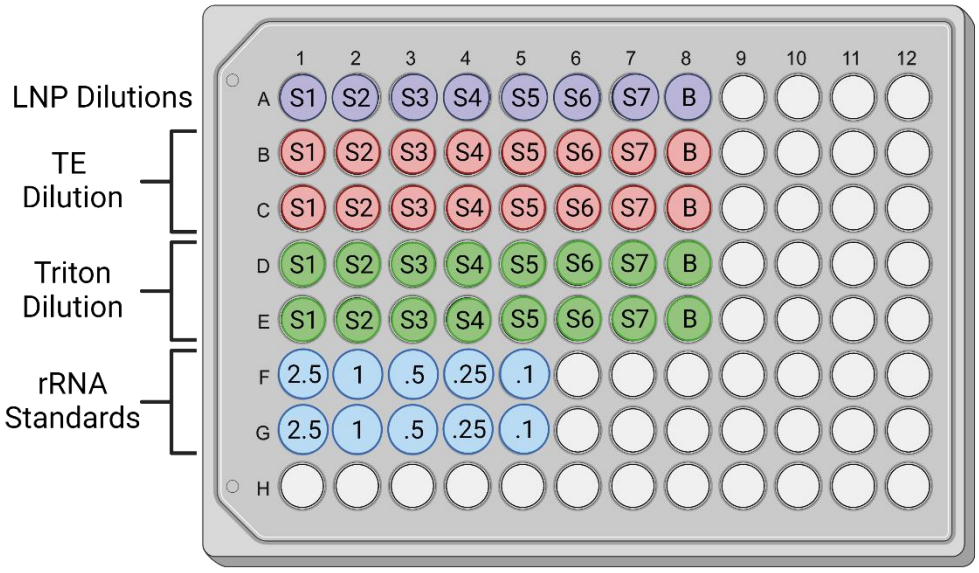

Figure 2.4.1. Set up of the RiboGreen Assay in a black 96-well plate. LNP dilutions were performed in row A. LNPs from row A were further diluted in either TE buffer (Row B and C) to measure un-encapsulated RNA, or Triton Buffer (Row D and E) to lyse LNPs and measure total RNA content. A range of rRNA standards from 2.5-0.1 ng/µl were set up according to Table 6, and 100 µl were added to Rows F and G in duplicate. The plate was then incubated at 37°C to lyse LNPs in the presence of detergent, 100 µl of RiboGreen dye was added to Rows B-G, and fluorescence was measured using excitation and emission filters of 475 nm and 500-550 nm respectively. Wells labled "B" indicate the blank control.

Table 6. Standard curve for Ribogreen Assay set up using provided rRNA standards

Final RNA concentration (µg/ml)	Volume of 20 µg/ml stock (µl)	1× TE Buffer (µl)	1× Triton Buffer (µl)	Volume Added per well (µl)	Volume of RiboGreen Dye Added per Well (µl)
2.5	65	65	130	100	100
1	26	104	130	100	100
0.5	13	117	130	100	100
0.25	6.5	123.5	130	100	100
0.1	2.6	127.4	130	100	100

2.5. Cell culture experiments

2.5.1. Transfection of cells with eGFP-self-amplifying RNA

HEK293 (Human Embryonic Kidney) cells were used to examine delivery efficiency of RNA-LNPs. Cells were maintained in complete Dulbecco's Modified Eagle's Medium (DMEM, 4.5 g/L glucose; Gibco, ThermoFisher Scientific, MA, USA) containing 10% foetal bovine serum (FBS), penicillin (100 000 U/ml) and streptomycin (100 µg/mL; Appendix 5.7.1). Cells were seeded in a 48-well plate (30 000 – 36 000 cells/well) the day before transfection. Two hundred nanograms of saRNA-LNPs were used per well. RNA-LNPs were diluted to a final concentration of 6.67 ng/µl and 30 µl was added to each well. Lipofectamine™ MessengerMax™ (LMMax; Invitrogen, MA, USA) was used as a positive control as it is a liposomal formulation that yields remarkably high transfection efficiency in cell culture. LMMax was diluted in OptiMEM and incubated for 10 minutes at room temperature. RNA was diluted in OptiMEM, added to the LMMax dilution, mixed, and incubated at room temperature for 5 minutes before 30 µl (200 ng) was added per well. Transfection efficiency was examined at 24- and 48-hours post-transfection unless otherwise stated. For eGFP RNA transfections, the EVOS Fluorescence Microscope (Invitrogen, MA, USA) was used to examine transfection efficiency.

2.5.2. Luciferase Assay

The Luciferase® Reporter Assay System kit (Promega, WI, USA) was used to assess transfection efficacy of HEK293 cells transfected using RNA-Luc2-LNPs. At 24- or 48-hours post-transfection, media was removed from cells. Cells were lysed by incubation in passive lysis buffer with shaking for 15 minutes at room temperature. LARII substrate (50 µl) was mixed with 10 µl of cell lysates in a white 96-well plate, and relative light units were detected using the GloMax® Explorer (Promega, WI, USA). Background luminescence values from the negative control were subtracted from experimental luminescence values.

2.5.3. Cell viability assay

To ensure no substantial cellular toxicity was being caused by saRNA-LNPs, an MTT assay was performed. Viable cells metabolise MTT [3-(4, 5-dimethylthiazol-z-yl)-2, 5-diphenyltetrazolium bromide] (Sigma-Aldrich, MO, USA) into a purple formazan that can be detected by absorbance at 570 nm. HuH7 cells were maintained in low glucose (1g/L) Dulbecco's Modified Eagle's Medium (DMEM; Gibco, ThermoFisher Scientific, MA, USA) containing 10% foetal bovine serum (FBS), penicillin (100 000 U/ml) and streptomycin (100

µg/mL; Appendix 5.7.1). HuH7 cells (10 000 cells/well) were seeded in a 96-well plate 24-hours prior to transfection with 100 ng of saRNA-LNPs. Cells transfected with delivery vehicle alone (empty LNP or Lipofectamine) served as controls. Cells treated with 25% DMSO for 30 min were included as a positive control for cellular toxicity. MTT assays were performed 24 hours post transfection. Media was aspirated from the cells. A mixture of 20 µl of 5 mg/ml MTT (in PBS) and 80 µl of cell culture media was added per well and incubated for one hour at 37 °C (5% CO_2). The growth media/MTT mix was then aspirated, and the formazan product was resuspended in 200 µl DMSO, absorbance was measured at 570 nm using an iMark microplate reader (BioRad, CA, USA). Background absorbance was measured at 690 nm (an unrelated wavelength to the purple formazan) and subtracted from experimental values.

2.6. *In vivo* experiments

Animal experiments were conducted according to protocols approved by the University of the Witwatersrand Animal Research Ethics Committee (AREC, AESC2021/08/03/C). NMRI mice (3-5 weeks old, approximately 20 g) were injected intramuscularly (IM) in the hindlimb with 5 µg saRNA-cLNPs or empty LNPs. HBS injections were used a negative control. Two RNA-Ext-cLNP candidates were assessed. Three mice were included per group, and an empty LNP per LNP candidate and saline control group were included.

For bioluminescence imaging, mice were injected intraperitoneally with 150 mg/kg of D-luciferin (GoldBio, MO, USA), anaesthetised with 1% isoflurane, and imaged using the CaliperLS IVIS bioluminescence system (PerkinElmer, MA, USA). Imaging was undertaken using bioluminescence exposure times of 1-30 seconds. Mice were imaged at 6- and 24-hours post injection, followed by imaging every other day (days 3, 5 and 7). Retro-orbital bleeding was performed after exposure to isoflurane at 6 hours for assessment of innate cytokine production and day 7 for toxicity assessment if expression was observed.

2.7. Figures and Statistical Analysis

Figures were created using Biorender.com and GraphPad Prism 5. Statistical analysis was performed using GraphPad Prism 5 using either a two-tailed unpaired student t-test, or a one-way ANOVA followed by a Tukey post-hoc test. Experiments were performed with a minimum of 3 biological replicates.

Chapter 3

Results

3.1. Optimisation of *in vitro* transcription using bi-cistronic saRNA constructs

The original saRNA production plasmids contained nsP1-4 from the Venezuelan equine encephalitis (VEE) Alphavirus, with a poly A sequence of 25 bp (Supplementary Figure 7). Two constructs were used: one encoding eGFP and a puromycin resistance gene, linked by an internal ribosomal entry site (IRES, Supplementary Figure 7A); the other contained Fluc (Firefly luciferase) and mCherry (a red fluorescent protein), also linked by an IRES (Supplementary Figure 7B). Restriction analysis of T7-VEE-eGFP-Puro yielded the expected band sizes of 11 521 bp from *Eco*R I digestion and 5948, 3651, 1093, and 829 bp from *Pst* I and *Sac* I digestion (Figure 3.1.1). Similarly, for VEE-Fluc-mCherry expected bands of 12 523 bp from *Eco*R I digestion and 6950, 3651, 1093 and 829 bp from *Pst* I and *Sac* I digestion (Figure 3.1.1).

Linearisation of pDNA was performed using *Mlu* I for 2 hours, purified by sodium acetate-ethanol precipitation, and complete linearisation was confirmed using agarose gel electrophoresis (Figure 3.1.2A). Initially, *in vitro* transcription was performed using the AmpliScribe T7-Flash Transcription Kit (Epicentre Biotechnologies, WI, USA) according to the kit instructions with a 30-minute incubation at 37°C. While the control IVT yielded a single, distinct band when electrophoresed on a denaturing formaldehyde agarose gel, the saRNA-eGFP and -Fluc IVTs showed degradation or incompletely transcribed RNA as seen by the light bands at the estimated sizes (9699 and 10 701 nt for saRNA-eGFP-Puro and saRNA-Fluc-mCherry respectively) followed by a smear under the band (Figure 3.1.2B). When the incubation time was increased to 2 hours, there was an improvement, however a significant smear was still visible (Figure 3.1.2C). Temperature optimisation was attempted using the Ampliscribe IVT kit, however no improvement was observed (Supplementary Figure 12A). IVT was also performed using the TranscriptAid T7 High Yield Transcription Kit (ThermoFisher Scientific, MA, USA) and the T7 RiboMAX™ Express Large Scale RNA Production System (Promega, WI, USA) at a 20 µl scale, however no improvement in saRNA quality was observed (Figure 3.1.2D).

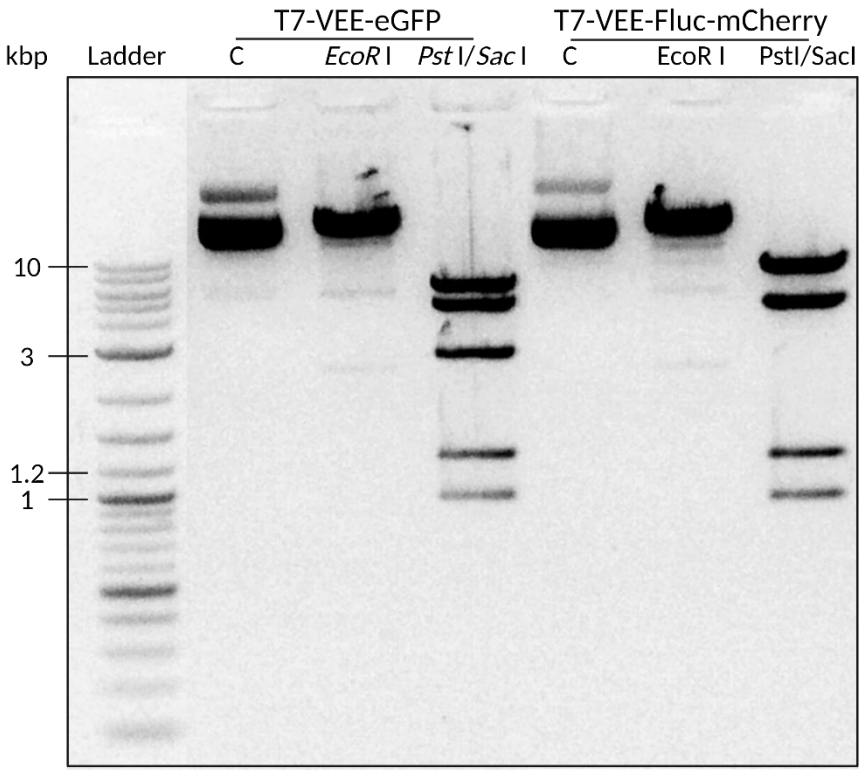

Figure 3.1.1. Screening of original template pDNA for saRNA *in vitro* transcription. saRNA template pDNA containing the VEE non-structural replication genes and either eGFP-IRES-Puro or Fluc-IRES-mCherry were used as templates for IVTs. The identity of these plasmids was confirmed using restriction digest analysis. pDNA was restricted with *Eco*R I and *Pst* I/*Sac* I. The expected bands were observed for VEE-eGFP-Puro and VEE-Fluc-mCherry. Wells labelled "C" indicate undigested pDNA controls. A forward slash indicates a double digest. NEB 1 kb Plus Ladder shown in Supplementary Figure 11A.

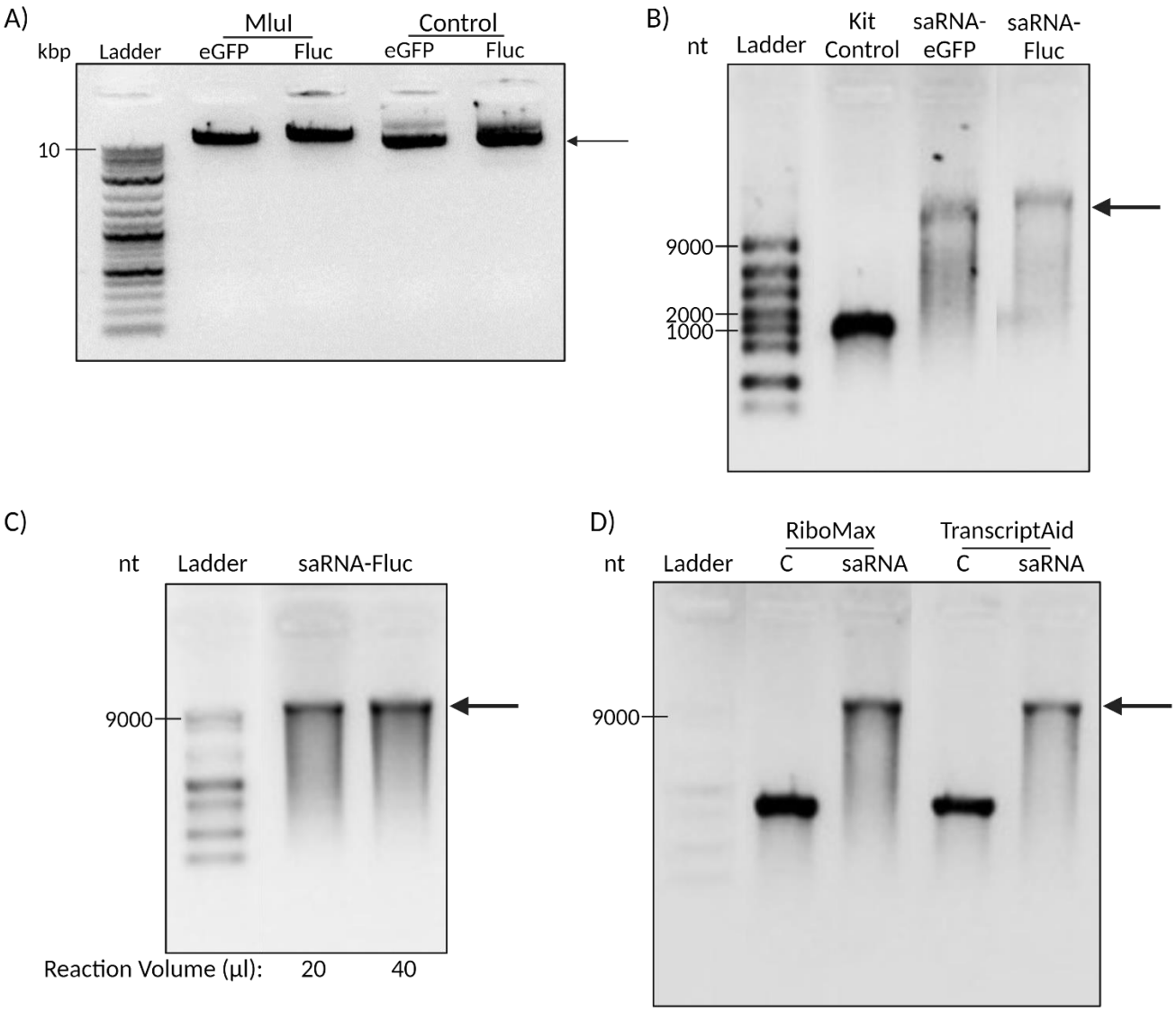

Figure 3.1.2. Optimisation of IVT for production of saRNAs. A) Complete linearisation of pDNA using *Mlu* I was confirmed. (B-D) IVT of saRNA was optimised. Initially, the AmpliScribe kit was used, with incubation times of 0.5 hours (B) and 2 hours (C). A slight band is present at the expected sizes; however, smears can be observed for both incubation times. D) The RiboMax and TranscriptAid IVT kits were also examined (20 µl reactions). A shows a Tris-EDTA agarose gel. B, C and D show formaldehyde agarose gels. Wells labelled "C" indicate kit IVT controls. Arrows indicate linearised product (A) and expected size of saRNA band (B-D). NEB ssRNA Ladder shown in Supplementary Figure 11B.

Eventually, only a 100 µl reaction using the RiboMAX kit was successful, with the majority of the saRNA visibly intact on the gel (Figure 3.1.3A). However, enzymatic capping of this saRNA using the Vaccinia Capping System (Promega, WI, USA) resulted in further degradation (Figure 3.1.3B).

Using the rationale that since saRNA is significantly longer than mRNA and hence requires a specific buffer and IVT composition, two in-house buffers and IVT reactions were set-up (Appendix Tables 2-4). These were based on the TriLink CleanCap AU protocol (107) and a preprint design of experiments (DOE) journal article (106), which are specific to saRNA. Although the TriLink-based IVT did not yield intact or complete saRNA transcripts (Figure 3.1.4A), the DOE-based IVT yielded a single, strong saRNA band (Figure 3.1.4B) prompting the use of this methodology going further. The DOE method was specifically designed for saRNA and included increased rNTP concentrations, the use of Magnesium Acetate ($MgOAc_2$) in place of $MgCl_2$ as a source of Mg^{2+} ions and an increased amount of linear pDNA at 0.1 µg/µl instead of 0.05 µg/µl. As enzymatic capping resulted in saRNA degradation, co-transcriptional capping using the anti-reverse cap analogue (ARCA, Figure 3.1.4C) and TriLink's CleanCap AU cap analogue (CCAU, Figure 3.1.4D) was performed using the DOE IVT method. These reactions yielded intact saRNA similar to that of the uncapped saRNA control. While ARCA is a dimer, cap 0 structure, CCAU is a trimer cap 1 analogue, making it more specific, with a higher capping efficiency and improved translation of protein from RNA.

Functionality of saRNAs was examined by transfection of HEK293 cells. saRNA-eGFP-Puro expressed eGFP as analysed by fluorescence microscopy (Figure 3.1.5A). As expected, CCAU-saRNA-eGFP showed a clear increase in fluorescence intensity compared to ARCA-saRNA-eGFP. Expression of saRNA-eGFP continued until day 15, after which the study was ended due to poor cell health caused by over-confluency (Figure 3.1.5B). However, neither mCherry, nor Fluc expression was detected after transfection using saRNA-Fluc-mCherry. This was attributed to possible interference caused by the IRES, as upstream and downstream genes can have an inhibitory impact on one another (108). As a result of this, new pDNAs were cloned to remove the IRES and downstream gene and lengthen the poly A sequence to improve expression and stability of the saRNA constructs.

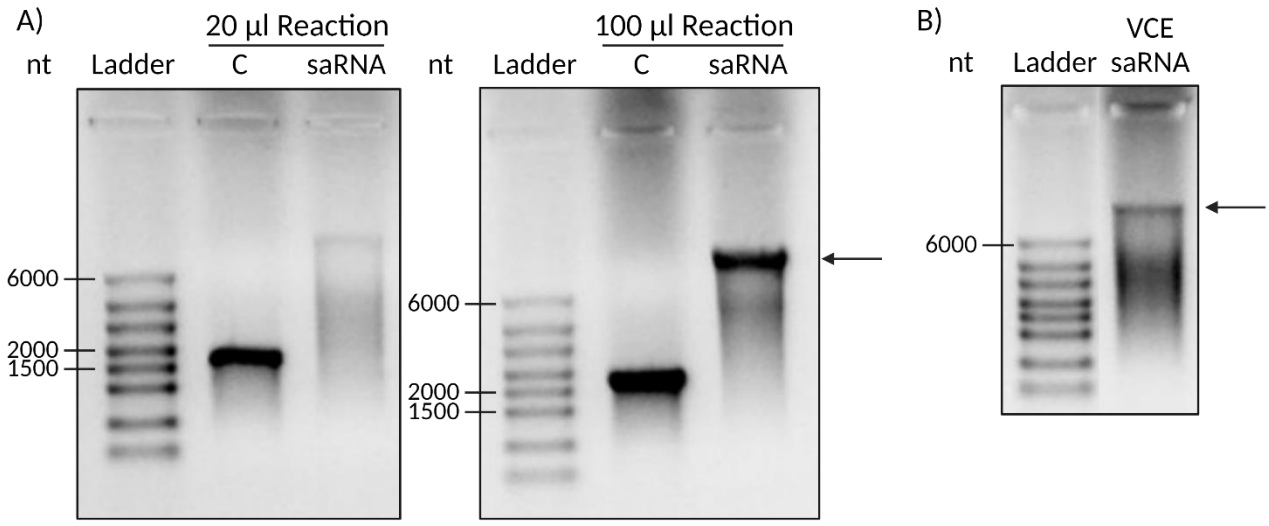

Figure 3.1.3. Successful saRNA IVT through scale-up of RiboMax Kit. A) Scale up of the RiboMax kit from a small-scale (20 µl, left) to a large-scale (100 µl, right) IVT reaction yielded a strong band above 6000 nt on the formaldehyde agarose gel. (B) Upon enzymatic capping of this saRNA using the vaccinia enzymatic capping (VCE) system, saRNA degradation was observed. All gels shown are formaldehyde agarose gels. Wells labelled "C" indicate kit IVT controls. Arrows indicate expected size of saRNA band. RiboRuler HR RNA Ladder is shown in Supplementary Figure 11C.

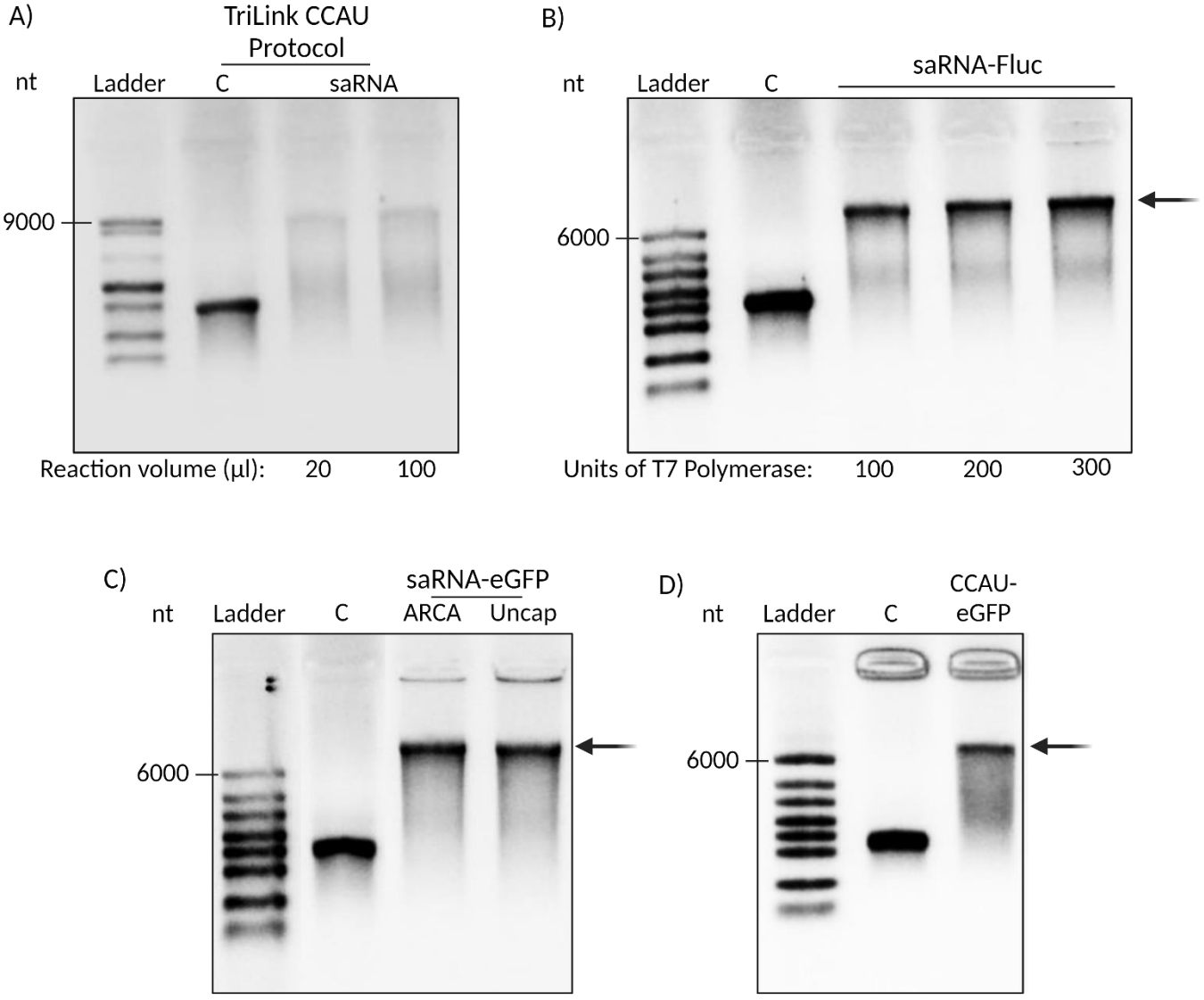

Figure 3.1.4. Development of a saRNA-specific in-house IVT reaction. In-house IVT reactions were set-up according to the TriLink CCAU, and a DOE pre-print journal article. While the TriLink-based IVT did not produce intact saRNA (A), a design of experiments (DOE)-based approach based on a pre-print journal article showed strong bands at three different T7 polymerase concentrations (B). This IVT was successful when ARCA (C) or CleanCap AU (CCAU, D) co-transcriptional capping reagents were used, when compared to an uncapped control. All gels shown are formaldehyde agarose gels. Wells labelled "C" indicate kit IVT controls. Arrows indicate expected size of saRNA band (B-D). NEB ssRNA and ThermoFisher RiboRuler HR RNA Ladders shown in Supplementary Figures 11B and C, respectively.

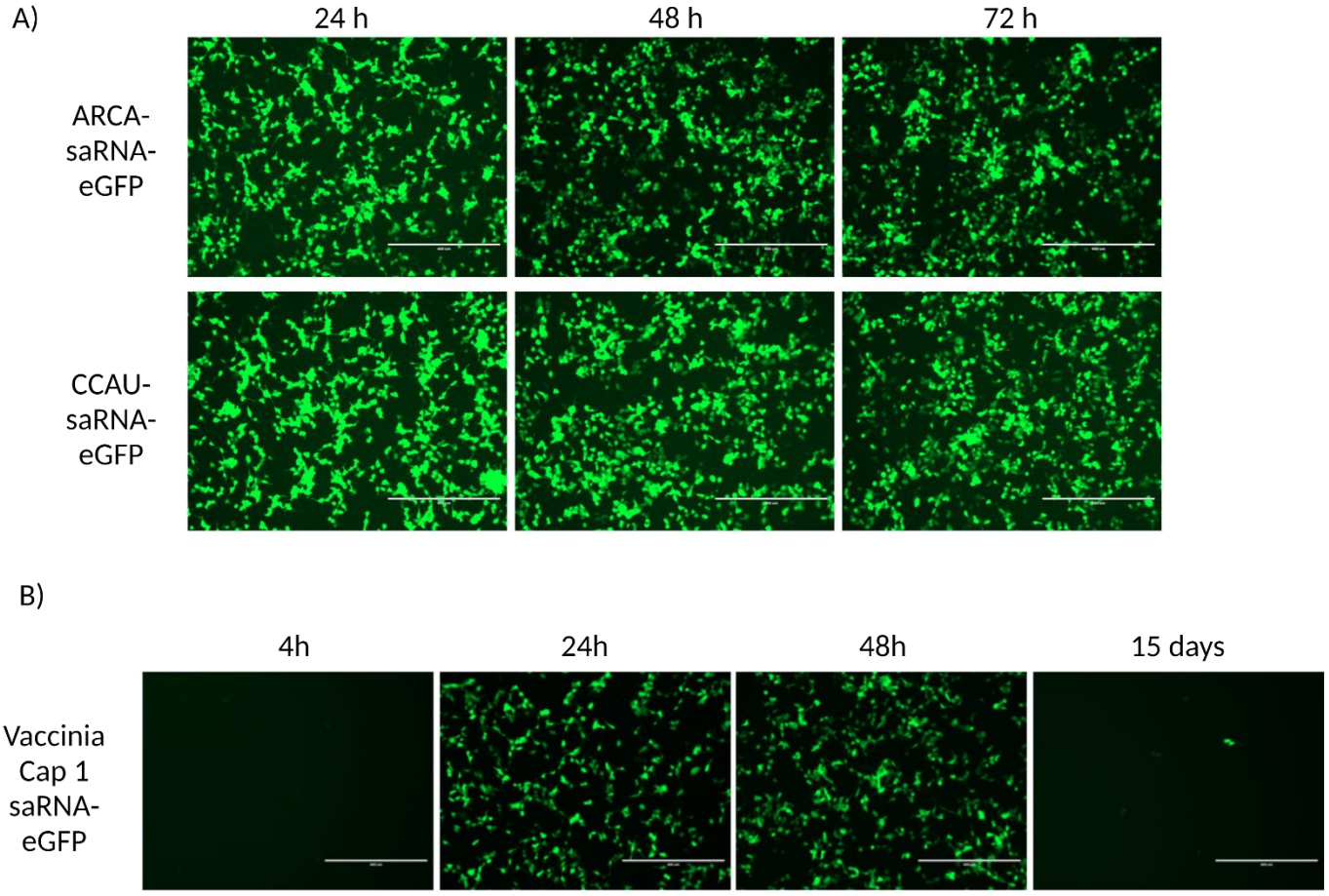

Figure 3.1.5. Comparison of different capping techniques for saRNA in cell culture. HEK293 cells were transfected with saRNA and visualised using a fluorescence microscope. A) Strong expression of saRNA-eGFP was visualised using ARCA (Cap 0) and CCAU (Cap 1), at 24, 48 and 72 hours. B) Despite degradation, enzymatically (Vaccinia) capped saRNA-eGFP showed good expression of eGFP at 24 hours. Expression could be visualised up to day 15 in cell culture. Scale bar = 400 µm.

3.2. Cloning of saRNA vectors and *In Vitro* Transcription of RNA

To solve lack of Fluc expression from saRNA-Fluc-IRES-mCherry, basic cloning was used to generate two saRNA production plasmids expressing reporter sequences: T7-saRNA-VEE-Luc2-pA(60) and T7-saRNA-VEE-eGFP-pA(60) (Figure 3.2.1; Supplementary Figures 10 and 11). These plasmids were generated using T7-VEE-eGFP (Supplementary Figure 7A) as the backbone.

The IRES, puromycin resistance selection gene, VEE 3' UTR and poly A sequence were removed from the original T7-VEE-eGFP plasmid (Figure 2.1.1). These were then replaced with the VEE 3' UTR and 60 bp poly A sequence of the subcloning vector to generate T7- saRNA-VEE-eGFP-pA(60) (Figure 3.2.1A; Supplementary Figure 8B). The eGFP gene was also replaced with Luc2, a codon optimised Fluc gene to generate T7-saRNA-VEE-Luc2-pA(60) to produce a reporter RNA for *in vivo* experiments (Figure 3.2.1A; Supplementary Figure 8A).

These plasmids were confirmed by restriction digestion (Figure 3.2.2). T7-saRNA-VEE-eGFP-pA(60) was screened, with expected bands of 10 343 bp from *Bgl* II digestion, and 4967, 3972 and 1404 bp from *Kpn* I and *Xba* I digestion observed. T7-saRNA-VEE-Luc2-pA(60) screening yielded expected bands of 11 296 bp for *Bgl* II digestion and 4967, 3972 and 1404 bp for *Lgu* I and *Bsp*1407 I digestion, confirming pDNA identity. eGFP and Luc2 saRNA plasmid sequences were further confirmed by sanger sequencing (Supplementary Figures 9 and 10).

To prepare pDNA for IVT, linearisation was performed with *Mlu* I for saRNA. Complete linearisation was confirmed by agarose gel electrophoresis (Figure 3.2.3A). IVT using the modified DOE protocol was performed and intact saRNA was confirmed by denaturing agarose gel electrophoresis (Figure 3.2.3B). saRNA was intact regardless of cap analogue, as ARCA and CCAU were successfully incorporated without degradation (Figure 3.2.3C).

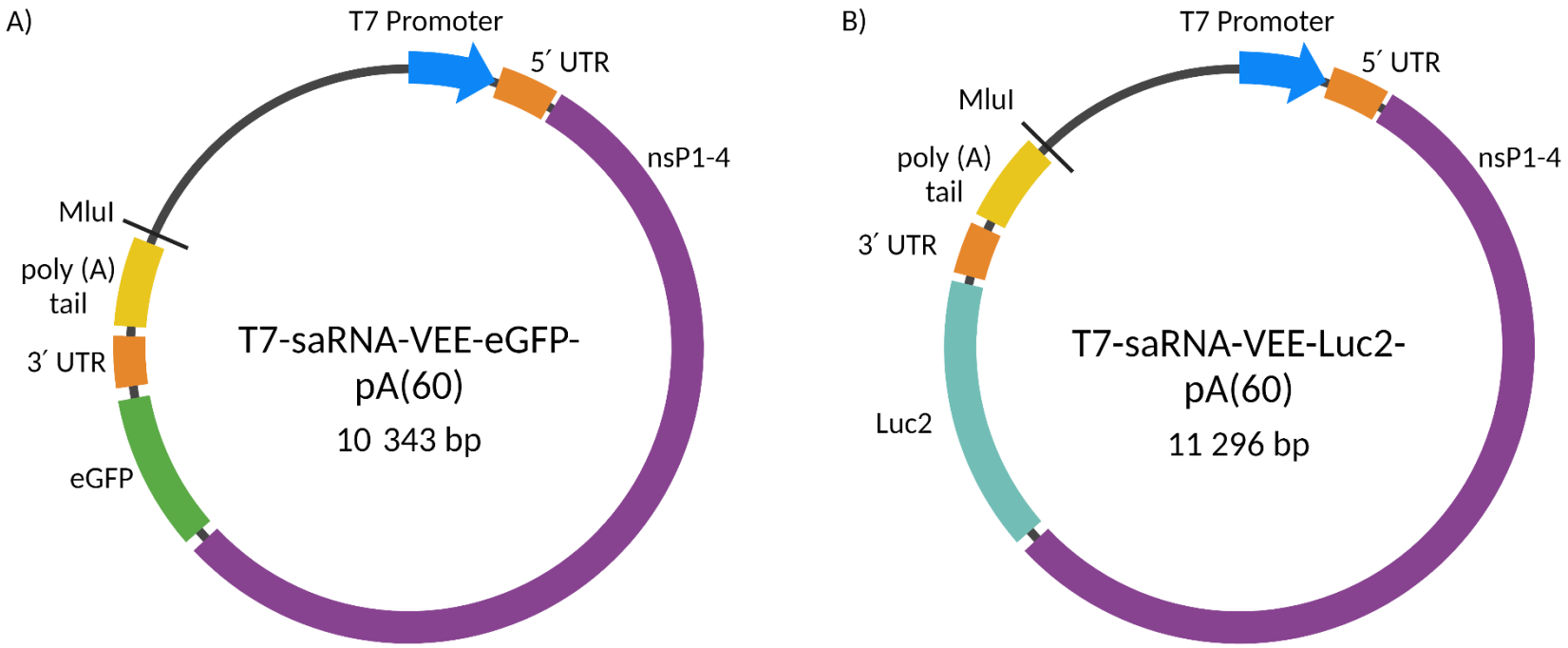

Figure 3.2.1. Schematic diagrams of cloned saRNA constructs. As a result of failure of the Fluc-IRES-mCherry construct to express the desired transgenes, new constructs were designed and cloned. Cloned saRNA constructs increased the length of the poly A sequence and removed the IRES, keeping the original eGFP gene (A) or replacing it with a codon optimised Fluc gene (Luc2; B). pDNA sizes for eGFP and Luc2 are 10 343 and 11 296 bp, respectively. Full plasmid maps shown in Supplementary Figure 8.

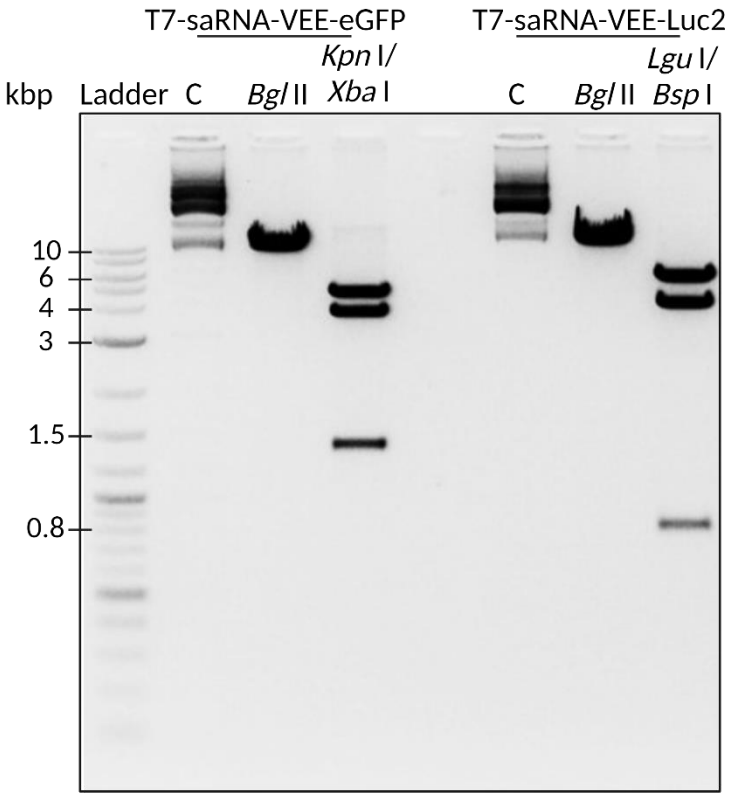

Figure 3.2.2. Screening of propagated saRNA plasmids. Prior to use of pDNA for IVT, saRNA pDNA production vectors were screened using restriction digestion and agarose gel electrophoresis. T7-saRNA-VEE-eGFP-pA(60) and T7-saRNA-VEE-Luc2-pA(60) were screened with *Bgl* II and *Kpn* I/*Xba* I, and *Bgl* II and *Lgu* I/*Bsp*1407 I respectively and yielded the expected bands. Wells labelled "C" indicate undigested pDNA controls. "*Bsp* I" denotes digestion with *Bsp*1407 I. A forward slash indicates a double digest. NEB 1 kb Plus Ladder shown in Supplementary Figure 11A.

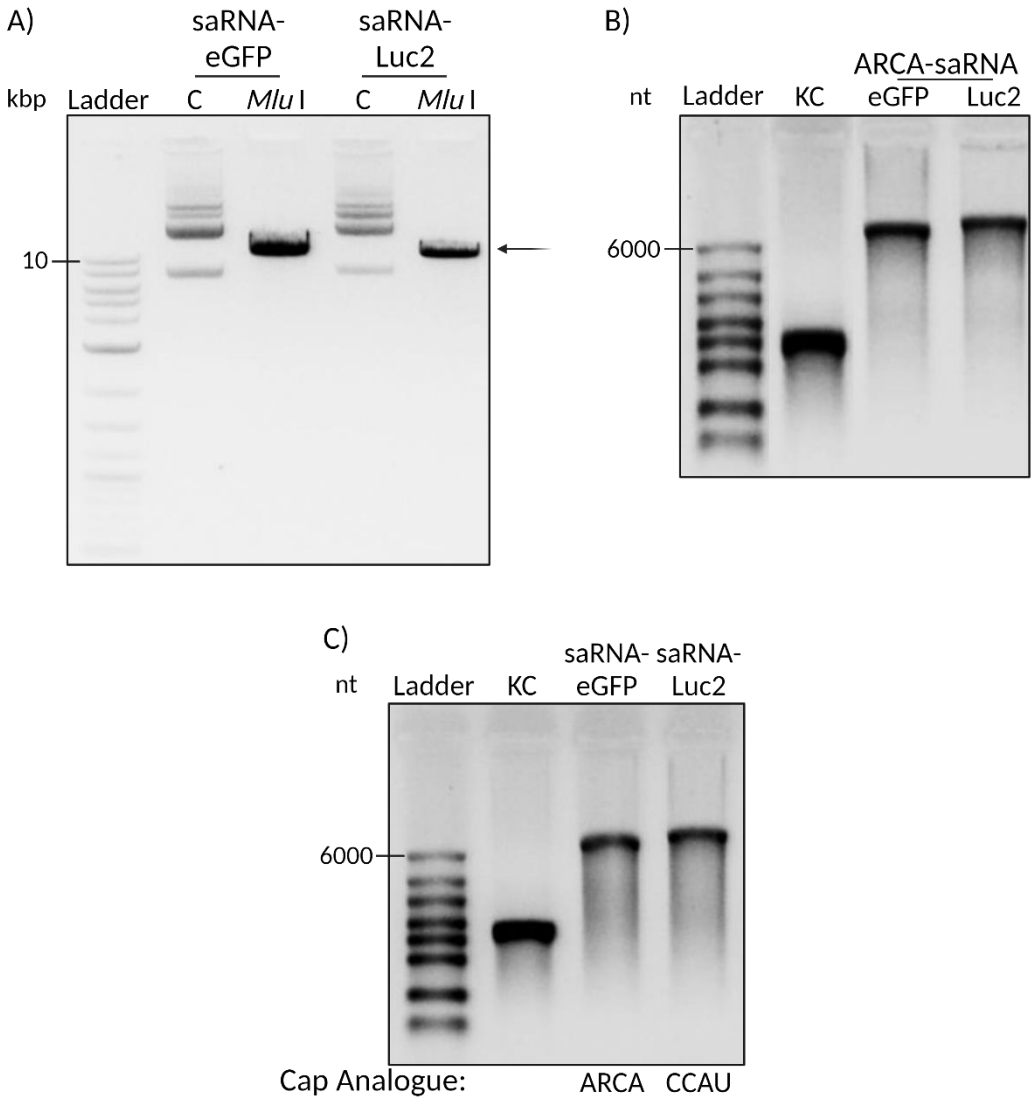

Figure 3.2.3. Preparation of pDNA and *in vitro* transcription of new saRNA constructs. (A) Linearisation of saRNA constructs with *Mlu* I were confirmed using agarose gel electrophoresis. A single band could be visualised on the gel. (B) saRNA-eGFP and saRNA-Luc2 were successfully transcribed using the DOE protocol. Formaldehyde agarose gels show full-length intact band visible above 6000 nt on the ladder. (C) Co-transcriptional capping using ARCA and CCAU was successfully performed with no indication of IVT inhibition, degradation, or incomplete transcription. A) Wells labelled "C" indicate undigested plasmid controls. Arrows indicate linearised pDNA product, NEB 1 kb Plus Ladder shown in Supplementary Figure 11A. B and C) Wells labelled "KC" indicate IVT kit controls. ThermoFisher RiboRuler HR RNA Ladder shown in Supplementary Figure 11C.

RNA function was examined following HEK293T cell transfection, ARCA-capped saRNA expressed eGFP high levels, with the new saRNA construct outperforming the original saRNA-eGFP (Figure 3.2.4A). Unlike saRNA-eGFP-Puro, the saRNA-eGFP transgene expression could already be observed at 6 hours. Amplification of eGFP expression can be clearly seen from 6- to 24-hours and 24- to 48-hours post-transfection, especially for the saRNA-eGFP construct. Hence, ARCA-saRNA-eGFP instead of ARCA-saRNA-eGFP-Puro was used for optimisation of LNPs in cell culture and *in vitro* experiments. It is also important to use a similar saRNA construct for eGFP and Fluc to improve consistency, as both new constructs do not contain an IRES. This improved expression is most likely as a result of removal of the IRES and additional Puromycin gene, which may have been dampening eGFP expression, and lengthening of the poly A sequence, which may improve stability and half-life of the saRNA.

ARCA-saRNA-Luc2 was able to successfully express Fluc (Figure 3.2.4B). As expected, CCAU capped saRNA improved translation significantly, with CCAU-saRNA-Luc2 expressing similar to that of pDNA at 24 hours post-transfection (Figure 3.2.4B). CCAU-saRNA-Luc2 had a 1.7-fold increase in expression compared to ARCA-saRNA-Luc2.

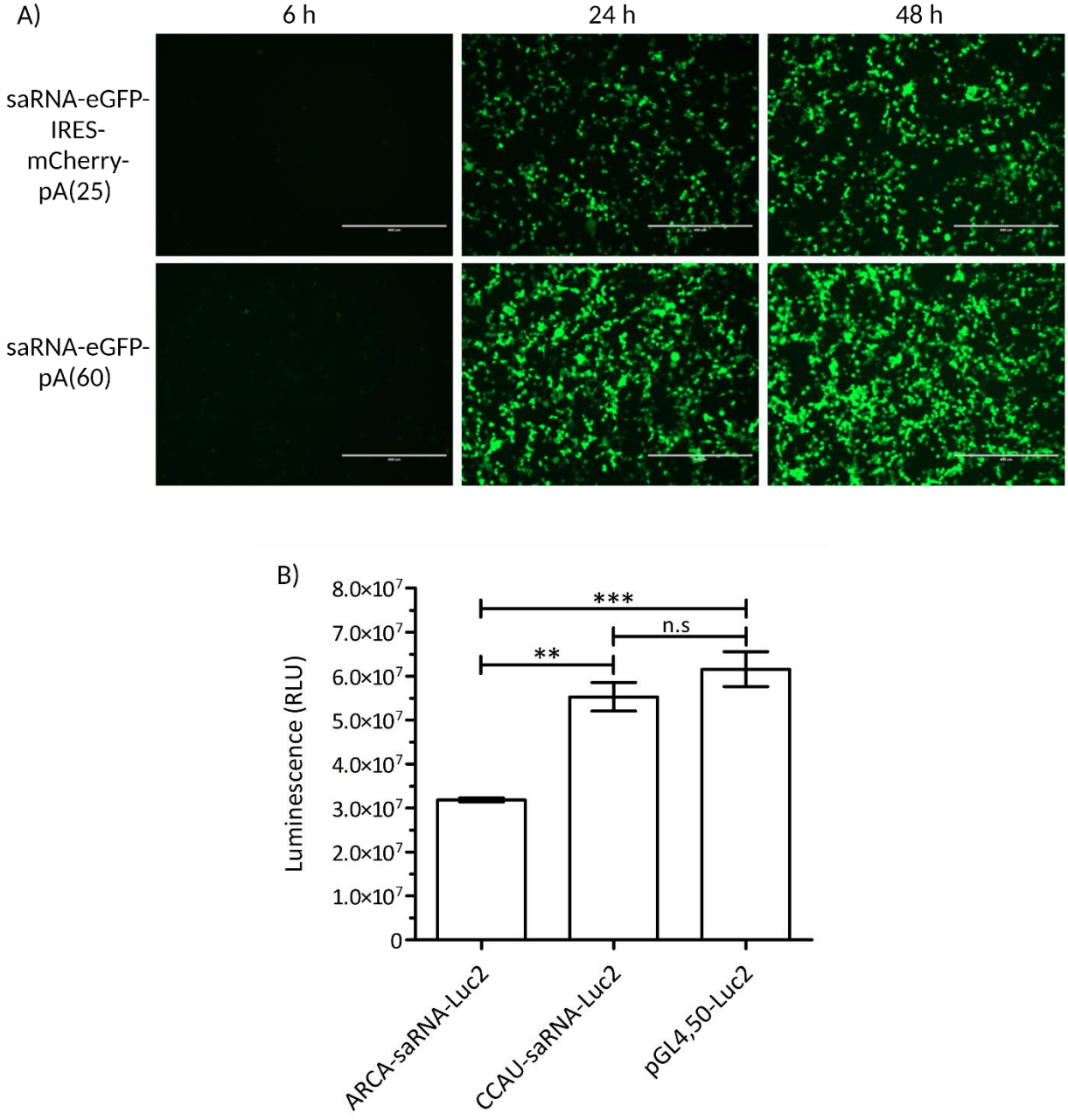

Figure 3.2.4. Successful transgene expression of new RNA transcripts in cell culture. HEK293 cells were seeded in 48-well plates 24 hours prior to transfection with saRNA. Improved expression was observed with new saRNA-eGFP constructs at all timepoints. A) Comparison of old and new saRNA-eGFP transcripts at 6-, 24-, and 48-hours post-transfection (Scale bar = 400 µm). B) Expression of saRNA-Luc2 co-transcriptionally capped with ARCA or CCAU compared to pDNA 24-hours post transfection. Statistical analysis performed using a one-way ANOVA followed by a Tukey post-hoc test (C) or a two-tailed, unpaired T-test (D); $p \leq 0.01$ (**) $p \leq 0.001$ (***), not significant (n.s); n=3.

3.3. Formulation and Optimisation of LNPs By Lipid Film Hydration

Cationic lipids, mainly DOTAP and DDA, have shown great success in formulation and delivery of saRNA vaccines (62,103). With this information, three main permanently cationic lipids: DOTAP and DDA along with DOTMA, were formulated alongside a helper lipid (either DSPC or DOPE), and cholesterol (Chol). A library of lipid combinations was assembled based on previous literature or new lipid molar ratios (see Appendix Table 5). CaliVax, a commercial liposome comprised of DOTAP:Chol in a 1:1 molar ratio, was also investigated. Initial saRNA-LNP formulations were assessed using ARCA-saRNA-eGFP.

3.3.1 Optimisation of LFH and production of empty LNPs for formulation of saRNA-Ext-cLNPs

Initially, DOTAP:Chol cLNPs (50:50 molar ratio) were produced using LFH to optimise the bath sonication step. A bath sonication of 12.5 minutes reduced the size of the LNPs sufficiently for extrusion using membranes with a pore size ≤ 200 nm (Figure 3.3.1A). However, it was later observed that bath sonication produced empty cLNPs of various sizes, and therefore, prior to extrusion, sizing was performed to confirm which filters would be required.

A library of LNPs were produced by LFH using different ratios of cationic lipid, cholesterol, and phospholipid (Appendix Table 5). Empty LNPs were successfully produced by LFH with sizes below 150 nm after extrusion (Figure 3.3.1B, Supplementary Table 1). However, this method was not very consistent, as seen with empty DOTAP and DOTMA B1, where there is a difference in size between two different LNP batches (sets A and B). saRNA-Ext-cLNPs were complexed at different N:P ratios and were used to transfect cells with saRNA-eGFP to optimise the N:P ratio.

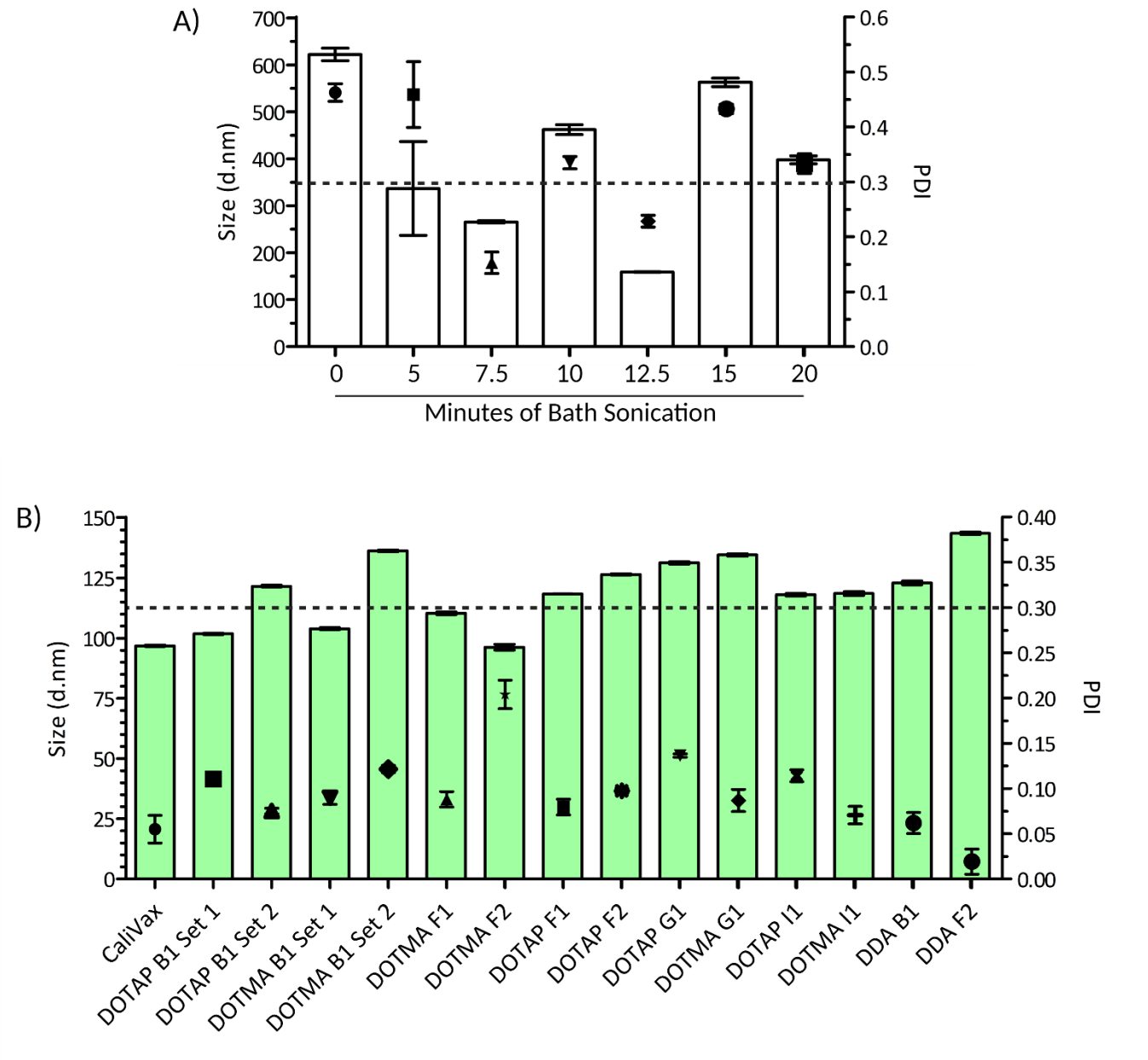

Figure 3.3.1. Optimisation of LFH production of empty cLNPs and formulation of a library of empty cLNPs. A) After overnight hydration of the lipid film bath sonication of DOTAP:Chol (50:50 mol ratio) was optimised to achieve the lowest size before extrusion. The smallest size was achieved with 12.5 minutes of sonication. B) Size and PDI of empty cLNPs formulated by LFH. Lipid compositions can be found in Appendix Table 5. Bars and symbols represent size (left y-axis) and PDI (right y-axis) of cLNPs respectively; dotted line indicates PDI cut-off of 0.3. n=3 for A) and B). Size (d.nm) is a measure of the particle diameter in nm.

3.3.2. Transfection Efficiency of saRNA-Ext-cLNPs is More Dependent on N:P Ratio and Less on Particle Size

Adsorption of saRNA on the surface of cLNPs was initially assessed (saRNA-Ext-cLNPs). CaliVax, a commercially available empty cLNP consisting of DOTAP:Cholesterol at a 1:1 weight:weight (w:w) ratio initially performed best at a N:P ratio of 3:1. However, after fine optimisation, a 2.5:1 ratio was found to improve expression (Figure 3.3.2A). Transfection efficiency and saRNA expression was amplified after 48- and 72-hours. At day 5, expression persisted, with CaliVax 2.5:1 N:P outperforming the 3:1 ratio (Figure 3.3.2B).

Based on this, in-house cLNPs produced using LFH were assessed. Initially DOTAP and DOTMA B1 saRNA-Ext-cLNPs based on previous literature were optimised (Figure 3.3.3A). After 24 hours, all N:P ratios appeared to have similar efficacy, and hence 12:1 and 8:1 N:P were further analysed as these are common ratios in the literature for saRNA. When these were analysed at both 24 and 48 hours, important information on the effect of the LNPs on saRNA replication was obtained (Figure 3.3.3B and C). DOTAP B1 12:1 showed minimal amplification of expression, while an 8:1 N:P displayed improved expression at 48 hours. Hence, examining transfection efficiency past 24 hours is crucial to optimise N:P ratio and lipid composition of the cLNPs. DOTMA B1 12:1 and 8:1 however appeared relatively similar at both 24 and 48 hours. As expected, transfection of cells grown in serum-free media showed improved transfection efficacy, as it is known that FBS has an inhibitory effect on cLNPs (109,110).

Based on these results, other saRNA-Ext-cLNPs were optimised. Some saRNA-Ext-cLNPs such as DOTMA F1 and F2 performed optimally at higher ratios (Figure 3.3.4A and B), while others such as DOTAP F2 and F1, performed better at a lower N:P (4:1, Figure 3.3.5A and B). Although DOTAP F1 4:1 showed a clear improvement in performance at 48 hours, F1 LNPs all generally performed well. DOTMA saRNA-Ext-cLNPs appear to be the most efficient at RNA delivery, followed by DOTAP, especially the “F1” and “F2” formulations. The “G1” and “I1” formulations appeared to perform secondary to these (Figure 3.3.6 and 3.3.7). Although G1 8:1 N:P cLNPs performed optimally at 24 hours, expression at 48 hours was either barely maintained or reduced for DOTAP and DOTMA (Figure 3.3.6A and B). This is in contrast to the lower ratios, as DOTAP G1 6:1, 4:1, and 3:1 N:P ratios resulted in a dramatic increase in saRNA expression (Figure 3.3.6A and B).

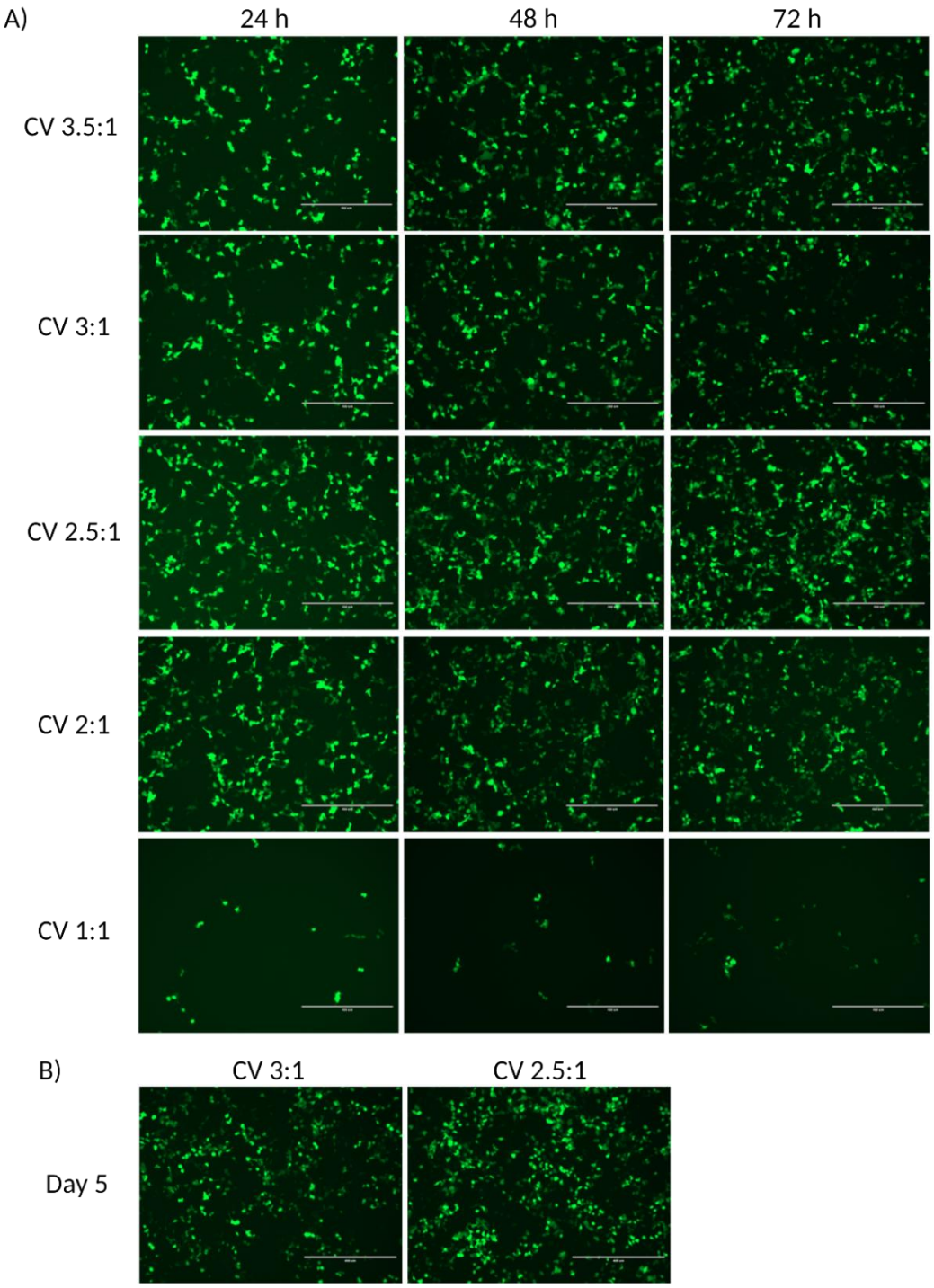

Figure 3.3.2. Formulation optimisation of saRNA-Ext-cLNPs with CaliVax in HEK293 cells. A) Fine-tuned optimisation of CaliVax saRNA-cLNPs. CaliVax was formulated with saRNA-eGFP at different N:P ratios and used to transfect cells. Delivery efficacy indicated by eGFP expression was examined and compared at 24-, 48-, and 72-hours post-transfection by fluorescence microscopy. B) Expression of saRNA for the 3:1 and 2.5:1 N:P ratio CaliVax RNA-cLNPs can still be observed at day 5 post-transfection. CaliVax is abbreviated to "CV." N:P ratios are labelled adjacent to the relevant fluorescence microscopy image. Scale bar = 400 µm.

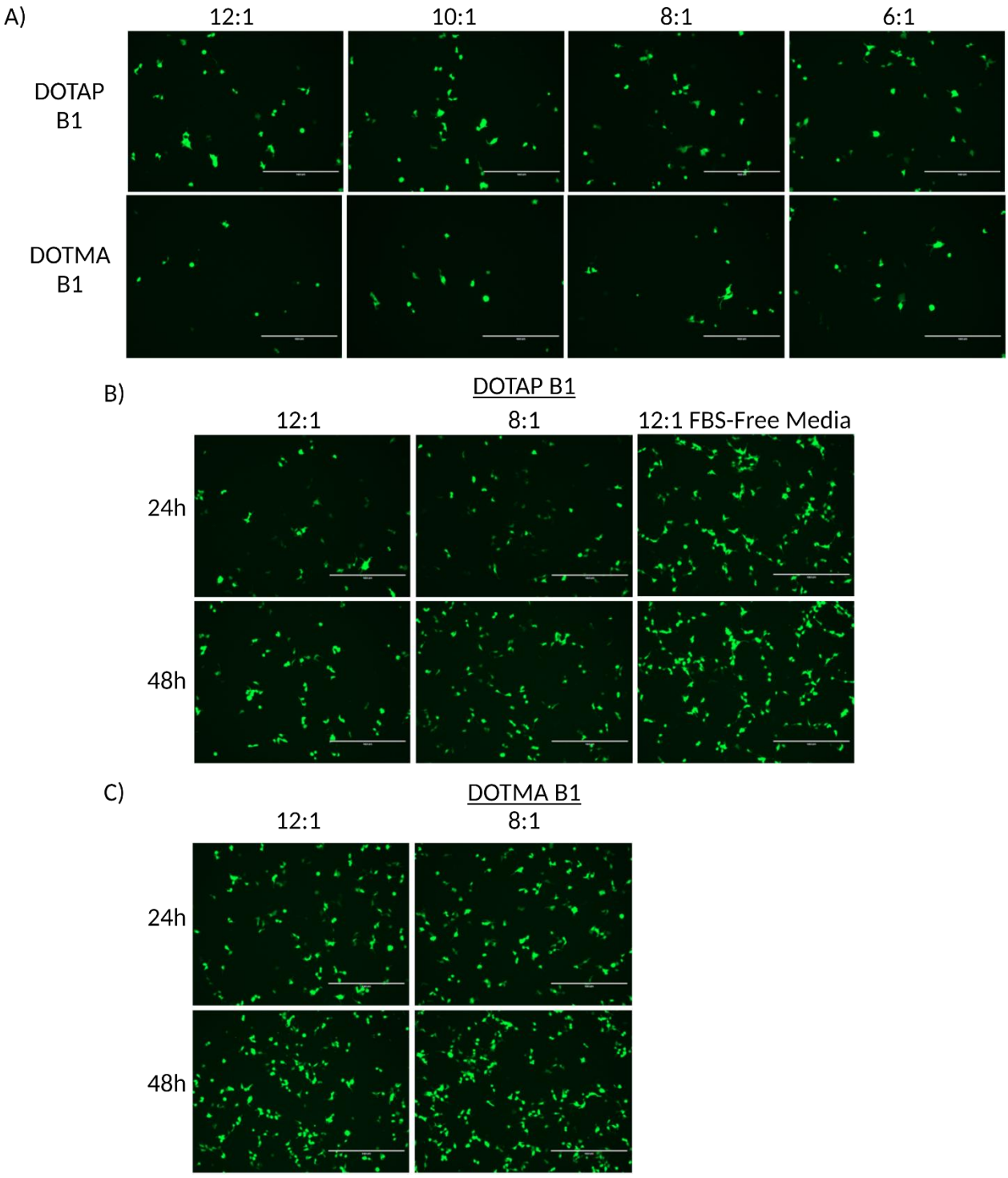

Figure 3.3.3. B1 saRNA-Ext-cLNPs and the effect of serum on transfection efficacy. A) DOTAP and DOTMA B1 LNPs formulated at different N:P ratios were used to transfect HEK293 cells. Fluorescence microscopy was used to examine transfection efficacy only at 24 hours initially. B and C) N:P ratios of 12:1 and 8:1 were further examined for DOTAP (B) and DOTMA (C) B1 saRNA-Ext-cLNPs at 24 and 48 hours to allow comparison of saRNA amplification kinetics. Removal of FBS by transfecting HEK293 cells grown in serum-free media was also examined for DOTAP B1 (B). N:P ratios are labelled above the relevant fluorescence microscopy image. Scale bar = 400 µm.

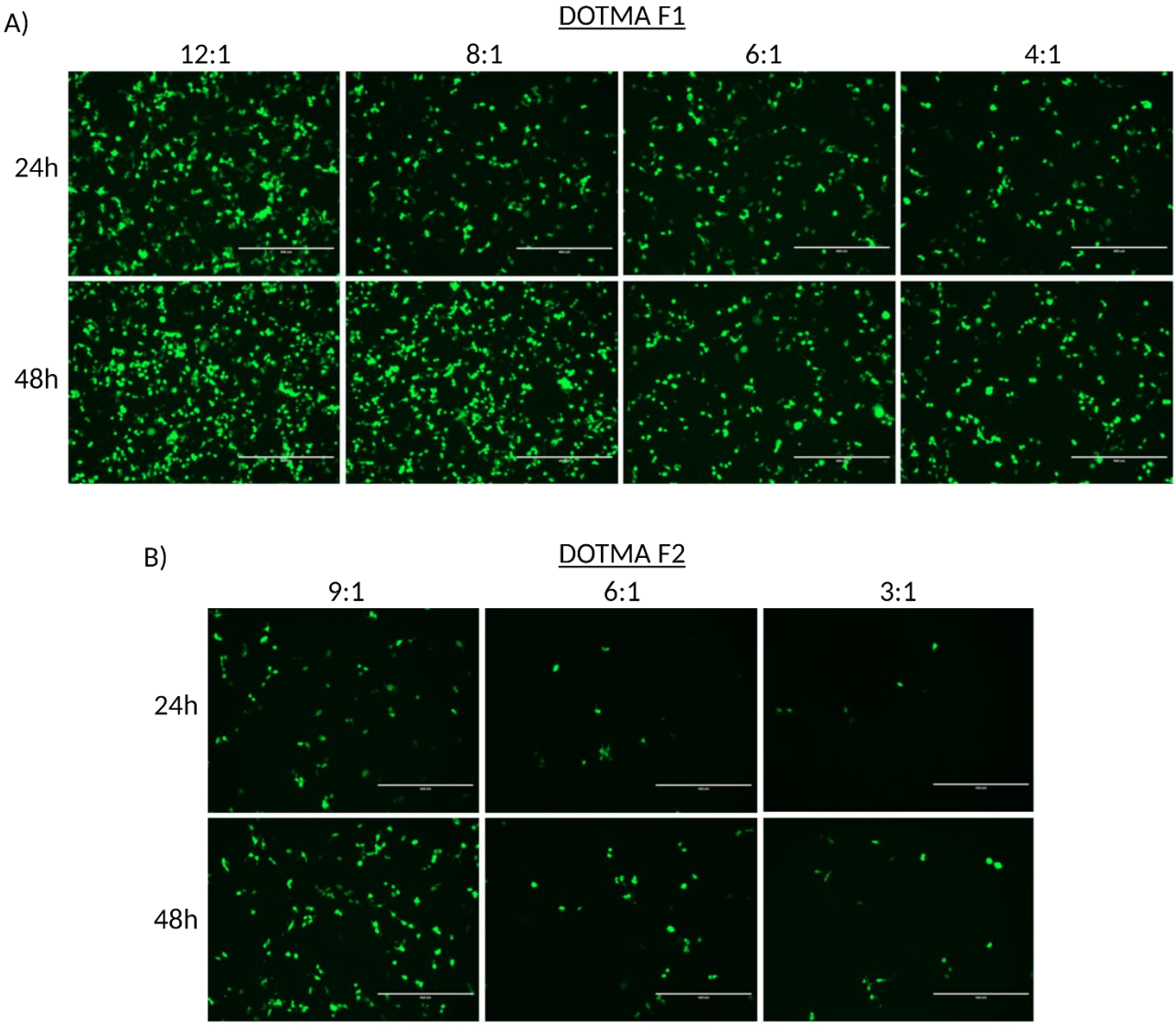

Figure 3.3.4. DOTMA F1 and F2 cLNPs show improved efficiency at higher N:P ratios. DOTMA F1 and F2 LNPs were complexed at different N:P ratios and used to transfect HEK293 cells. Transfection efficacy was examined by fluorescence microscopy after 24 and 48 hours. A) DOTMA F1 saRNA-Ext-cLNPs performed the best at a 12:1 N:P ratio, however at 48 hours the 8:1 ratio performed similarly to the 12:1 ratio. B) At higher (9:1) ratios, similar cLNPs exchanging the phospholipid DOPE with DSPC, also showed improved efficacy compared to the lower (6:1 and 3:1) N:P ratios. N:P ratios are labelled above the relevant fluorescence microscopy image. Scale bar = 400 µm.

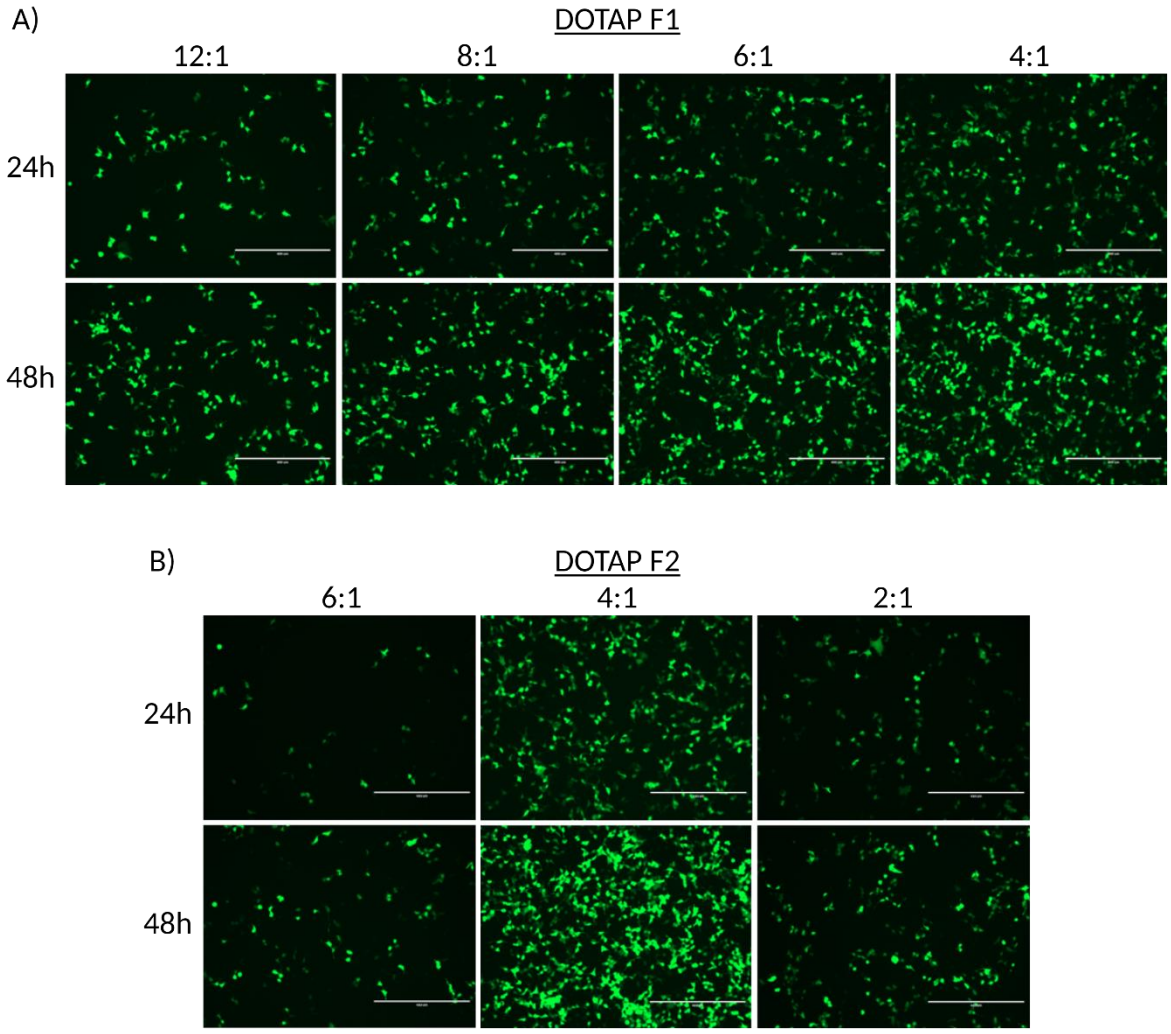

Figure 3.3.5. Larger DOTAP saRNA-Ext-cLNP sizes do not affect transfection efficacy in HEK293 cells. DOTAP F1 (A) and F2 (B) LNPs displayed improved delivery efficacy when complexed with saRNA at lower N:P ratios. Although both LNPs have the same DOTAP:Cholesterol:Phospholipid mol percentage composition, the phospholipid used in F1 LNPs is DOPE, while F2 LNPs exchange this for DSPC. For DOTAP F1 (A), although lower N:P ratio worked optimally, there was no N:P that worked distinctively poorly. This was much more distinct for F2 LNPs (B), where 4:1 clearly performed optimally. N:P ratios are labelled above the relevant fluorescence microscopy image. Scale bar = 400 µm.

G1 formulations contain reduced cationic lipid, and increased phospholipid percentage compared to the F1 formulations, indicating that an increased molar percentage of the main cationic (complexing) lipid appears to be a significant factor in improved saRNA delivery. I1 saRNA-Ext-cLNPs were able to maintain their expression from 24 to 48 hours. Although all DOTAP I1 cLNP N:P ratios appeared to have a similar transfection efficacy, only the 8:1 N:P ratio performed well for DOTMA I1 LNPs (Figure 3.3.7A and B). I1 LNPs consisted of a 50:50 mol% ratio (~1:1 w:w ratio) of cationic lipid:DOPE, as opposed to CaliVax's 1:1 w:w ratio of DOTAP:cholesterol, which shows that although DOPE assists with endosomal escape, replacing it with Cholesterol may not necessarily reduce transfection efficacy by limiting RNA release. Since LNPs with 3 components including both Cholesterol and a phospholipid show better delivery efficacy, this implies a synergistic effect of the two in cLNPs. Overall, it also changes the characteristics of the LNPs as the optimal N:P is also altered.

DDA saRNA-Ext-cLNPs consistently showed lower expression at 24 hours compared to DOTAP and DOTMA, as seen by the F2 and B1 formulations (Figure 3.3.8A and B). While DDA F2 cLNPs expressed poorly at 24 hours, a marked amplification of saRNA expression was observed at 48 hours, with a 12:1 N:P ratio outperforming the other ratios. B1 DDA LNPs showed improved expression at 24 hours, however this was not amplified as drastically, and more so maintained at 48 hours. Although DDA saRNA-Ext-cLNPs did not perform as well as DOTAP and DOTMA at 24 hours, previous studies have shown they are efficient vaccine delivery vehicles and may still be good candidates to explore further *in vivo* (62), especially the F2 cLNPs, where expression is significantly amplified at 48 hours.

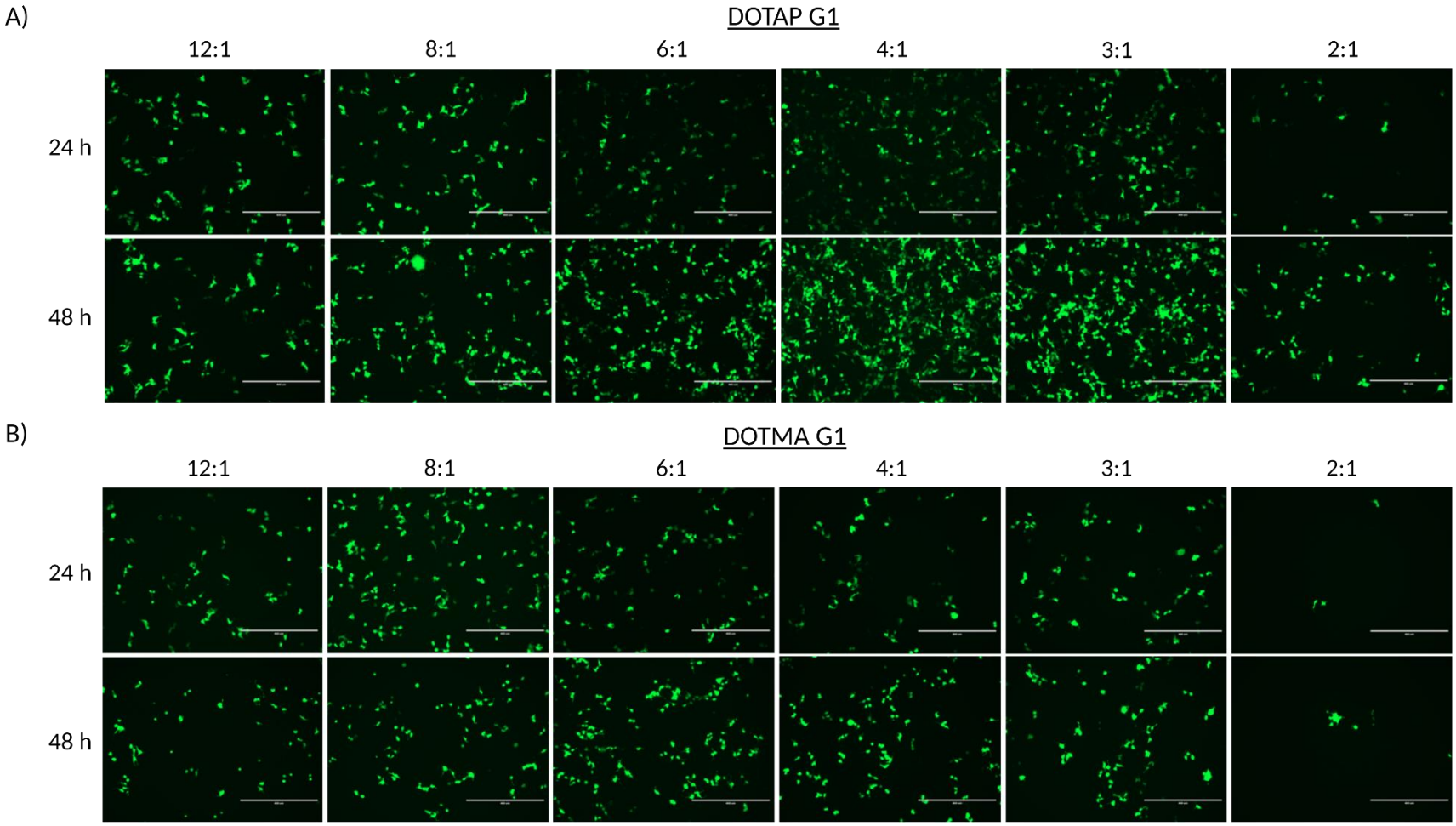

Figure 3.3.6. G1 formulations follow the trends of DOTAP and DOTMA B1 saRNA-Ext-cLNPs. DOTAP and DOTMA G1 cLNPs were complexed with saRNA-eGFP at a range of N:P ratios and examined for transfection efficacy of HEK293 cells at 24 and 48 hours. A) DOTAP G1 cLNPs performed better at lower ratios, particularly 6:1, 4:1 and 3:1. Although these did not work as well as 8:1 at 24 hours, they outperform the 8:1 ratio at 48 hours post-transfection. B) DOTMA G1 8:1 performed optimally at 24 hours, however this was reduced at 48 hours, where 8:1-3:1 N:P ratios performed similarly. N:P ratios are labelled above the relevant fluorescence microscopy image. Scale bar = 400 µm.

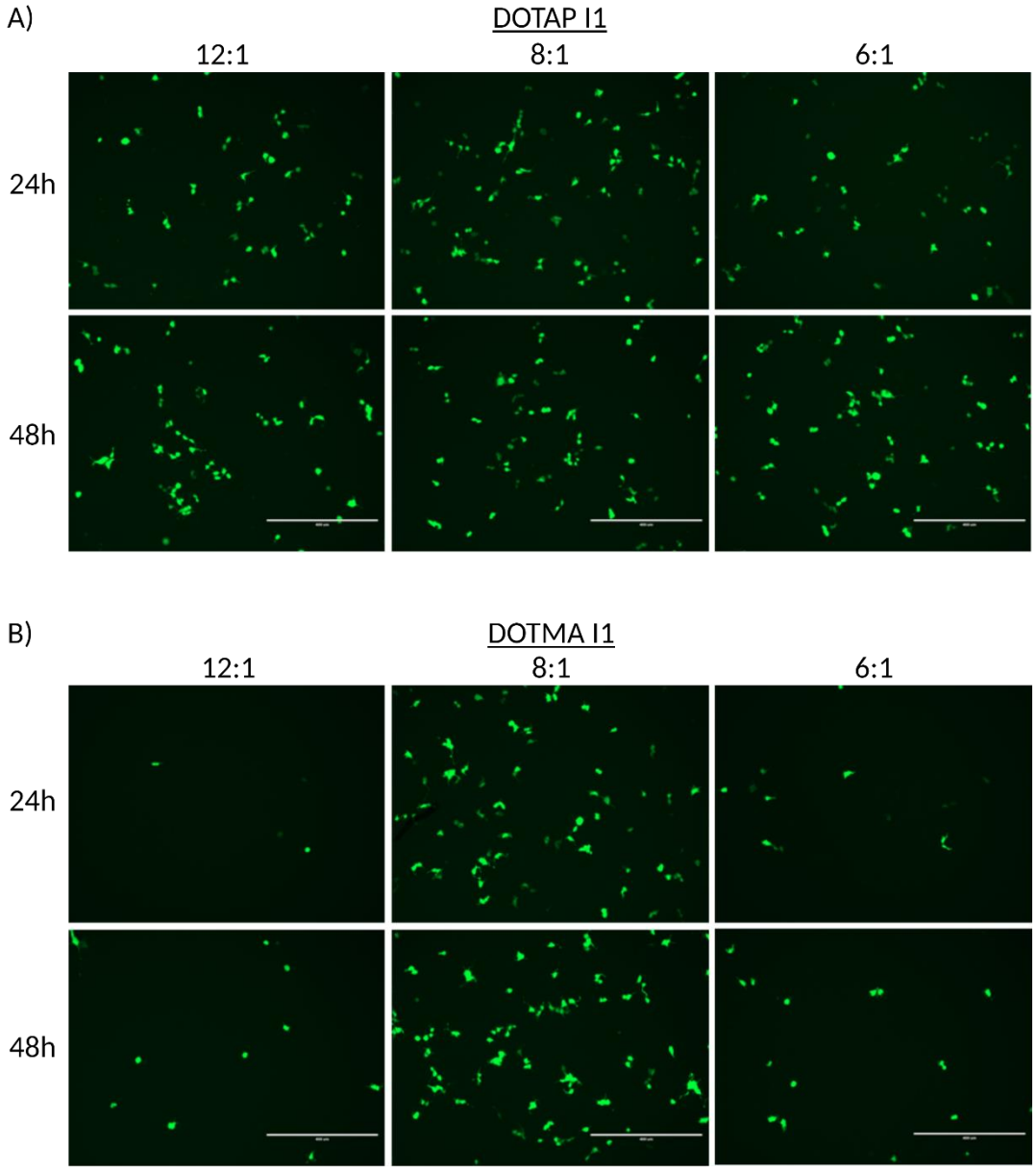

Figure 3.3.7. Optimisation of I1 saRNA-Ext-cLNPs by transfection of HEK293 cells. I1 cLNPs were complexed with saRNA at N:P ratios of 12:1, 8:1 and 6:1. Transfection efficacy was examined by fluorescence microscopy after 24 and 48 hours. A) While DOTAP I1 8:1 LNPs performed the most efficiently at 24 hours, all N:P ratios worked similarly at 48 hours. B) In contrast, only an 8:1 ratio performed well at 24- and 48-hours post-transfection for DOTMA I1 saRNA-Ext-cLNPs. N:P ratios are labelled above the relevant fluorescence microscopy image. Scale bar = 400 µm.

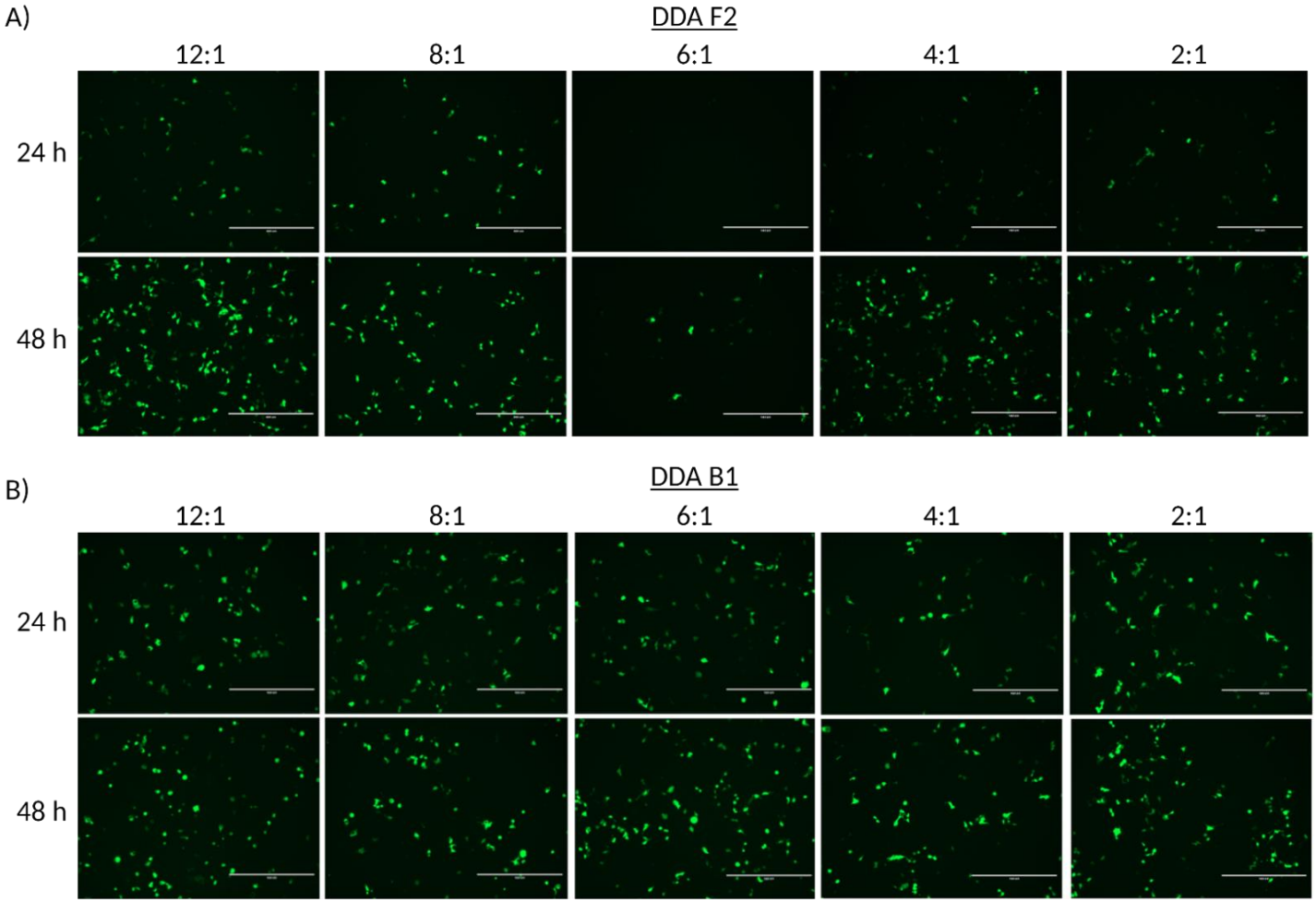

Figure 3.3.8. The important effect of DDA cLNPs on amplification of saRNA expression. DDA F2 and B1 cLNPs were complexed with saRNA at a wide range of N:P ratios and used to transfect HEK293 cells. Transfection efficacy was examined by fluorescence microscopy after 24 and 48 hours. A) F2 DDA saRNA-Ext-cLNPs performed poorly at 24 hours, while at 48 hours post transfection, a marked boost in expression was observed, especially for the 12:1 N:P ratio. B) B1 LNPs expressed better than F2 cLNPs at 24 hours, however there was more of a maintenance than an amplification of RNA expression at 48 hours. N:P ratios are labelled above the relevant fluorescence microscopy image. Scale bar = 400 µm.

Importantly, although particle sizes differed vastly between optimally performing LNP compositions, it was ultimately the N:P ratio that determined cell transfection efficacy. While empty LNP sizes were similar (Figure 3.3.1B), the sizes of optimal saRNA-Ext-LNPs ranged from 162 nm for DOTMA F1 12:1 to 575 nm when DOTAP F2 4:1 was complexed (Figure 3.3.9A, Supplementary Table 1). Similarly, empty CaliVax had an average size of 97 nm, this increased to 348 nm upon addition of saRNA (Figure 3.3.9A). As expected, when saRNA was complexed exteriorly, LNP size increased with decreasing N:P as the number of RNA molecules per LNP increases (Figure 3.3.10). The PDI range was also quite large, with some PDIs above the 0.3 threshold (Figure 3.3.9A). While the size and PDI of some of these LNPs may not be suitable for human injection, this is most likely to be a result of limitations of LFH. Alternatively, empty LNPs could be made smaller using microfluidics while LFH is a cheaper alternative to screen potential saRNA-Ext-LNP candidates. The zeta-potentials of these were very positive, as expected of the permanently cationic nature of the LNPs (Figure 3.3.9B). While adding saRNA did decrease the zeta potential, it was still very positive even at lower N:P ratios (Figure 3.3.9B).

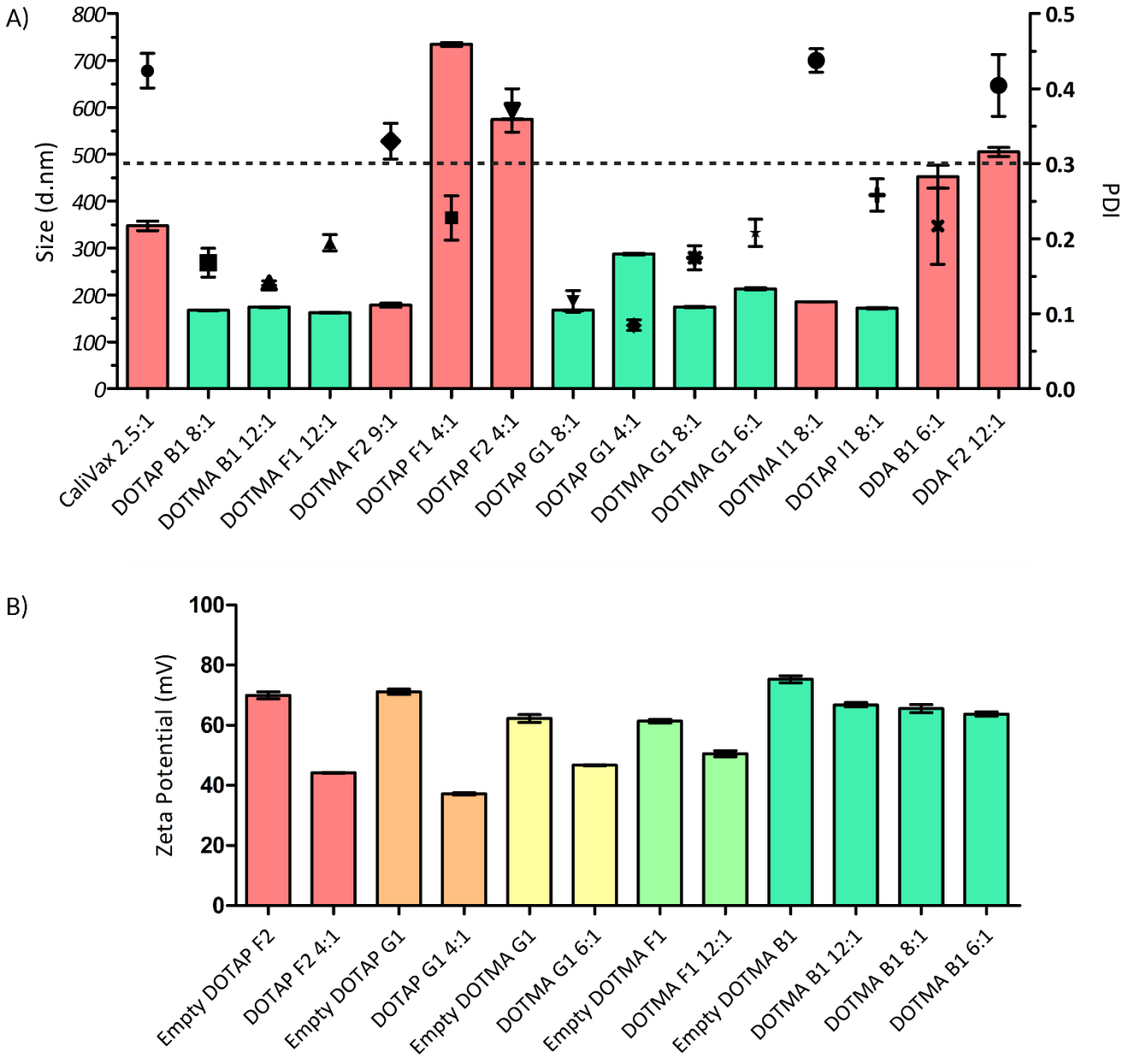

Figure 3.3.9. Physical characteristics of formulated saRNA-Ext-cLNPs. A) Size of optimal saRNA-Ext-cLNPs. A large range of sizes was observed despite optimal performance in cell culture experiments. PDIs were generally below 0.3, with some being greater than the 0.3 cut off. Green bars represent saRNA-Ext-cLNPs that meet both the size and PDI criteria, red bars indicate cLNPs with large sizes, PDIs or both. B) As expected, cLNPs were very positive (>60 mV, millivolts). Upon addition of saRNA, zeta potential decreased proportionally to N:P ratio. A) Bars and symbols represent size and PDI of cLNPs respectively; dotted line indicates PDI cut-off of 0.3. n=3 for A) and B). Size (d.nm) is a measure of the particle diameter in nm.

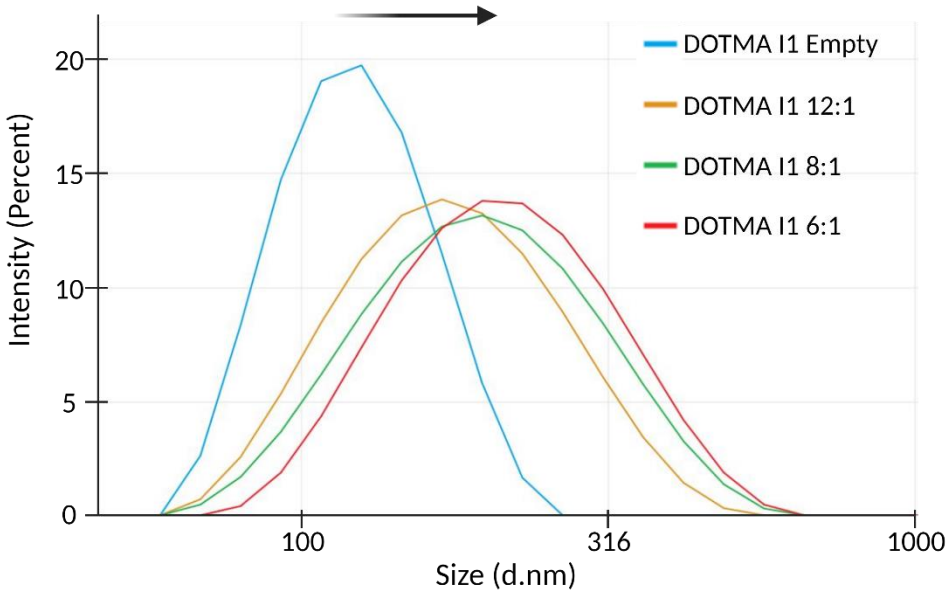

Figure 3.3.10. Dependence of size on N:P ratio of saRNA-Ext-cLNPs. ZetaSizer graph for DOTMA I1 saRNA-Ext-cLNPs is shown, there is a shift in size with different N:P ratios. Empty LNPs were the smallest, as N:P ratio decreased from 12:1 to 6:1, corresponding to addition of more RNA molecules, the size of the saRNA-Ext-cLNPs increased (arrow). Size (d.nm) is a measure of the particle diameter in nm.

3.4. *In vitro* toxicity and *in vivo* assessment of saRNA-cLNP candidates

As a result of good *in vitro* eGFP expression, CaliVax and DOTMA and DOTAP F1 were assessed for *in vivo* efficacy. Initially, expression was confirmed by formulating RNA-Ext-cLNPs using saRNA-Luc2, transfecting cells, and assessing Fluc expression at 72 hours (Figure 3.4.1A). DOTAP F1 8:1 and 6:1 N:P ratios were chosen as opposed to a 4:1 N:P ratio as the size and PDIs were poor as seen earlier. saRNA-Ext-cLNPs showed reduced expression when compared to LMMax, which was expected. However, CaliVax 2.5:1 saRNA-Ext-cLNPs performed significantly better. The reduction in expression could also be as a result of the duration of cell growth affecting cell health, and hence expression. LMMax seems to deliver saRNA at a much higher efficiency, hence a more appropriate control, such as an established saRNA-LNP (e.g., using SM-102 or Dlin-DMA-MC3) would probably result in a more accurate comparison. DOTAP saRNA-Ext-cLNPs expressed at similar levels at both an 8:1 and 6:1 ratio, and hence an

8:1 ratio was chosen going forward in accordance with general higher N:P ratios used for saRNA.

Based on these results, an MTT assay was performed, no significant toxicity was observed (Figure 3.4.1B). Cellular toxicity did increase when RNA was complexed with LNPs as compared to empty LNPs, however this toxicity was not statistically significant.

cLNPs for *in vivo* studies were produced by LFH. The sizes of these empty LNPs were 74 and 122 nm with PDIs of 0.177 and 0.098 for DOTAP F1 and DOTMA F1 respectively (Figure 3.4.2A). However, upon addition of saRNA, sizes increased to 355 and 222 nm for DOTAP F1 and DOTMA F1 respectively, with PDIs above or approximately equal to the 0.3 cut-off. Regardless, the encapsulation efficiencies for all saRNA-cLNPs were very high (~98%; Figure 3.4.2B), and RNA-cLNPs were still able to express in cell culture (Figure 3.4.2C). Blakney et al. (62) were able to utilise larger saRNA-Ext-cLNPs *in vivo*, showing good expression and anti-viral immune responses. Although, these studies used microfluidics to produce empty cLNPs and not LFH.

For *in vivo* studies NMRI mice were either injected with 5 µg of saRNA-cLNPs or an equal dose of empty LNPs (negative control). Bioluminescent imaging was performed at 6 and 24 hours, followed by every other day until day 7. Unfortunately, none of the mice displayed any protein expression from saRNA-Luc2 delivery using the LNPs (Supplementary Figure 12). Similarly, saRNA-CaliVax showed no expression at day 3 or day 7 post-injection, where peak expression is expected.

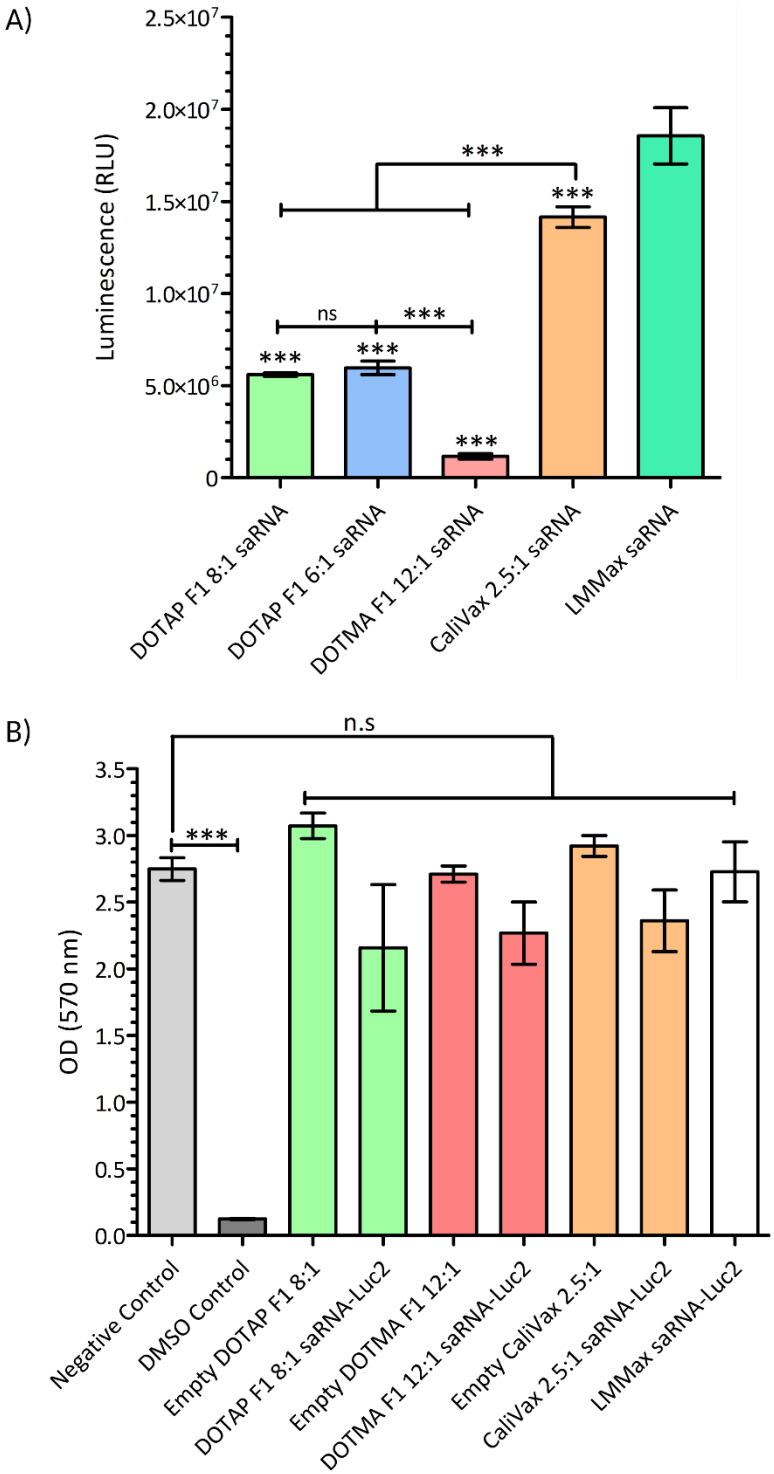

Figure 3.4.1. Expression comparison and toxicity assessment of *in vivo* saRNA-Ext-cLNP candidates using saRNA-Luc2. A) Comparison of saRNA-Ext-cLNP expression at 72 hours using RNA-Luc2. CaliVax showed the best performance, followed by DOTAP F1 and lastly DOTMA F1 cLNPs. LMMax was used as a positive control. B) An MTT assay was performed at 24 hours post-transfection to assess toxicity, none of the cLNPs show a significant reduction in viability compared to the negative control. Statistical analysis performed using a one-way ANOVA followed by a Tukey post-hoc test; $p \leq 0.01$ (**) $p \leq 0.001$ (***), not significant (n.s). A) Symbols above bars represent statistical analysis compared to the relevant LMMax control. RLU – relative light units. n=3 for A) and B)

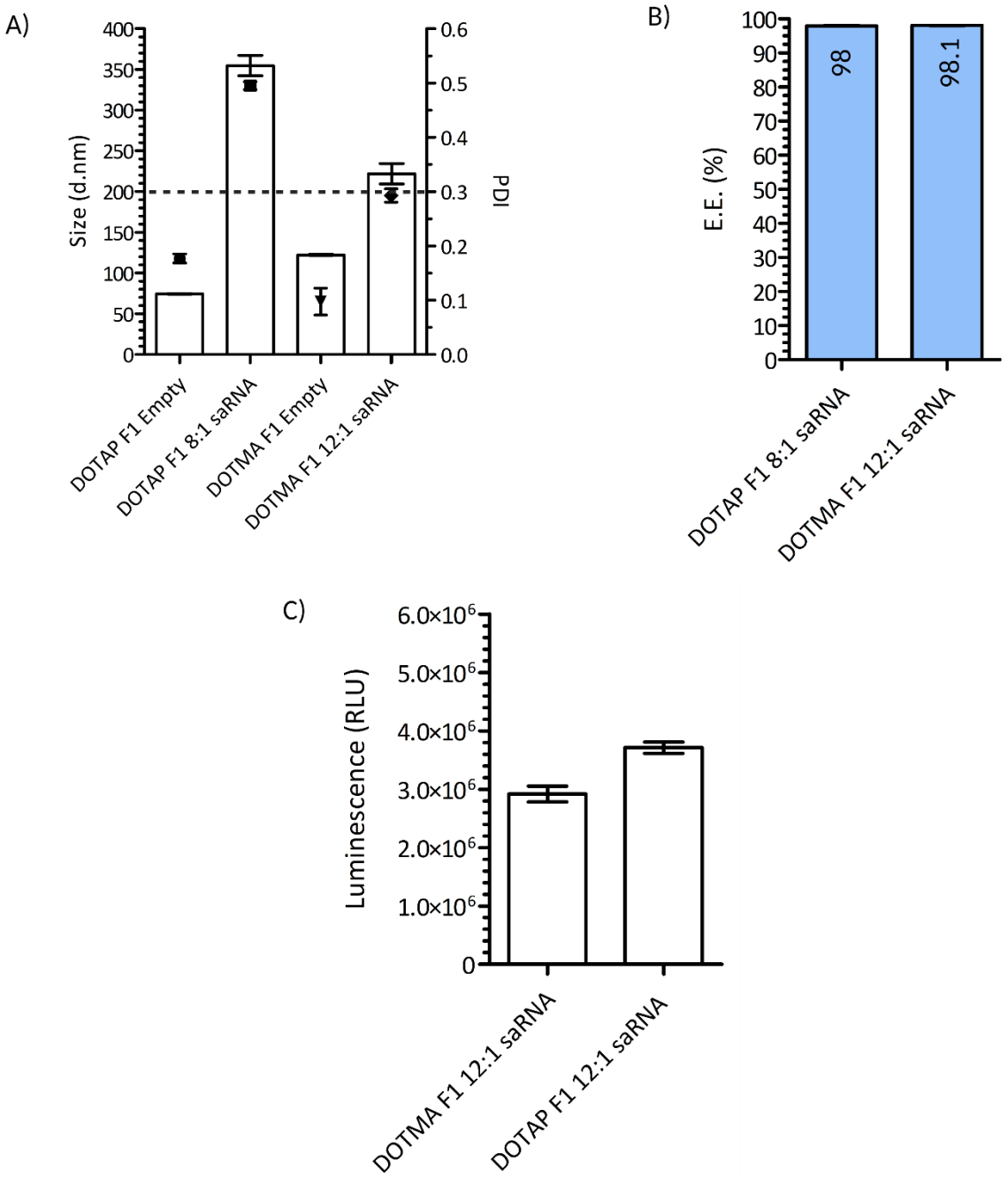

Figure 3.4.2. Formulation and characterisation of DOTAP and DOTMA F1 RNA-Ext-cLNPs for *in vivo* assessment. A) cLNPs were produced using LFH and complexed exteriorly with saRNA-Luc2. Sizes and PDIs were quite large, particularly for saRNA-DOTAP F1 8:1, which was <250 nm with a PDI approximately equal to the 0.3 cut-off. B) Encapsulation efficacies were assessed by a RiboGreen Assay, showing very high encapsulation efficiencies of 98% of saRNA within the cLNPs. C) Expression of injected cLNPs was assessed in cell culture, and expression was confirmed after 24 hours. A) Bars and symbols represent size and PDI of cLNPs respectively; dotted line indicates PDI cut-off of 0.3.

3.5. Internal Formulation of saRNA-cLNPs (saRNA-Int-cLNPs)

To examine alternative saRNA formulation strategies, saRNA-Int-cLNP formulation was performed. This was achieved by two methods: microfluidics and a modified SI method adapted from Zhang *et al.* (111) and Melo *et al.* (112).

3.5.1. Microfluidics formulation of PEGylated saRNA-Int-LNPs

DOTAP E1 cLNPs (DOTAP:Chol:DOPE:DMG-PEG2000) at an 8:1 N:P ratio was formulated using microfluidics with a size, PDI and Zeta Potential of 76.3 nm, 0.11 and 10.47 mV respectively (Figure 3.5.1A and B, Supplementary Table 1). The zeta potential is significantly lower than the un-PEGylated cLNPs produced by LFH, this is possibly due to the PEGylated lipid "shielding" the charge of the cationic lipid. These delivered saRNA-eGFP poorly, however upon use of serum-free media, a marked increase in expression was observed (Figure 3.5.2). This suggests an influence of serum constituents on the cLNPs, agreeing with literature showing that cLNPs interact with serum proteins and are not stable when injected systemically due to permanent positive charges (109,110). However, these have been utilised previously for saRNA vaccines, even when un-PEGylated (62). Hence, this may be a case of *in vitro* results often not aligning with *in vivo* results (113). iLNPs were also examined as these are currently the most utilised platform for RNA vaccines. DLin-DMA-MC3 has been extensively used in iLNPs, and hence was examined as a comparison. E2 iLNPs were formulated at 12:1 and 8:1 N:P ratios and were <50 nm after purification by concentration columns (Figure 3.5.1A, Supplementary Table 1). These had a high encapsulation efficiency of 95% (Figure 3.5.3A). Although the 12:1 N:P performed better than 8:1, poor efficacy of both was observed (Figure 3.5.3B). Considering these have been successfully applied to saRNA vaccines, this result was surprising (97). This could be as a result of kidney as opposed to liver cells being used, as these LNPs intrinsically target cells overexpressing LDLR. It also exposes a poor correlation between cell culture and *in vivo* efficacy (113). These LNPs were optimized for encapsulation of significantly smaller siRNAs, as this LNP is used in Onpattro® (Patisiran) (114), which could also explain poor release of encapsulated saRNA. The zeta potentials of all the PEGylated LNPs were close to neutral, however cLNPs were slightly more positively charged, while iLNPs were more negatively charged (Figure 3.5.1B).

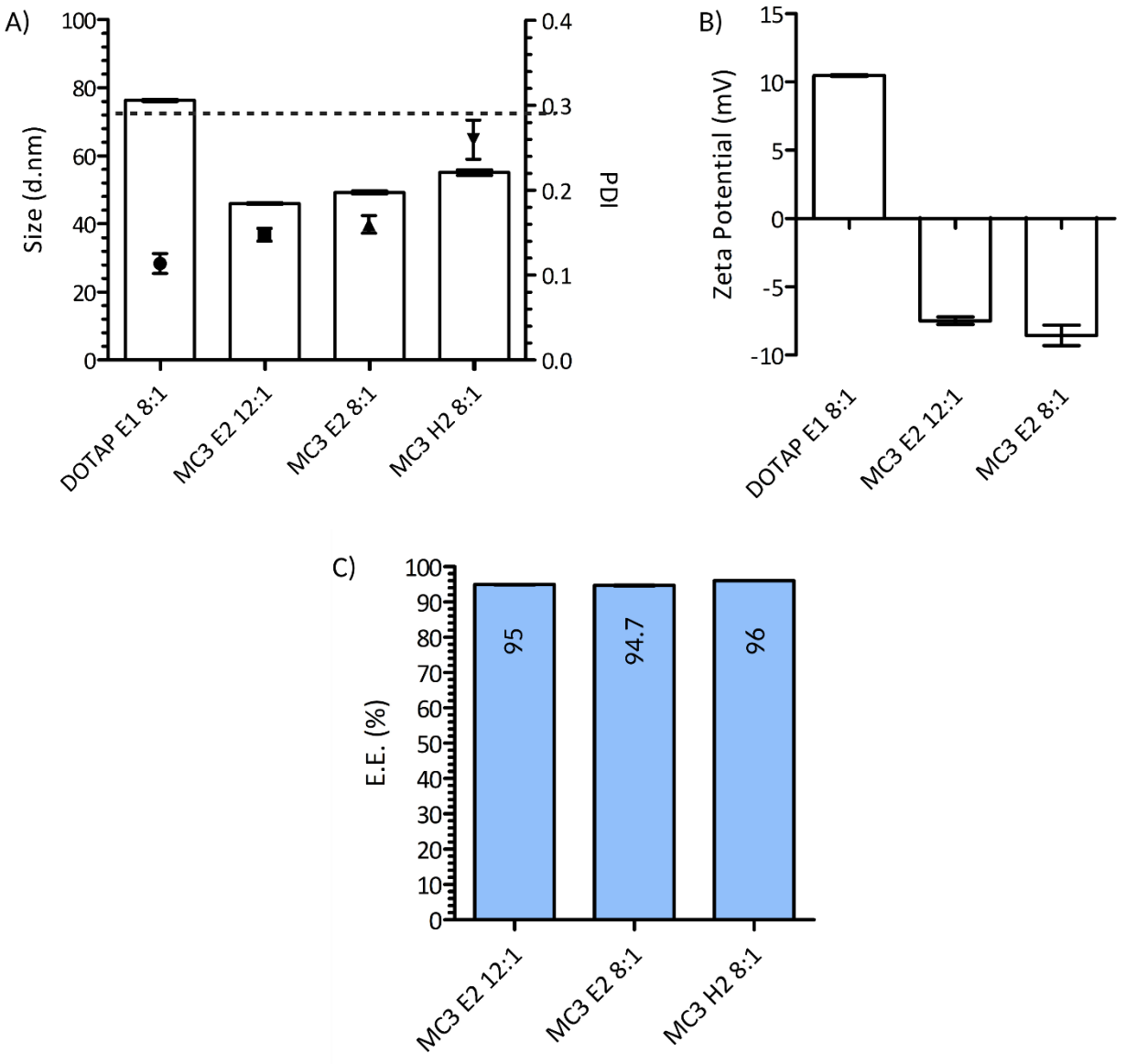

Figure 3.5.1. Characteristics of saRNA-Int-LNPs formulated using microfluidics. A) saRNA-Int-cLNPs and -iLNPs were successfully produced using microfluidics with sizes <100 nm and low PDIs. B) While all LNPs were relatively neutral, PEGylated E1 cLNPs were slightly positively charged, while PEGylated iLNPs were slightly negatively charged. C) All microfluidics formulated LNPs showed high encapsulation efficiency (>90%). A) Bars and symbols represent size and PDI of cLNPs respectively; dotted line indicates PDI cut-off of 0.3. Size (d.nm) is a measure of the particle diameter in nm.

MC3 H2 8:1 N:P LNPs were also produced with low sizes (Figure 3.5.1A, Supplementary Table 1), and these worked more efficiency showing improvement in Fluc expression compared to MC3 E2 iLNPs (Figure 3.5.5B). This is possibly as a result of a lower percentage of the PEGylated lipid (DMG-PEG2000), reducing hinderance of the LNPs from interacting with and entering cells. A higher ionisable lipid percentage and less cholesterol could have also improved expression, which was similar to what was observed for the RNA-Ext-cLNPs (Appendix Table 5).

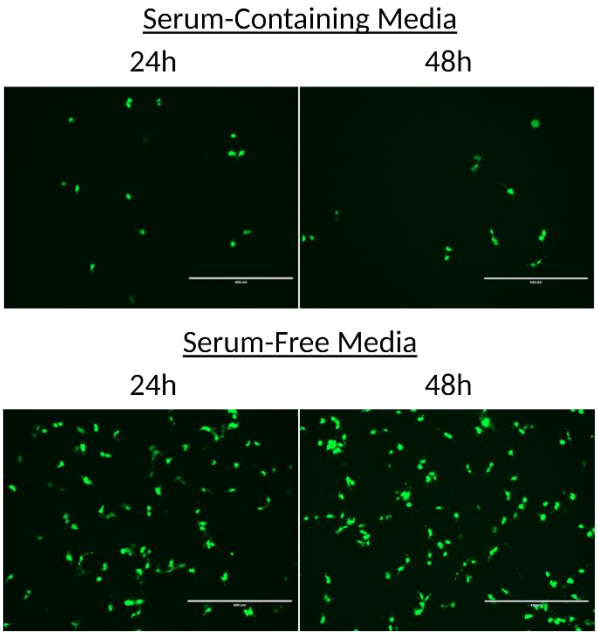

Figure 3.5.2. Delivery efficacy of DOTAP E1 saRNA-Int-cLNPs in HEK293 cells. DOTAP E1 cLNPs did not perform well in serum-containing media, showing minimal eGFP expression, however this increased upon removal of serum from the media. Scale bar = 400 µm.

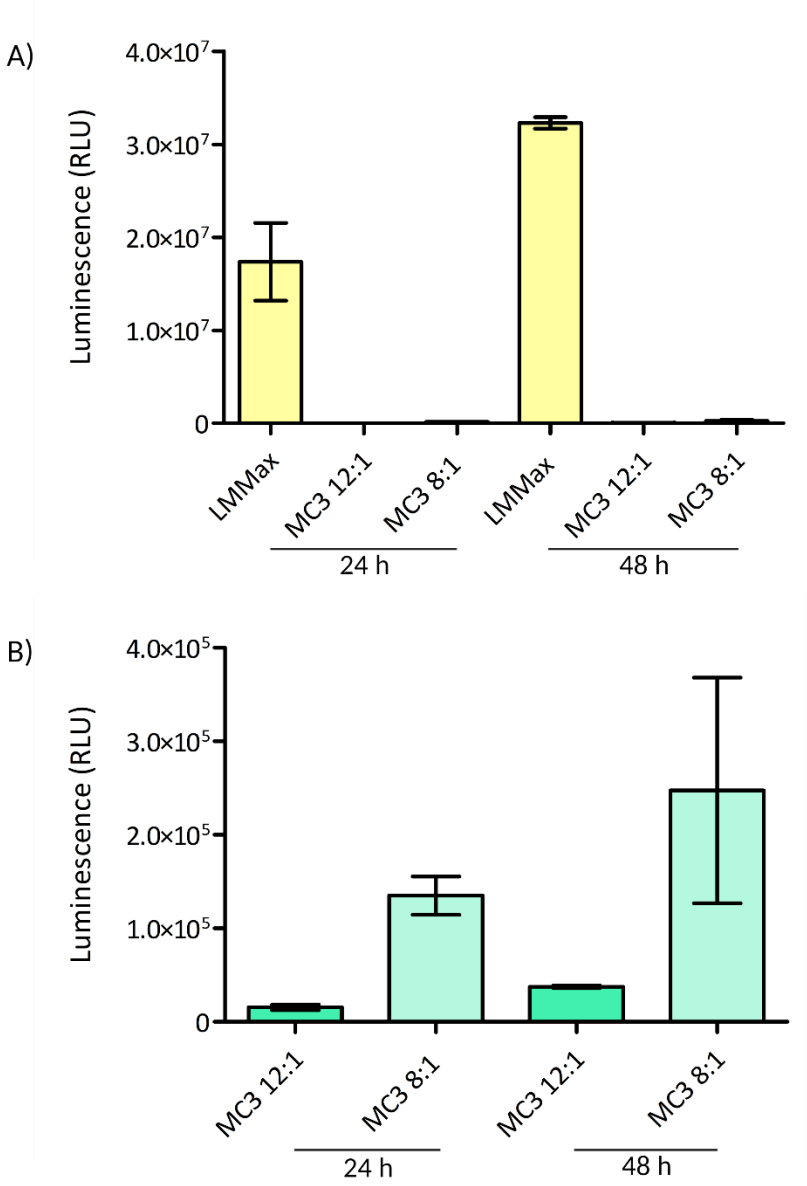

Figure 3.5.3. Unexpected poor delivery efficacy of MC3 E2 saRNA-Int-iLNPs in cell culture. MC3 E2 iLNPs did not perform well in cell culture experiments, showing minimal Fluc (Luc2) expression at 24 and 48 hours compared to LMMax (A). When LMMax is omitted from the graph, some luminescence can be observed (B). The 8:1 N:P performed better than the 12:1 N:P.

3.5.2. A simple modified solvent injection can produce functional saRNA-Int-cLNPs

To screen saRNA-Int-cLNPs without the need to formulate using microfluidics, a modified SI method was used. This involves simply adding the lipids in ethanol to the diluted RNA and vortexing for a few seconds. This was able to produce saRNA-Int-cLNPs with efficiently encapsulated saRNA, albeit with variable size distributions (Figure 3.5.4A, Supplementary Table 1). Some had multiple peaks, poor PDIs, larger sizes or aggregation (e.g., DDA B1 12:1), while others had single peaks with acceptable PDIs and sizes (DOTAP and DOTMA B1). This results from a cruder method of mixing as compared to microfluidics, which makes use of highly controlled flow rates and low turbulence. Nonetheless, high encapsulation efficiencies were observed (>90%, Figure 3.5.4B) and were used for internal LNP screening prior to microfluidics formulation. In contrast, iLNPs had poor encapsulation efficiency when formulated using SI independent of buffer composition, pH, and ionisable lipid used, as neither SM-102 nor DLin-MC3-DMA LNPs H2 cLNPs were able to efficiently encapsulate saRNA using this method (<70%, Figure 3.5.4B).

Transfection efficiency of saRNA-cLNPs using the modified solvent injection method was evaluated using saRNA-Luc2. Once again transfection efficacy was mainly dependent on N:P ratio. For B1 saRNA-Int-cLNPs (Figure 3.5.5A), although DOTAP B1 12:1 performed the best at 24 hours post-transfection, at 48 hours a reduction in expression was noted. Regardless, DOTAP B1 8:1 saRNA-LNPs showed a slight increase in expression from 24 to 48 hours, which is expected, considering the amplifying nature of saRNA. DOTMA B1 12:1 performed poorly and showed drastically reduced expression at 48 hours, while DDA B1 cLNPs aggregated and were therefore not assessed for transfection efficiency.

Similar to saRNA-Ext-cLNPs, F1 saRNA-Int-cLNPs formulated using the modified solvent injection method displayed improved performance (Figure 3.5.5B). Although DOTAP F1 8:1 cLNPs performed the best at 24 hours, only a small increase in expression was observed at 48 hours post-transfection. However, at 12:1 and 15:1 N:P ratios, although a lower expression level was observed at 24 hours, the expression more than doubled at 48 hours. DDA F2 12:1 saRNA-cLNPs, showed a similar pattern to DOTAP F1 15:1 and 12:1, however a substantial 4-fold increase was observed from 24 to 48 hours. This was an impressive result, showing how

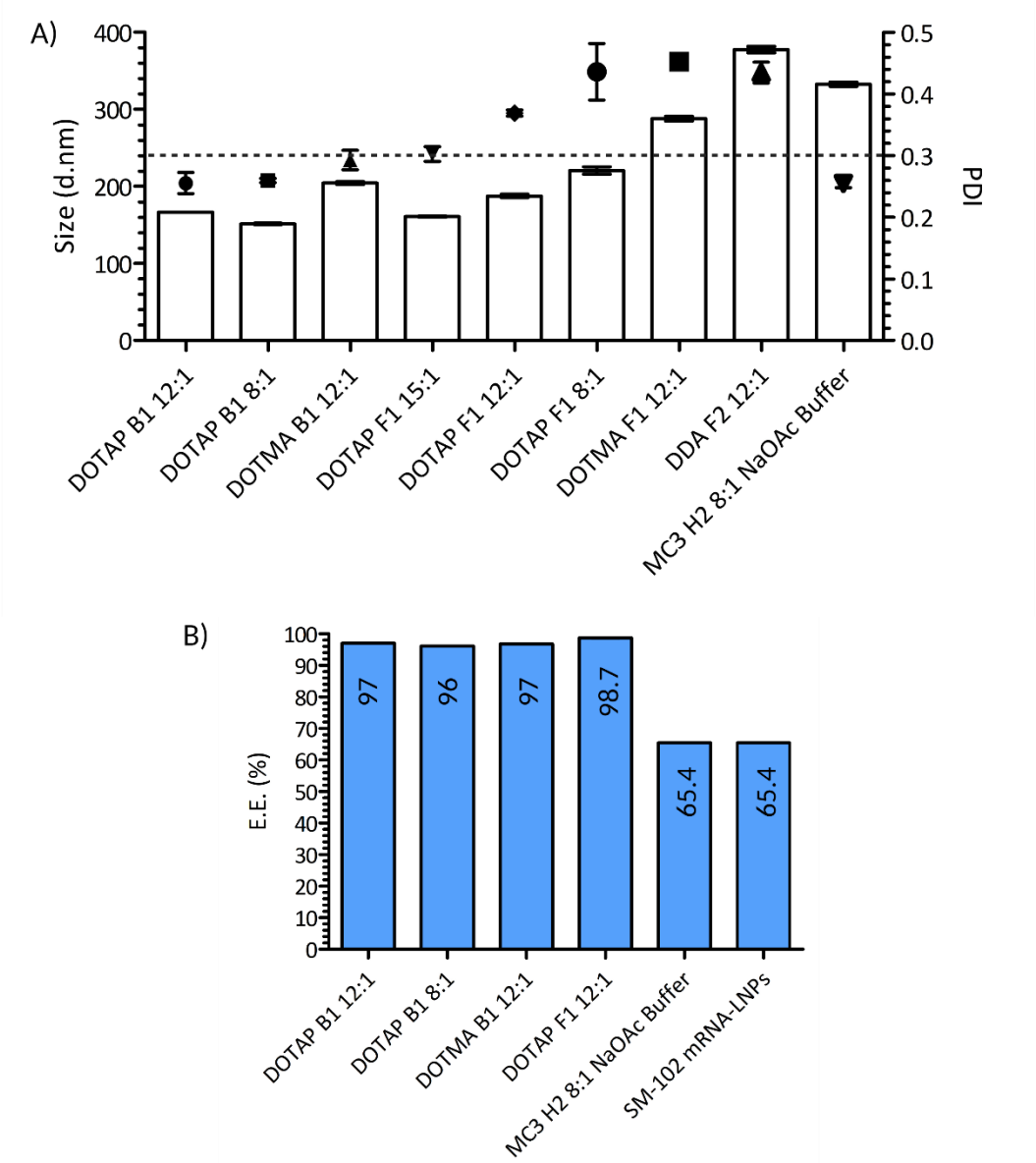

Figure 3.5.4. Formulation of saRNA-Int-cLNPs using a modified solvent injection method. A) cLNP sizes were all above 100 nm with variable PDIs. B) Despite larger sizes and PDIs, cLNPs displayed high encapsulation efficacy of saRNA. iLNPs were unable to efficiently encapsulate RNA using this method. A) Bars and symbols represent size and PDI of cLNPs respectively; dotted line indicates PDI cut-off of 0.3. Size (d.nm) is a measure of the particle diameter in nm.

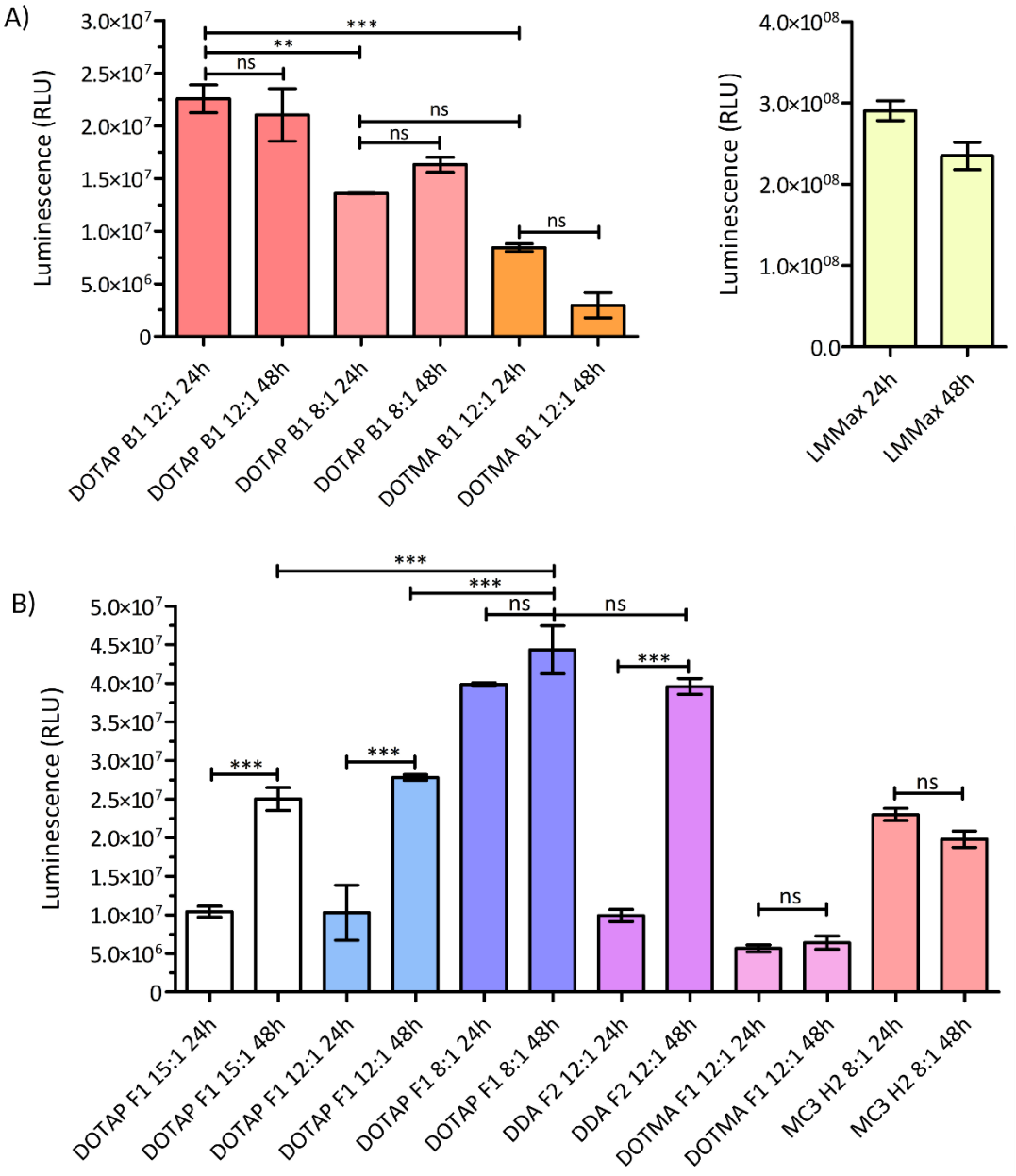

Figure 3.5.5. The effect of lipid choice and N:P ratio on transfection efficacy of saRNA-Int-cLNPs produced using the modified solvent injection method. A) For B1 cLNPs, DOTAP B1 at an N:P ratio of 12:1 performed the best, with a reduction in efficacy for an 8:1 ratio (left). Transfection efficacy did not seem to amplify at 48 hours; however, the expression kinetics were similar to the LMMax control (right). B) Effect of saRNA-Int-cLNP lipid composition and N:P ratio on saRNA expression kinetics for F1/F2 cLNPs. N:P ratio altered initial delivery, and amplification kinetics of saRNA. While DOTAP 15:1 and 12:1, and DDA F2 12:1 show minimal expression at 24 hours post-transfection, they show a significant increase in expression after 48 hours. Statistical analysis performed using a one-way ANOVA followed by a Tukey post-hoc test; $p \leq 0.001$ (***), not significant (n.s). n=3 for both A) and B).

different cationic lipids can significantly alter saRNA expression kinetics, making it a strong candidate for *in vivo* assessment. DOTMA F1 12:1 performed relatively poorly, with no substantial increase in expression from 24 to 48 hours. Only DOTMA saRNA-Int-cLNPs performed worse than the MC3 control included, which also did not result in amplification of Fluc expression as discussed previously.

3.5.3. Comparison of Microfluidics and Solvent Injection is Limited by Purification Difficulties

In an attempt to compare the modified solvent injection method and microfluidics, DOTAP F1 12:1 and DDA F2 12:1 saRNA-Int-cLNPs were produced using both methods. While the LNPs produced using the modified SI method were not purified (crude), LNPs produced using microfluidics were dialysed prior to use in transfection. Dialysis resulted in a loss in sample, which limited their use in *in vivo* studies, however purification using concentrator columns resulted in aggregation of LNPs, prompting favour of LNP dialysis. Microfluidics LNPs were generally smaller compared to the modified solvent injection method, with a minor size increase after dialysis (Figure 3.5.6A). Upon transfection of HEK239 cells, a marked reduction in transfection efficacy was shown compared to crude LNPs produced using the modified SI method (Figure 3.5.6B) despite maintenance of encapsulation efficiency. The saRNA-Int-cLNPs produced using the modified SI method were able to replicate transfection efficacy and expression dynamics as before (Figures 3.5.6B and 3.5.5B)

Similar loss in potency was observed after purification of PEGylated D1 cLNPs. Although sizes, PDIs and encapsulation efficiency remained the same before and after dialysis (Figure 3.5.6C and D), potency was reduced. Expression almost tripled from 24 to 48 hours when crude saRNA-Int-cLNPs were used to transfect cells (Figure 3.5.6E). However, purified LNPs showed no expression of Fluc transgene. Despite issues with purification, which can be optimised, DOTAP D1 8:1 saRNA-Int-cLNPs were able to deliver saRNA to cells and allow for amplification of saRNA, and hence, these D1 LNPs still show strong potential for *in vivo* use. Similarly, other saRNA-Int-cLNPs such as DDA F2 12:1 and DOTAP F1 12:1 were very promising candidates when evaluated using the modified SI method, which should be translatable to microfluidics after the purification is optimised.

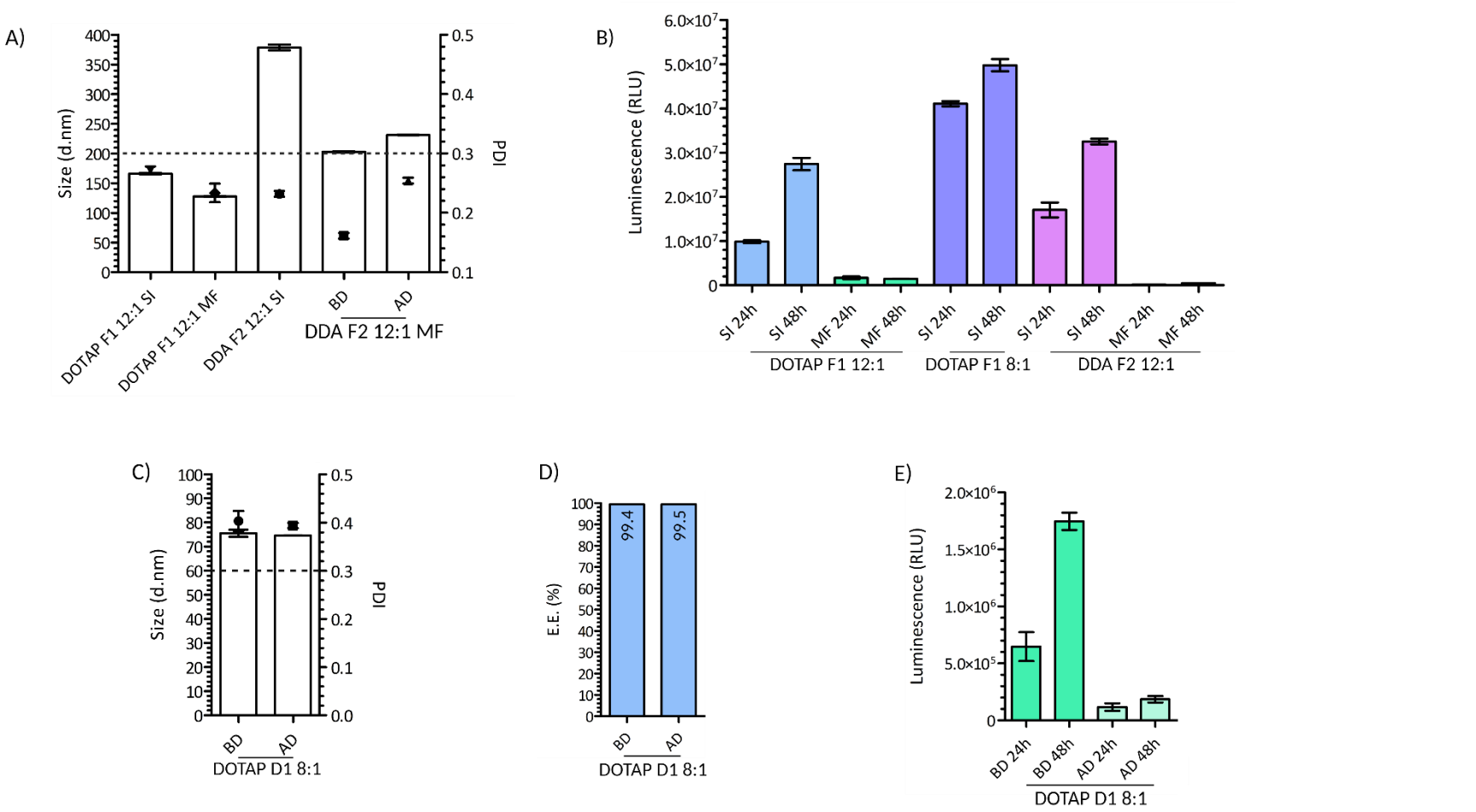

Figure 3.5.6. Loss in saRNA-Int-cLNP potency upon purification of saRNA-Int-cLNPs. A) saRNA-Int-cLNPs produced using microfluidics (MF) were smaller than those formulated with the modified SI, although all LNPs were >100nm with the exception of DDA F2 SI formulated cLNPs. However, all PDIs were <0.3. A minimal increase in size was observed from before (BD) to after dialysis (AD) of DDA F2 12:1 saRNA-Int-cLNPs. B) Dialysed cLNPs formulated using microfluidics lost their delivery efficacy in cell culture compared to crude LNP controls formulated using SI. PEGylated D1 LNPs formulated using MF had similar sizes and PDIs (C), and encapsulation efficiencies (D) before and after dialysis. However, their potency is lost after purification (E). A and C) Bars and symbols represent size and PDI of cLNPs respectively; dotted line indicates PDI cut-off of 0.3. Size (d.nm) is a measure of the particle diameter in nm.

Chapter 4

Discussion

The COVID-19 pandemic has brought mRNA to the forefront as an effective platform for vaccines. Improvements in RNA and antigen design, and delivery of these vaccines is essential to the progression of mRNA as a versatile and accessible drug substance (20). saRNA has advantages over conventional mRNA such as use of unmodified nucleotides in place of modified nucleotides which reduces production costs, and the requirement of significantly lower doses (80), which may improve vaccine equity. Although saRNA has been studied alongside conventional mRNA, with its first use in an influenza vaccine in 1994 (54), it has only been further investigated and become more relevant recently, especially after successful delivery of an RSV vaccine with a non-viral vector (97). This highlights the importance of developing non-viral vector platforms to drive the success of RNA vaccines, however much is still to be investigated to optimise these platforms. The work in this dissertation provides a platform for both development of saRNA for vaccines, and the vectors required for successful delivery and subsequent immune responses.

4.1. rNTP: Mg^{2+} ratio and pDNA template dose are crucial factors in IVT of longer RNA transcripts

IVT optimisation was performed as kits used for conventional mRNA IVTs were not efficient at producing RNA with significantly longer transcripts. Agreeing with the literature, the Magnesium ion (Mg^{2+}) to NTP ratio appears to be very important for *in vitro* transcription, especially of saRNA (106). While the TriLink protocol used a total NTP: $MgOAc_2$ ratio of 1:1.35, the DOE buffer 1:1.88 with additional sodium acetate. These Mg^{2+} ions have a dual function: (a) They bind to NTPs and act as a co-factor resulting in incorporation of nucleotide monophosphates into the synthesised RNA strand; (b) they are required for the binding of the T7 polymerase onto the linearised pDNA template (30,31), which is an essential step in transcription initiation. The concentration of Spermidine, which allows dissociation of RNA polymerase from the DNA template (115), is also important for saRNA. The DOE buffer uses 10× less Spermidine, which may promote prolonged association of the T7 polymerase with a much longer DNA template, and hence prevent premature dissociation of the enzyme before a complete saRNA is transcribed. An increase in DNA template concentration was also shown

to be important as using a lower concentration in the High Yield and AmpliScribe IVTs did not show successful IVT. However, doubling the concentration such as in the RiboMax kit and DOE protocol, produced intact saRNA transcripts. Although these factors were important for saRNA, they seemed less important for production of conventional mRNA, as all kits successfully transcribed the mRNA kit controls.

4.2. Successful cloning of new saRNA templates and expression kinetics of saRNA

The cloning strategy for the new saRNA pDNA templates is simple and has a high success rate. These constructs allow for efficient linearisation and *in vitro* transcription of saRNA, which were able to express prominent levels of transgene (eGFP and Fluc). This was dependent on the capping mechanism used, while enzymatically capped saRNA was able to be expressed, this was not as strong as co-transcriptional capping. This was most likely as a result of degradation of saRNA during capping, and this method may not be suitable for capping of significantly longer RNAs. Co-transcriptional capping however, especially TriLink's CleanCap AU reagent, resulted in significantly higher transgene expression, similar to that of pDNA after 24 hours. This is a highly efficient and specific system as it is a trimer as opposed to previous dimer analogues (116). Co-transcriptional capping also holds the advantage over enzymatic capping as it eliminates an additional purification step between the IVT and capping reactions, which will be essential in large scale production of saRNA to reduce degradation of the longer RNA through turbulent handling.

4.3. LFH as a useful, cost-efficient tool for cell culture screening of RNA-Ext-LNP candidates

Non-viral vectors are vital to deliver the encapsulated RNA into cells, prevent RNase-mediated degradation, and act as an adjuvant. These all ensure that antigens can be translated, and an effective immune response can be developed. In this body of work, LNPs were chosen as these have been successfully utilised in approved vaccines and therapies. Empty cLNPs were successfully formulated using lipid film hydration, and saRNA could be formulated externally with high encapsulation efficiency. LFH is a "top-down" approach, and hence may not be the most optimal method of production, as seen with the variability in sizes between batches of empty LNPs such as the DOTAP and DOTMA B1 cLNPs. These cLNPs also had larger sizes compared to those produced using microfluidics. There were difficulties in producing DDA cLNPs, such as ones containing DOPE (such as F1), which is why it was substituted for DSPC. Requirement of heating the lipids above their phase transition temperature during hydration,

sonication, and extrusion increases the difficulty of this method as this temperature is relatively high in certain cases (the phase transition temperature of DSPC is 55°C [114]). Hence, at a larger scale, "bottom-up" approaches such as microfluidics and solvent injection, may be more suitable to produce these LNPs in a simpler, more reproducible manner. Nonetheless, this method is a relatively cheap method of producing cLNPs to examine saRNA-Ext-cLNPs candidates *in vitro*, as this is significantly cheaper than screening using microfluidics. Cationic lipids have the advantage of reduced cost compared to ionisable lipids, and cLNPs have an extensive track record in successful use for non-RNA therapeutics (66), emphasising their clinical relevance. These have recently shown success in the saRNA vaccine field (62,103–105).

4.4. Promising cell culture results for potential saRNA-Ext-cLNPs

Many of the saRNA-Ext-cLNP candidates showed prominent levels of RNA delivery as seen by transgene expression. The composition and N:P ratios were the most important LNP considerations influencing the delivery, as larger sizes were often able to deliver more efficiently that smaller sizes and vice versa. While Lipofectamine MessengerMax (LMMax) delivered saRNA much more efficiently, this was used as a control for transfection rather than a comparison for saRNA-Ext-cLNPs, as LMMax is not used for *in vivo* delivery of saRNA. A more appropriate comparison would be an LNP that is known to deliver saRNA efficiently *in vivo*, such as the MC3 iLNPs used for the saRNA-Int-cLNPs (97). Nonetheless, high transfection efficacy for optimised formulations was clearly evident. No significant toxicity was measured in cells transfected with these LNPs. Interestingly, LNPs formulated with RNA were generally more toxic than LNPs alone, suggesting a combinational effect when the RNA is complexed to the LNP in the non-significant toxicity observed.

4.5. Possible explanations for failure of saRNA-Ext-cLNP candidates *in vivo*

Despite positive cell culture results, *in vivo* results for the top candidates were negative, with no expression of saRNA visible after any of the timepoints. This could be due to a multiplicity of reasons including the size of the LNPs. While the large size may not be detrimental in cell culture, factors such as immune responses and organ architecture may affect LNP pharmacology. The immune system may result in clearance of LNPs by the mononuclear phagocyte system before cell transfection can occur (reviewed in (67)). It has been shown that larger LNPs are cleared more rapidly due to an increase in surface area for immune recognition

(117). However, Blakney *et al*. formulated saRNA-Ext-LNPs with relatively large sizes (>175 nm) despite being formulated with microfluidics. These saRNA-cLNPs expressed transgene and resulted in an immune response (62,104). A study published by Moderna also found that the immunogenicity of mRNA-LNPs increased with increasing size up to 105 nm, after which immunogenicity decreased with an increase in size, albeit only up to 150 nm. Regardless, larger LNPs still resulted in robust immune responses (118). Therefore, microfluidics may be the distinguishing difference, and may be required for positive *in vivo* results as it is a more robust method of LNP production.

Addition of a PEGylated lipid may further improve delivery efficacy by preventing clearance by the immune system by reducing size and opsonisation of the LNP surface. PEG is also beneficial for LNP stability *in vivo* and during storage (reviewed in (119)). It may also negatively impact the LNP depot effect, which may be favourable for RNA vaccine efficacy (88). The difference in organ architecture between 2D versus 3D cell layout may affect transfection efficacy, as cell culture results also do not strictly correlate with *in vivo* efficacy (111). Zhang *et al.* (111) screened their library of LNPs, and some LNPs that did not perform well in cell culture, showed the highest expression *in vivo*. Secondary tissue structure, and different cell types in cell culture versus *in vivo* environments may be the reason for these inconsistencies.

Generally, mice showed no weight loss and were healthy when performing welfare checks based on physical examinations. Innate cytokines and *in vivo* toxicity were not examined as the candidates failed to efficiently deliver the RNA and result in expression. However, cytometric bead arrays would be used to assess cytokine production, and measurement of alanine and aspartate transaminases would determine whether any toxicity was caused.

4.6. Effects of saRNA-Int-LNP formulation on saRNA expression kinetics

mRNA vaccines are generally formulated inside the LNPs using microfluidics for clinical use. In this study, multiple cLNPs and iLNPs were formulated with saRNA internally using microfluidics. These generally had small sizes and high encapsulation efficiencies, however there was variability in their delivery. This could be a result of cell culture versus *in vivo* efficacy as some of these, in particular the MC3 formulations, were utilised by Geall *et al*. with successful *in vivo* results (97). Regardless, MC3 H2 LNPs showed relatively good cell culture efficacy. Interestingly, the expression kinetics of the saRNA were not expected, with no increase in expression despite the expected RNA replication. However, this could be a result

of the lipid being developed for use with siRNAs (114), which are even smaller than mRNAs. Hence, MC3 may not be suitable or require more optimisation to be used efficiently with saRNA. The disadvantage of microfluidics, especially at a smaller scale, is the cost. The equipment and cartridges are quite costly, especially if the goal is screening *in vivo* candidates. However, this platform is scalable, streamlined, and provides a highly precise, chaotropic and non-turbulent method for internal and external formulation of saRNA-LNPs (120).

To overcome costs associated with microfluidics when screening saRNA-Int-LNPs, a modified solvent injection method was used to formulate based on the solvent injection method. Although larger cLNPs with higher PDIs were produced, the formulation was successful in producing saRNA-Int-cLNPs with high encapsulation efficiencies. The larger sizes and PDIs of LNPs formulated by modified solvent injection would be solved by using microfluidics. however, iLNPs showed low encapsulation efficacy, and hence should only be produced using microfluidics.

Overall, for saRNA-Int-cLNPs and saRNA-Ext-cLNP candidates examined, DOTMA and DOTAP showed the most potential for saRNA delivery, in particular the F1, B1 and F2 formulations. DOTMA has generally not been examined in the literature, as DOTAP has been preferred. DOTMA is the non-ester analogue of DOTAP, which could improve LNP stability *in vivo* and during storage, and is simpler to synthesise. This could be an advantage over ester analogues, as no toxicity was observed in cell culture by omission of this feature. However, one important result that could have easily been omitted if only short-term expression was analysed is the potential of DDA for saRNA delivery. In both saRNA-Ext-cLNPs and saRNA-Int cLNPs, while DDA saRNA-LNPs showed minimal expression at 24 hours post-transfection, after 48 hours this was significantly boosted. This shows a difference in the delivery kinetics of DDA, possibly affecting endosomal escape or RNA release kinetics from the LNP. Hence this formulation should not be omitted from future studies. PEGylated D1 saRNA-Int-cLNPs, despite showing lower expression than non-PEGylated cLNPs, also have potential *in vivo* to minimise clearance and improve expression. Importantly, the difference between the E2 cLNPs, which showed minimal expression, and these D1 cLNPs, is the omission of cholesterol. Unlike with iLNPs, cholesterol may have an inhibitory effect on these PEGylated cLNPs. While the DOTAP B1 saRNA-Int-cLNP 12:1 showed a reduction in expression from 24- to 48-hours, the

lipofectamine control displayed a similar trend which may indicate the possibility of an issue with the transfection itself (cell health etc.) rather than the LNPs themselves.

saRNA-Luc2 was used in these experiments, and showed how quantification of the transgene expression is especially useful for assessment of LNP efficacy and expression kinetics. For saRNA-eGFP, a technique such as flow cytometry should be used to allow for this quantification in future. These results showed that studying LNP composition in combination with N:P ratio is especially important in developing the optimal LNP formulation that accommodates saRNA delivery as well as efficient RNA replication to allow a lower dose to be used in humans. This emphasises the importance for comparisons of saRNA and mRNA, due to the short-lived expression of conventional mRNA. Although this may seem like an extensive process, this could be improved by using a design of experiments approach (104).

4.7. Solutions to successfully purify saRNA-cLNP candidates

Purification of saRNA-Int-cLNPs was attempted using two methods: concentrator columns and dialysis, with multiple difficulties persisting. Loss of sample and LNP potency were the main setbacks, the loss in sample suggests interaction of the LNPs with the dialysis membrane. Suggestions such as pre-wetting the membrane and washing the membrane after dialysis did not improve this. To solve these obstacles, different dialysis cassettes could be tested to try and reduce membrane binding. However, dialysis is not a scalable method, and a method closer to a tangential flow filtration system should be optimised, such as improving the use of the concentrator columns. Centrifugal concentrator column use resulted in membrane fouling, preventing buffer exchange and concentration. The reason for this could be as a result of high centrifugation speeds (2000 ×g), which could be lowered. Membrane fouling could also be due to instability and subsequent aggregation when a centrifugal force is applied to unPEGylated LNPs, as PEGylated iLNPs and cLNPs are purified well using this method. The buffer could be altered to change aspects such as pH and component concentrations as this may improve LNP stability.

One limitation of RNA-LNPs is their long-term storage stability, using sucrose to stabilise the LNPs may also assist downstream applications, such as lyophilisation which involves the removal of water by sublimation. This results in formation of a “cake” which can be reconstituted in water or a buffer of choice (20,121). This is a technique only applied more

recently to LNPs, and will assist in improving transportation stability in lower middle income countries such as South Africa (20).

Conclusions and Future Work

The work outlined in this dissertation will aid in development of LNPs and the processes for production, characterisation, and assessment of saRNA- and mRNA-LNP vaccines in South Africa. A flexible platform for saRNA vaccines in combination with LNP formulation has been successfully established. Three different production methods were examined. While modified solvent injection and LFH are substantially cheaper, they may not be optimal for clinical application due to size constraints. Microfluidics was able to produce consistently smaller and higher quality LNPs, however, purification still requires optimisation. Although positive results for LFH-produced LNPs were not observed *in vivo*, optimisation of a library of saRNA-cLNPs has been achieved. This includes both saRNA-Int-cLNPs and saRNA-Ext-cLNPs, which still have potential to be examined *in vivo*. Interesting results on the expression kinetics of saRNA and their relationship with composition of LNPs and the N:P ratio was observed. It is therefore essential to optimise these characteristics correctly to maximise the potential of the saRNA platform.

Future studies will resolve issues with saRNA-Int-cLNP purification to prevent aggregation and allow *in vivo* assessment. saRNA-Ext-cLNPs formulated using empty LNPs produced using microfluidics should be examined *in vivo* as this may be the determining factor for successful delivery. Different routes of injection, such as intradermal and intranasal administration, could also be examined. This will be important in examining less invasive vaccine administration, which could show an improvement in vaccine uptake as a result of reduced pain. This may have a beneficial effect on immune responses by delivering the RNA to different cell types, including an increased proportion of antigen display to immune cells (104). Novel LNPs should also be examined to specifically cater for mRNA and saRNA delivery and reduce reliance on lipids that require licencing for commercial use. Improving RNA-LNP stability by lyophilisation would increase storage and transportation temperatures from ultra-low temperatures to temperatures typically used for conventional vaccines (4°C). Following South Africa's reliance on first world countries for mRNA-LNP vaccine supply, this study represents an important development towards independence on mRNA vaccine production from the global North. This platform provides an advancement in the current RNA technologies in Africa, improving preparation for any future pandemics.

Chapter 5

Appendix

5.1. Bacterial culture

5.1.1 Luria Bertani (LB) medium (1 L)

Ten grams tryptone, 5 g yeast extract and 5 g NaCl were dissolved in one litre of dH_2O, mixed and autoclaved at 121 °C for 30 minutes.

5.1.2. LB-agar medium (1 L)

Fifteen grams of agar was added per 1 L LB media, mixed and autoclaved at 121 °C for 30 minutes. The solution was left to cool until it reached 55 °C after which 1 ml (100 mg) of ampicillin antibiotic stock (1000 ×, 100 mg/ml) was added. LB-Agar was poured into bacterial agar plates (25 ml per plate) at left to cool until solid. Agar plates were stored at 4 °C until needed or for no less than 2 months.

5.1.3. Ampicillin (1000 × stock, 100 mg/ml, 10 ml)

One gram of ampicillin was dissolved in 5 ml injection grade SABAX H_2O. Five millilitres of 100% ethanol were added to the solution. This was filter sterilised through a 0.2 µm filter and stored at -20 °C.

5.1.4. Transformation of chemically competent bacteria

Twenty nanograms of purified pDNA, or 5 µl of ligation mix was added to 50 µl of chemically competent NEB Turbo *E. coli* cells (New England Biolabs, NJ, USA) and incubated on ice for 30 minutes. This was heat shocked at 42 °C for 90 seconds, followed by incubation on ice for 5 minutes. The transformation mix was then added to an agar plate supplemented with ampicillin and evenly spread across the surface. Agar plates were incubated upside down overnight at 37 °C.

5.2. Plasmid DNA Extraction Buffers

5.2.1. Re-suspension Buffer (P1, one litre)

Re-suspension buffer was prepared by dissolving Tris Base (6.06 g) and EDTA (3.72) in 800 ml dH_2O. The pH was adjusted to pH 8 with NaOH and the volume was adjusted to one litre with dH_2O. The solution was autoclaved at 121 °C for 30 minutes and stored at 4 °C. After the solution had cooled, 100 mg of RNase A was added.

5.2.2. Lysis Buffer (P2, one litre)

Lysis buffer was prepared by dissolving 8 g NaOH and 10 g sodium dodecyl sulphate (SDS) in dH_2O. This was autoclaved at 121 °C for 30 minutes and stored at room temperature.

5.2.3. Neutralisation Buffer (P3, one litre)

Neutralisation buffer was prepared by dissolving potassium acetate (294.5 g) in 500 ml dH_2O, the pH was adjusted to 5.3 with glacial acetic acid. The volume was adjusted to 1 litre with dH_2O, autoclaved at 121 °C for 30 minutes, and stored at 4 °C.

5.2.4. Wash Buffer (QC, one litre)

Wash buffer was prepared by dissolving sodium chloride (NaCl, 58.44 g) and MOPS (3-morpholinopropane-1-sulphonic acid, 10.46 g) in 800 ml of dH_2O. The pH was adjusted to 7 using NaOH after which 150 ml of isopropanol was added. The volume was adjusted to 1 litre with dH_2O, autoclaved at 121 °C for 30 minutes, and stored at room temperature.

5.2.5. Equilibration Buffer (QBT, one litre)

Equilibration buffer was prepared by dissolving 43.83 g NaCl and 10.46 g MOPS in 800 ml dH_2O. The pH was adjusted to 7.0 with NaOH, and 150 ml of isopropanol and 15 ml of 10% Triton X-100 were added. The volume was adjusted to 1 litre with dH_2O.

5.2.6. Elution Buffer (QF, one litre)

Elution buffer was prepared by dissolving 73.05 g NaCl and 6.06 g Tris Base in 800 ml of water. The pH was adjusted to 8.5 using hydrochloric acid (HCl). Isopropanol was added (150 ml) and the volume was adjusted to 1 litre.

5.2.7. Small scale purification of pDNA (without column) for screening of ligation reactions

Bacteria were inoculated overnight at 37 °C in 10 ml of LB media supplemented with ampicillin. The was performed using a colony from a bacterial plate transformed with a ligation mix.

The next day, the bacterial culture was centrifuged at 3000 ×g for 15 minutes after which the supernatant was removed. The pellet was resuspended in 180 µl of re-suspension solution and transferred to a 1.5 ml microcentrifuge tube. Lysis buffer (160 µl) was added and vigorously mixed, this was incubated at room temperature for 5 minutes. One hundred and twenty microlitres of neutralisation solution was added to the solution and mixed thoroughly,

followed by incubation on ice for 5 minutes. The solution was centrifuged at maximum speed (12 000-14 000 ×g) at 4 °C for 10 minutes. The supernatant was transferred to a new tube and 600 µl of isopropanol was added and incubated for 2 minutes at room temperature to precipitate the DNA. This was centrifuged at maximum speed for 20 minutes at room temperature. The pellet was washed with 1 ml of 70% ethanol followed by centrifugation at maximum speed, 4 °C for 5 minutes. The supernatant was removed, and the pellet was air-dried, followed by resuspension in dH_2O.

5.2.8. Large-scale purification of plasmid DNA (QIAGEN Plasmid Maxi Kit (Qiagen, MD, USA))

Bacteria were inoculated overnight at 37 °C in 200-300 ml of LB media supplemented with ampicillin. The was performed using a colony from a bacterial plate, or a glycerol stock of bacteria containing the pDNA of interest.

The next day, the bacterial culture was centrifuged at 6000 ×g for 15 minutes. The pellet was resuspended in 10 ml re-suspension buffer, followed by addition of 10 ml lysis buffer, and mixed vigorously. This was incubated at room temperature for 5 minutes after which 10 ml of neutralisation buffer was added and the solution was mixed. This was incubated on ice for 20 minutes. The solution was centrifuged at 10 000 ×g, 4 °C for 45 minutes. A column was prepared by addition of 10 ml equilibration buffer and allowing the solution to empty by gravity flow. The supernatant of the centrifuged solution was added to the column and allowing it to flow through by gravity flow. The supernatant was filtered using biochemical cotton to remove any precipitants prior to addition to the column. The column was then washed twice with 30 ml of wash buffer. Plasmid DNA was eluted by adding 15 ml of elution buffer. To precipitate the pDNA, 10.5 ml of isopropanol was added to the eluted DNA and centrifuged at 10 000 ×g, 4°C for 40 minutes. The supernatant was removed, and the pellet was washed by adding 5 ml of 70% ethanol and centrifuging at 10 000 ×g, 4°C for 20 minutes. The supernatant was removed, the pellet was air-dried and re-suspended in injection grade dH_2O.

5.3. Cloning

5.3.1. Extraction and purification of restriction digest fragments from an agarose gel

Purification of gel fragments was performed using the QIAquick® Gel Extraction Kit (Qiagen, MD, USA). The DNA fragment of interest was excised from the gel. The gel slice was weighed and 3 volumes of buffer QG was added to 1 volume of gel and incubated at 50 °C for 10 minutes with vortexing every 3 minutes. One gel volume isopropanol was then added, and the sample was added to a spin column (800 µl maximum per spin). The column was centrifuged at maximum speed (12 000-14 000 ×g) for 1 minute and the flow through was discarded. This was repeated until all of the gel-mixture has been passed through the column. The column was washed twice by adding 750 µl buffer PE, incubating at room temperature for 5 minutes, and centrifuging at maximum speed for 1 minute. The DNA fragment was eluted into a clean tube by adding 30 µl of buffer EB, incubating at room temperature for 5 minutes, followed by centrifugation at maximum speed for 1 minute. A second elution was done into a separate tube to increase DNA yield. If possible, the fragment was re-electrophoresed on an agarose gel to confirm purity.

5.3.2. Ligation of DNA fragments

Ligations were set up according to the manufacturers' recommendations at vector:insert ratios of 1:0 (control), 1:3 and 1:5. The ligation reactions were incubated at room temperature for 10 minutes, or overnight at 4 °C and 16 °C followed by bacterial transformation.

Appendix Table 1. Primers used for plasmid sequencing.

Primer Name	Primer Use	Primer Sequence (5 ' → 3 ')
MCS Fw	saRNA and MCS pDNA Sequencing	CAGCTTGTCTGTAAGCGG
MCS Rv		CGGCTCGTATGTTGTGTG
Luc2 Fw		ATCAAATACAAGGGCTAC
eGFP IF		AGATCCGCCACAACATCGAG

Sequencing was performed by Inqaba Biotech (GP, RSA).

5.4. *In vitro* transcription of saRNA

5.5.1. Lithium Chloride precipitation solution (10 ml, 7.5 M LiCl, 50 mM EDTA)

A 0.5 M EDTA stock solution (10 ×, 50 ml) was made by dissolving 7.3 g EDTA in UltraPure™ DNase/RNase-Free Distilled Water (Invitrogen, MA, USA) and adjusting the pH to 8.0 using NaOH. LiCl solution was made by mixing 3.2 g LiCl with 1 ml of the 0.5 M EDTA solution and

topping up the solution to 10 ml with nuclease-Free water. This was filter sterilised and stored at 4 °C.

5.5.2. In-House IVT Buffers and Reactions

Spermidine (200 mM, 0.5 ml) and DTT (1 M, 0.5 ml) stock solutions were prepared by dissolving 77.1 mg and 14.5 mg respectively in nuclease-Free water, followed by filter sterilisation.

The 5 × DOE IVT buffer was set up according to the following table:

Appendix Table 2. Composition of 5× DOE-based saRNA IVT B

Component	Final Concentration (mM)	Stock Concentration (mM)	Volume of stock (µl)
HEPES	200	1000	100
Magnesium acetate	375	1000	187.5
DTT	200	1000	100
Spermidine	1	200	2.5
Sodium acetate	50	3000	8.3
Nuclease-Free Water			101.7

This was stored at -20 °C in foil for light protection.

Appendix Table 3. Composition of 10× TriLink CleanCap AU Protocol IVT Buffer

Component	Final Concentration	Stock Concentration (mM)	Volume of stock (µl)
Tris·HCl pH 8.0	400 mM	1000	400
Magnesium acetate	270 mM	1000	270
DTT	100 mM	1000	100
Spermidine	20 mM	200	100
Triton X-100	0.2% v/v		2
Nuclease-Free Water			128

Appendix Table 4. TriLink *In Vitro* Transcription Reaction Setup.

Component	Final Concentration
Nuclease-Free Water	(To Final Volume)
rNTPs (ATP, CTP, GTP, UTP)	5 mM each
Cap Analogue	4 mM
Transcription Buffer	1×
Linearised Template	50 ng/µl
RNase Inhibitor	1 U/µl
Yeast Inorganic Pyrophosphatase	0.002 U/µl
T7 RNA Polymerase	8 U/µl

5.5.3. Formaldehyde Agarose Gel Electrophoresis

10× MOPS Buffer (0.2 M MOPS, 0.05 M Sodium Acetate, 0.01 M EDTA; 1 litre):

To prepare 10× MOPS buffer for gel and running buffer preparation, 41.85 g MOPS (3-morpholinopropane-1-sulfonic acid), 3.72 g sodium acetate and 20 ml of a 0.5M EDTA solution were added to 800 ml of nuclease-free water. The pH was adjusted to 7.0 using sodium hydroxide, and the volume was adjusted to 1000 ml. This was stored at room temperature protected from light by foil.

Gel and running buffer preparation:

A 1% gel (100 ml) was prepared by adding 1 g of agarose in 72 ml of nuclease-free water. This was dissolved by microwaving the solution. This was left to cool down to ~55°C, after which 10 ml of 10× MOPS Buffer and 18 ml of 37% formaldehyde was added. The solution was poured into a gel casting tray and left to solidify before use.

5.6. LNP Production

5.6.1. HEPES Buffered Saline (HBS, 1 L, 20 mM HEPES, 150 mM NaCl, pH 7.5)

HEPES (4.8 g) and NaCl (8.8 g) were dissolved in UltraPure™ DNase/RNase-Free Distilled Water (Invitrogen, MA, USA). The solution was adjusted to pH 7.5 with NaOH and filter sterilised. HBS was stored at 4 °C and protected from light.

5.6.2. Sodium Acetate Buffer for iLNP Formulation (500 ml, 650 mM stock, pH 5)

Sodium Acetate (26.7 g) was dissolved in nuclease-free water, this was adjusted to pH 5 with acetic acid, adjusted up to 0.5 ml and filter sterilised. Buffer was stored at 4 °C and diluted to 6.25 mM before use.

5.6.3. Lipid Nanoparticle Stocks and Mixes

Lipids were dissolved in 100% ethanol at 20 mg/ml and stored at -20 °C. Lipid mixes were set up according to the table below:

Appendix Table 5. Composition of lipid mixes for LNP formulations.

LNP I.D.	LNP Composition	Molar Percentage	Source of Molar Ratio
B1	Cationic Lipid:Cholesterol:DOPE	35:49:16	(62)
D1	Cationic Lipid:DOPE:DMG-PEG2000	49:49:2	(103)
E1	Cationic Lipid:Cholesterol:DOPE:DMG-PEG2000	40:48:10:2	(103)
E2	Cationic Lipid:Cholesterol:DSPC:DMG-PEG2000	40:48:10:2	(103)
F1	Cationic Lipid:Cholesterol:DOPE	50:40:10	(122)
F2	Cationic Lipid:Cholesterol:DSPC	50:40:10	(122)
G1	Cationic Lipid:Cholesterol:DOPE	45:25:30	This study
H2	Cationic Lipid:Cholesterol:DSPC:DMG-PEG2000	50:38.5:10:1.5	(88)
I2	Cationic Lipid:DOPE	50:50	This study

5.6.4. Triton buffer for Ribogreen Assay (2% Triton X-100, 1× Tris-EDTA, 100 ml)

To prepare a 2% Triton X-100 buffer, 2 ml of Triton X-100, 10 ml of 10× TE Buffer (ThermoFisher Scientific, MA, USA) were added to 88 ml of nuclease-free water. This was mixed by magnetic stirring and stored at 4°C.

5.7. Mammalian Cell Culture

5.7.1. Penicillin/Streptomycin (1000 × stock, 100 000 U/ml Penicillin, 100 µg/ml Streptomycin)

Fifteen millilitres of stock solution were prepared by dissolving 0.9 g penicillin and 1.5 g streptomycin in PBS. The solution was filter sterilised (0.2 µm) and stored at -20 °C in 0.5 ml aliquots.

5.7.2. Transfection of RNA

Cells in 96- and 48-well plates were transfected with 100 ng and 200 ng, respectively. Lipofectamine MessengerMax (LMMax; ThermoFisher Scientific, MA, USA) was used to transfect RNA and used as a positive control in LNP comparison experiments. LMMax was diluted in OptiMEM and incubated for 10 minutes. RNA was diluted in OptiMeM (ThermoFisher Scientific, MA, USA) and then added to the LMMax dilution and incubated for 5 minutes after which the mix was added to the cells. LMMax was added at a ratio of 1:1.6 (1.6 µl LMMax per microgram of RNA). RNA-LNPs were diluted in OptiMEM prior to addition to cells.

Lipofectamine 3000 (L3000; ThermoFisher Scientific, MA, USA) was used to transfect cells with pDNA. L3000 was diluted in OptiMEM, and DNA was diluted in P3000 reagent and OptiMEM.

These were then mixed and incubated for 5 minutes, after which they were added to cells. L3000 was used at a ratio of 1:1 (1 µl L3000 per microgram of DNA).

Chapter 6

Supplementary Data

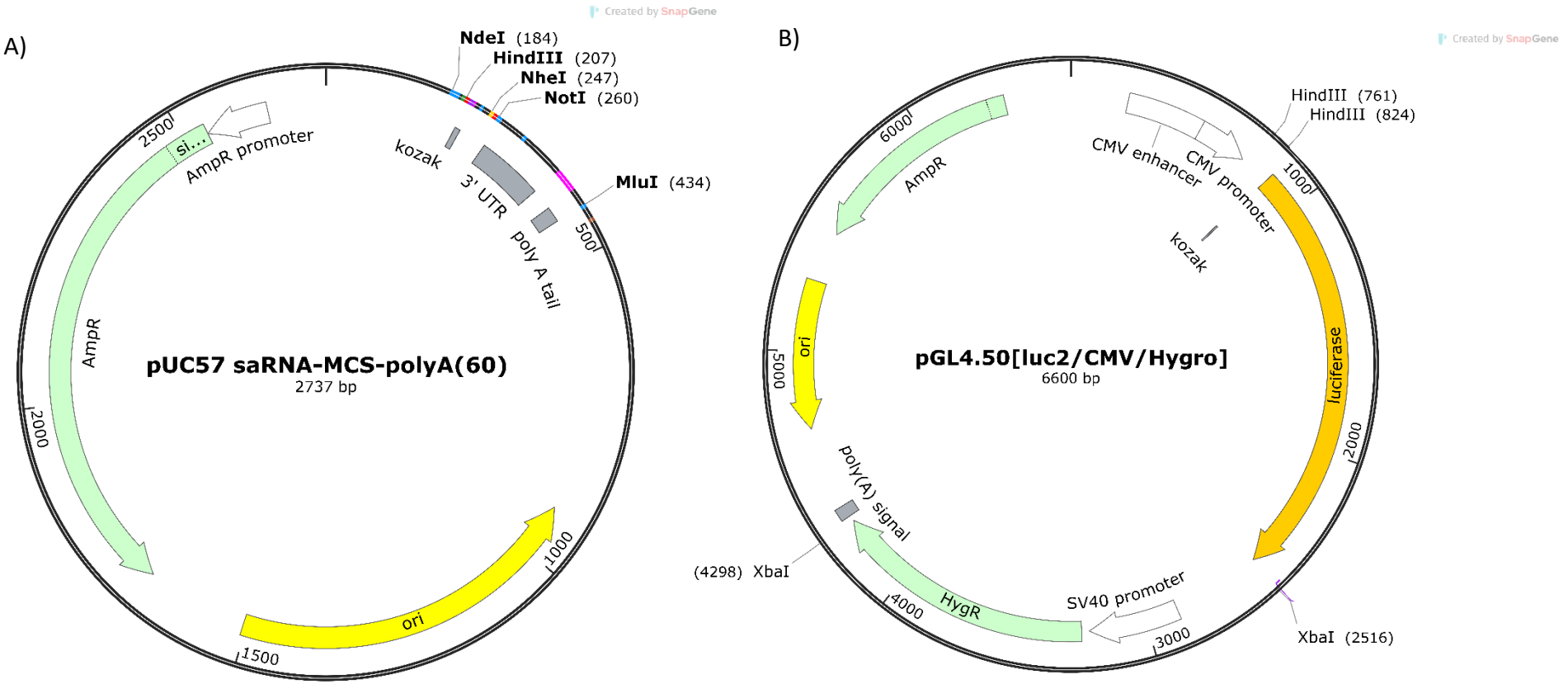

Supplementary Figure 1. Plasmid Maps of pUC57 saRNA-MCS-polyA(60) and pGL4.50[luc2/CMV/Hygro]. A) saRNA-MCS-polyA(60) contains the VEE 3' UTR and a 60 bp poly A sequence. B) pGL4.50 contains a codon optimised Firefly luciferase gene under the control of a cytomegalovirus (CMV) enhancer and promoter.

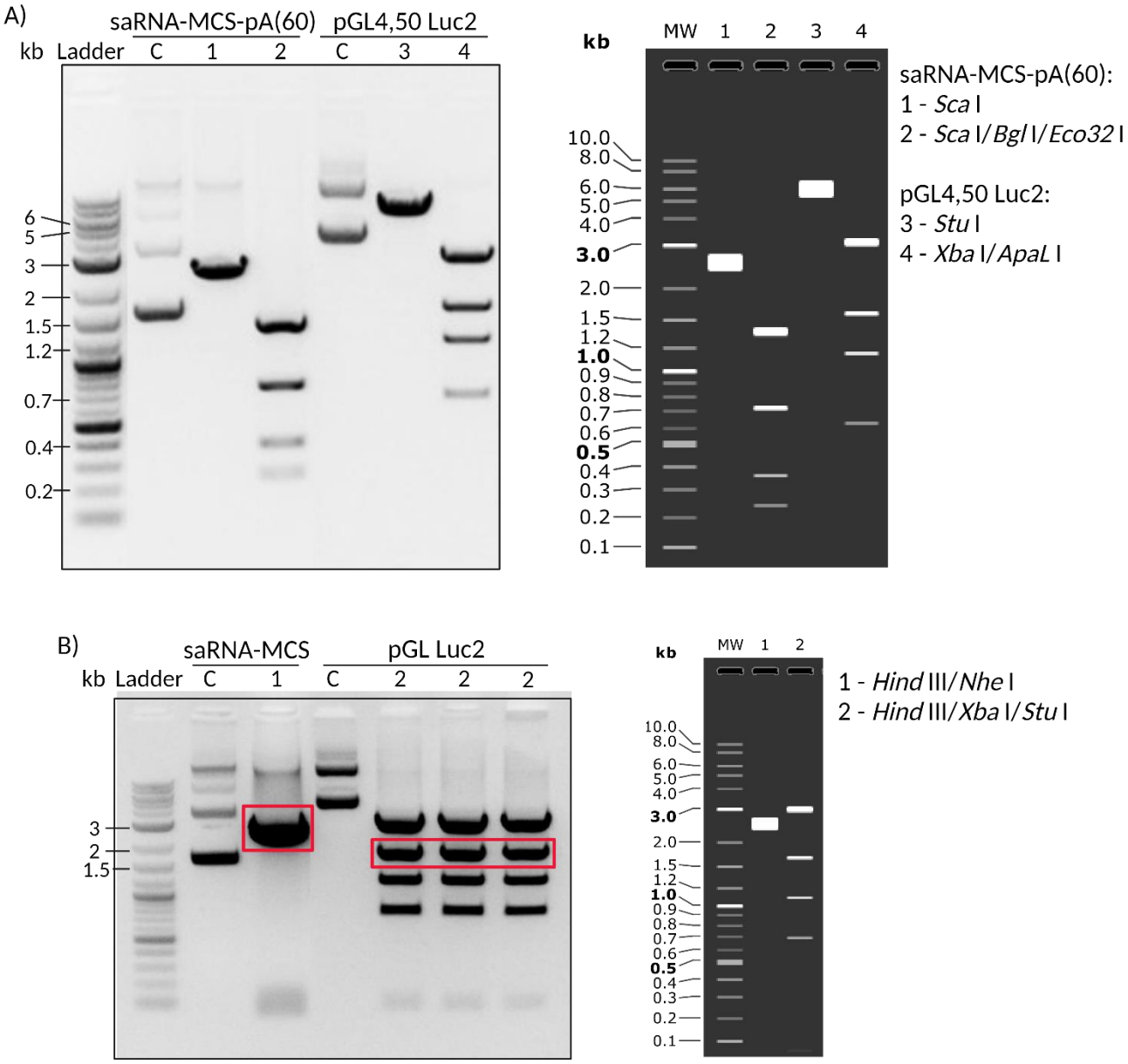

Supplementary Figure 2. Screening and digestion of pGL4.50 Luc2 and saRNA-MCS-polyA(60) for saRNA-MCS-Luc2 cloning. A) pUC57 saRNA-MCS-polyA(60) and pGL4.50[luc2/CMV/Hygro] (pGL4.50 Luc2) were screened by restriction digestion (left). Bands on the gel match the expected bands from the simulated gel (right). B) saRNA-MCS-pA(60) and pGL4.50 Luc2 were digested with *Hind* III and *Nhe* I and *Hind* III, *Xba* I, and *Stu* I, respectively. The desired fragments of 2697 bp and 1692 bp for saRNA MCS and pGL4.50 Luc2 respectively (outlined in red) were gel extracted.

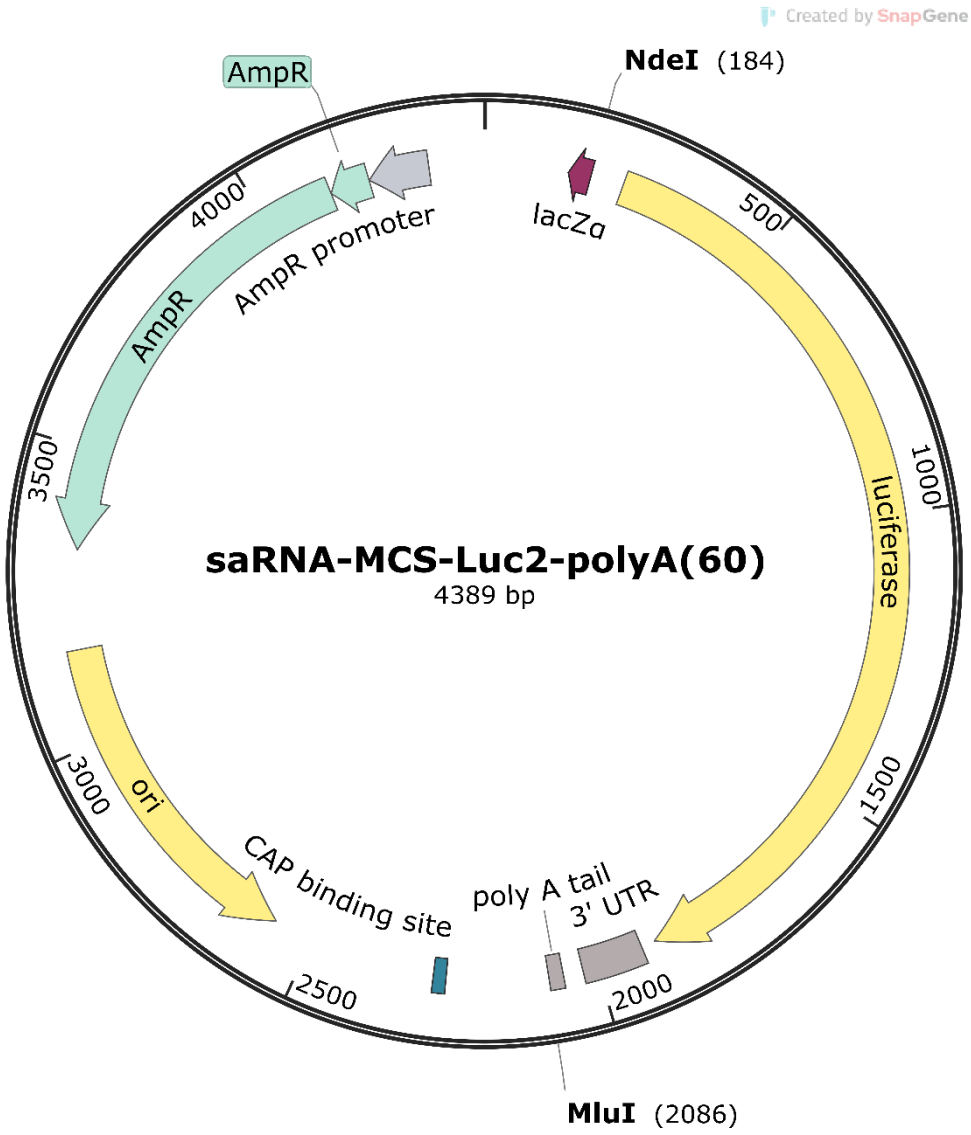

Supplementary Figure 3. Plasmid map of saRNA-MCS-Luc2-polyA(60). After ligation of the luciferase (Luc2) gene into saRNA-MCS-polyA(60), saRNA-MCS-Luc2-polyA(60) was generated. This contains the Luc2 gene upstream of a 60 bp poly A sequence and the VEE 3' UTR.

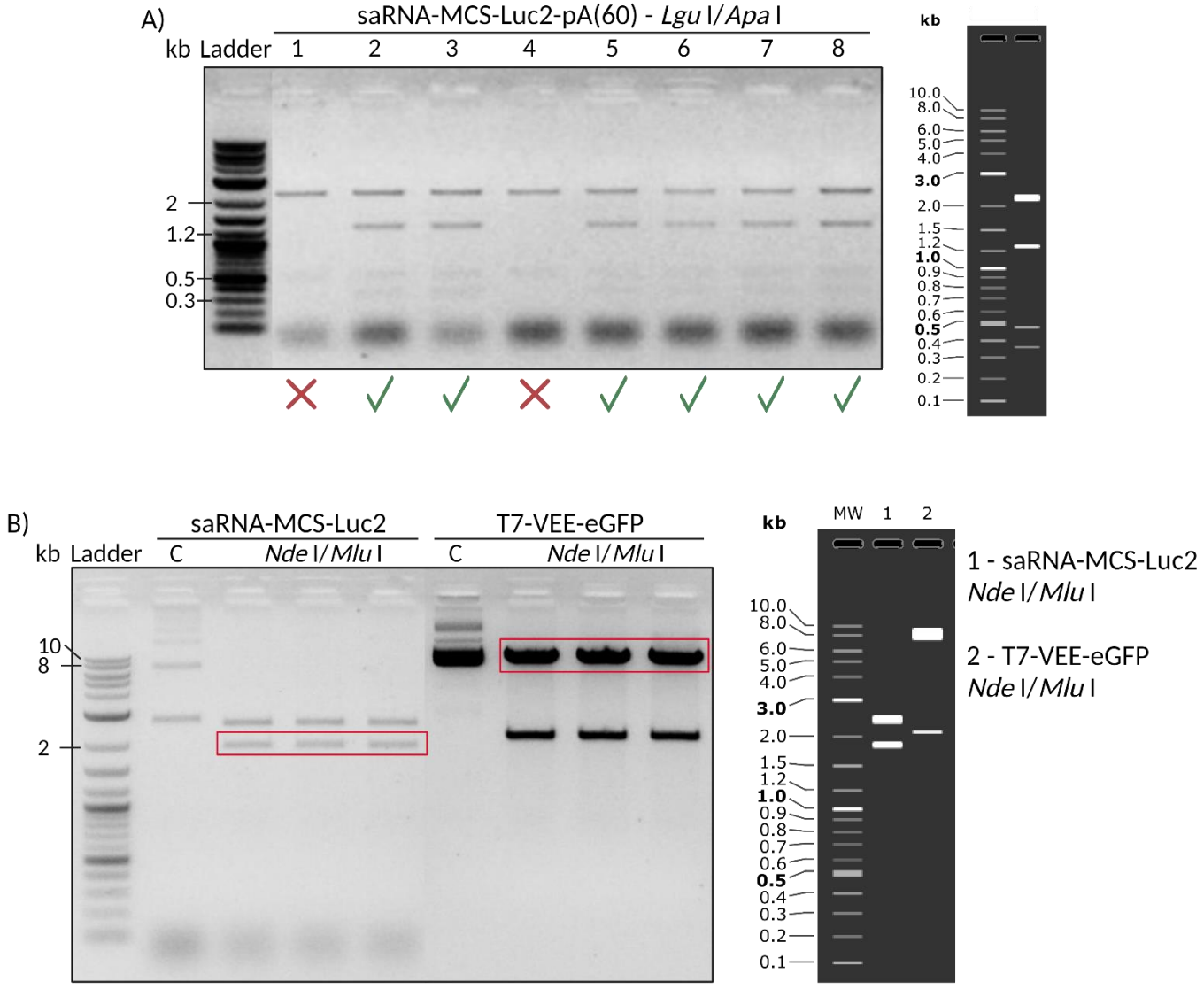

Supplementary Figure 4. Screening of saRNA-MCS-Luc2 and cloning of T7-saRNA-VEE-Luc2-polyA(60). A) After ligation of Luc2 into saRNA-MCS, clones screened by restriction digest with *Lgu* I and *Apa* I. The expected bands of 2268, 1278, 484 and 359 bp were present for 6 out of the 8 clones. B) saRNA-MCS-Luc2 and VEE-eGFP were digested with *Nde* I and *Mlu* I. The desired fragments of 9394 bp and 1902 bp for T7-VEE-eGFP and saRNA-MCS-Luc2 respectively (outlined in red) were gel extracted.

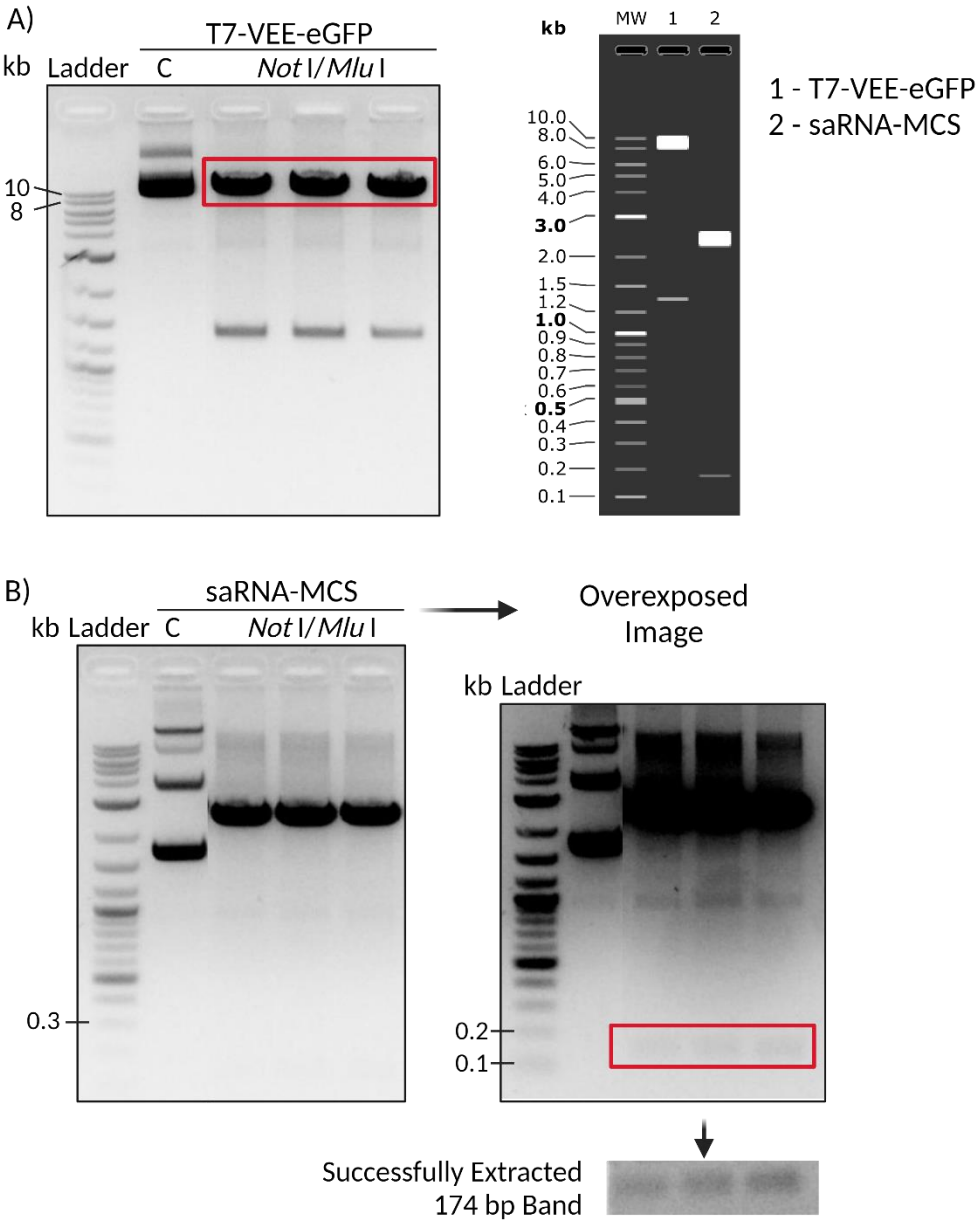

Supplementary Figure 5. Cloning of T7-saRNA-VEE-eGFP-polyA(60). The puromycin resistance selection gene, 3' UTR and poly A sequence of T7-VEE-eGFP were replaced with 3' UTR and poly A sequence of saRNA-MCS. A and B) T7-VEE-eGFP and saRNA-MCS were digested with *Not* I and *Mlu* I. The desired fragments of 10 169 bp and 174 bp for T7-VEE-eGFP and saRNA MCS respectively (outlined in red) were gel extracted. The 174 bp band was exceptionally light (B, left). However, upon overexposure of the gel with UV light, the band was visible and was able to successfully be extracted from the gel (B, right). Simulated gel pattern for both digestions is shown (A, right).

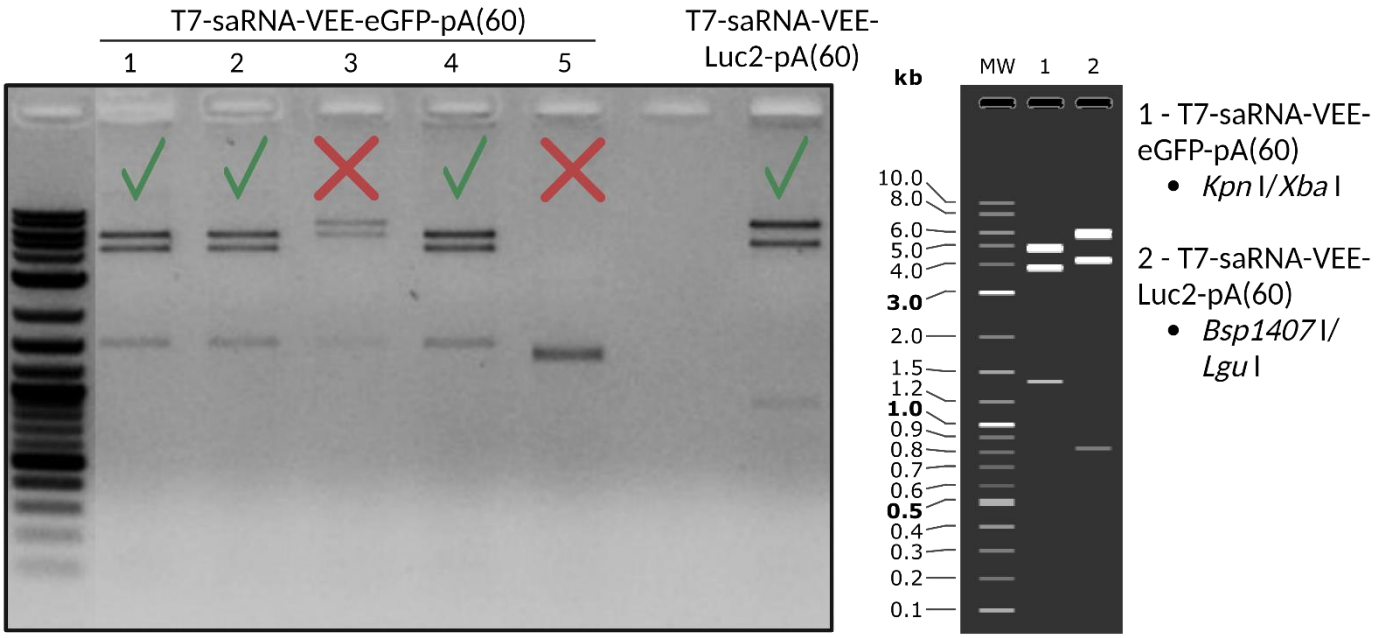

Supplementary Figure 6. Screening of T7-saRNA-VEE-eGFP-polyA(60) and T7-saRNA-VEE-Luc2-polyA(60) clones. Final ligations using pDNA fragments prepared in Supplementary Figures 2 and 3 for T7-saRNA-VEE-Luc2-polyA(60) and T7-saRNA-VEE-eGFP-polyA(60) respectively were performed. T7-saRNA-VEE-eGFP-polyA(60) and T7-saRNA-VEE-Luc2-polyA(60) clones were screened using *Kpn* I and *Xba* I, and *Bsp*1407 I and *Lgu* I respectively (left). Simulated gel pattern is shown (right).

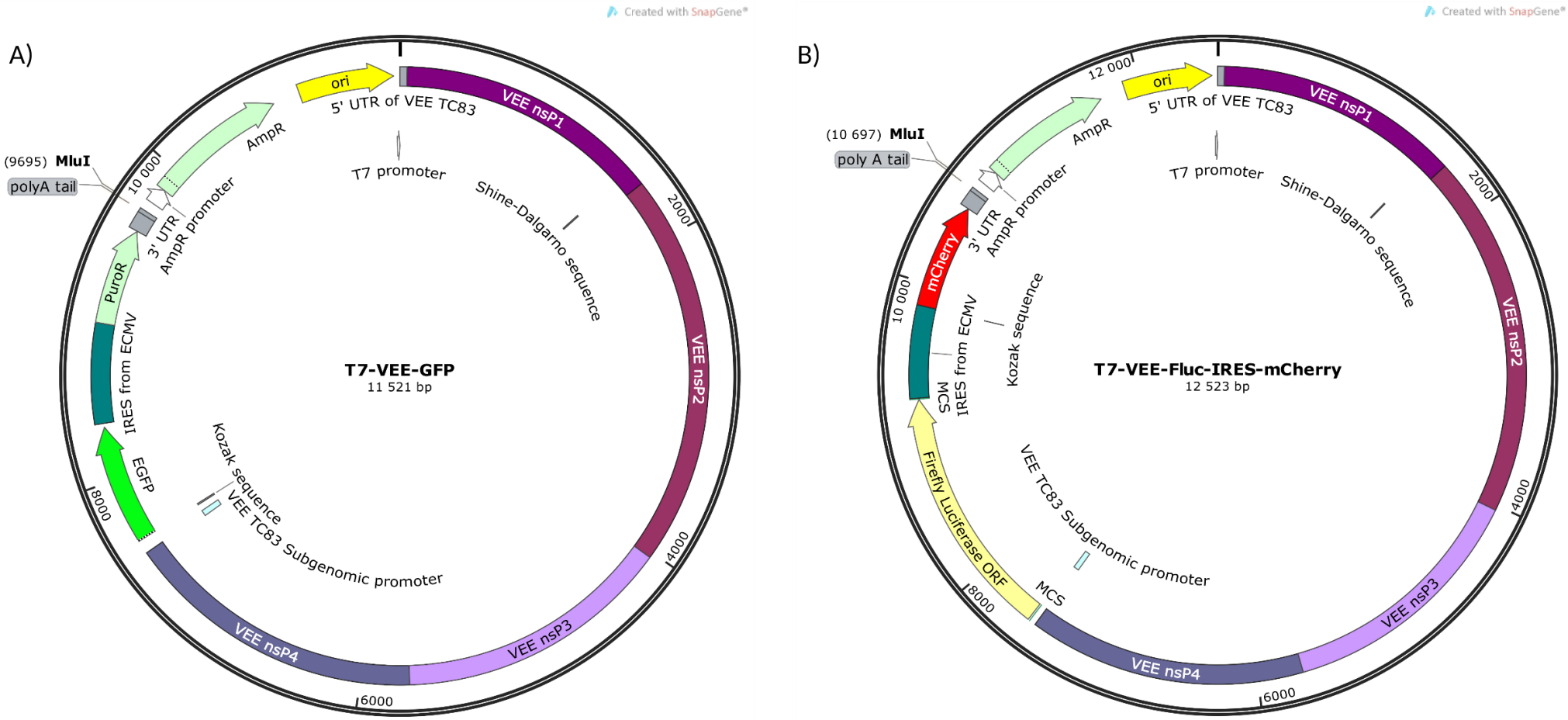

<u>Supplementary Figure 7. Plasmid maps of T7-VEE-eGFP and T7-VEE-Fluc-IRES-mCherry.</u> Production plasmids for *in vitro* transcription of saRNAs expressing eGFP/Puromycin resistance and Fluc/mCherry genes. Linearisation was performed with *Mlu* I to prepare plasmids for IVT.

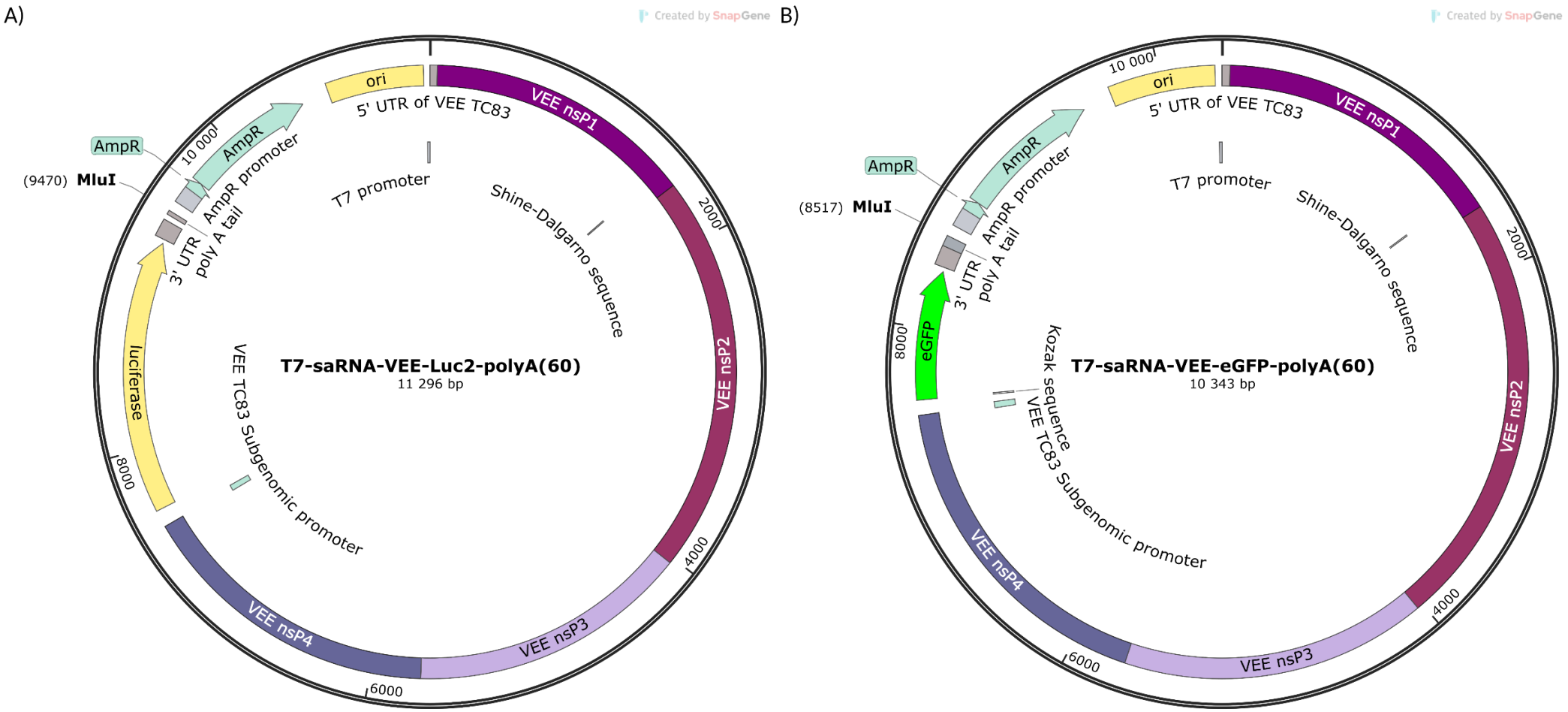

Supplementary Figure 8. Plasmid maps of T7-saRNA-VEE-Luc2-pA(60) and T7-saRNA-VEE-eGFP-pA(60). A) T7-saRNA-VEE-Luc2-pA(60) and B) T7-saRNA-VEE-eGFP-pA(60) are RNA template pDNA encoding the nsP1-4 for saRNA replication and a mono-cistronic reporter gene downstream of a subgenomic promoter. The RNA sequence is downstream of a T7 promoter, and the pDNA can be linearised using *Mlu* I.

Supplementary Figure 9. Sequence alignment of sequencing results with T7-saRNA-VEE-eGFP-pA(60) reference sequence (Ref Seq). Forward (nsP4 Fw), internal (GFP IF), and reverse (Amp Rv) primers were designed to sequence the beginning (A) and end (B) of the eGFP gene and the cloning site prior to the 3' UTR and at the poly A sequence (B) to ensure no significant mutations had occurred. Two guanine to cytosine substitutions were present in the non-coding region (B), however these were outside of the Kozak sequence (blue box). All other bases aligned completely, with a full 60 bp poly A-T sequence present (B, green boxes).

Supplementary Figure 10. Sequence alignment of sequencing results T7-saRNA-VEE-Luc2-pA(60) reference sequence (Ref Seq). Forward (nsP4 Fw), internal (Luc2 Fw), and reverse (Amp Rv) primers were designed to sequence the beginning (A) and end (B)of the Luc2 gene that was cloned, as well as the cloning site at the poly A sequence (C) to ensure no significant mutations had occurred. Degenerate bases (highlighted in yellow) were confirmed to be the correct base using the chromatogram. All other bases aligned completely, with a full 60 bp poly A-T sequence present.

A) NEB 1 Kb Plus DNA Ladder

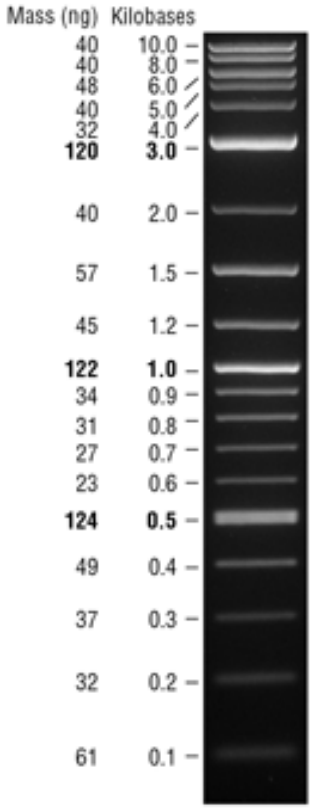

B) NEB ssRNA Ladder

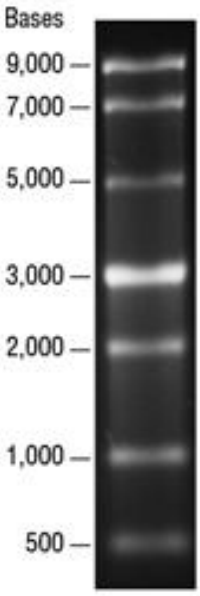

C) ThermoFisher Scientific RiboRuler HR RNA Ladder

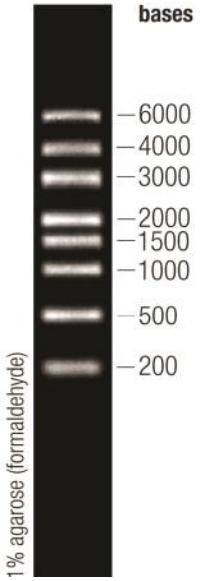

Supplementary Figure 11. DNA and RNA Ladders Used in Agarose Gel Electrophoresis. A) The NEB 1 Kb Plus DNA Ladder was used for agarose gel electrophoresis for pDNA screening and identifying DNA fragments to gel extract. NEB ssRNA (B) and ThermoFisher Scientific RiboRuler HR RNA (C) Ladders used for denaturing agarose gel electrophoresis analysis of IVT RNA.

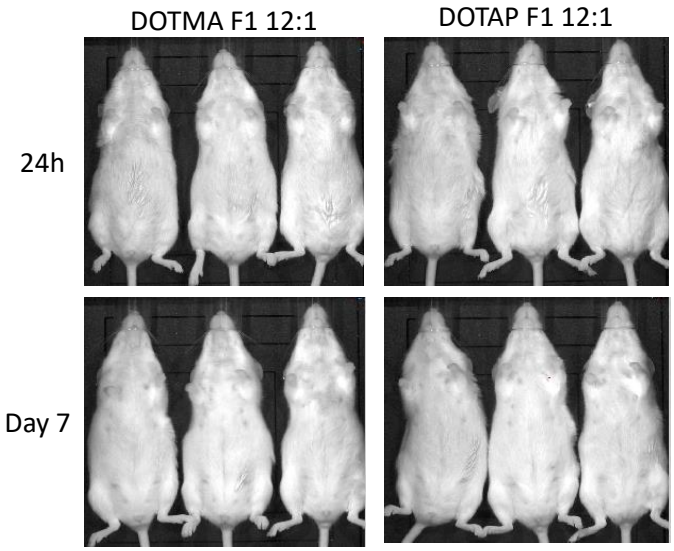

Supplementary Figure 12. *In vivo* bioluminescence images of NMRI mice injected i.m. with saRNA-Ext-cLNP candidates. Mice were injected with CCAU-saRNA-Luc2 formulated exteriorly to cLNPs produced using LFH. Images were obtained at 6- and 24-hours, and days 3, 5, and 7 post-injection. Representative images at 24-hours and day 7 post-injection have been included. Exposure time was set from 1-30 seconds, with 30 seconds of exposure shown. No expression can be seen at either time points. Expression of saRNA should peak at day 7.

Supplementary Table 1. Size and PDI numerical values of formulated Lipid Nanoparticles.

LNP Code	Formulation Method	RNA Formulation	Size (d.nm) ± SD	PDI ± SD
CaliVax	LFH	Empty	96.84 ± 0.550	0.055 ± 0.026
DOTAP F1	LFH	Empty	118.3 ± 0.084	0.079 ± 0.015
DOTMA F1	LFH	Empty	110.3 ± 0.943	0.088 ± 0.015
DOTAP G1	LFH	Empty	131.2 ± 0.882	0.136 ± 0.003
DOTMA G1	LFH	Empty	134.5 ± 0.871	0.087 ± 0.021
DDA B1	LFH	Empty	122.9 ± 1.389	0.062 ± 0.020
DOTAP B1 Set 1	LFH	Empty	101.8 ± 0.736	0.111 ± 0.012
DOTAP B1 Set 2	LFH	Empty	121.5 ± 0.864	0.075 ± 0.007
DOTMA B1 Set 1	LFH	Empty	103.9 ± 0.930	0.090 ± 0.015
DOTMA B1 Set 2	LFH	Empty	136.2 ± 0.815	0.122 ± 0.009
DOTAP F2	LFH	Empty	126.4 ± 0.459	0.098 ± 0.005
DOTMA F2	LFH	Empty	96.21 ± 2.081	0.204 ± 0.027
DOTMA I1	LFH	Empty	118.5 ± 1.478	0.071 ± 0.017
DOTAP I1	LFH	Empty	118 ± 0.9112	0.114 ± 0.011
DDA F2	LFH	Empty	143.5 ± 0.978	0.019 ± 0.024
CaliVax 2.5:1	LFH	saRNA-Ext-cLNPs	347.5 ± 17.31	0.424 ± 0.040
DOTAP F1 4:1	LFH	saRNA-Ext-cLNPs	734.0 ± 7.00	0.228 ± 0.051
DOTMA F1 12:1	LFH	saRNA-Ext-cLNPs	162.2 ± 1.51	0.195 ± 0.019
DOTAP G1 8:1	LFH	saRNA-Ext-cLNPs	167.8 ± 1.52	0.116 ± 0.025
DOTAP G1 4:1	LFH	saRNA-Ext-cLNPs	287.5 ± 3.21	0.258 ± 0.037
DOTMA G1 8:1	LFH	saRNA-Ext-cLNPs	174.3 ± 1.72	0.085 ± 0.013
DOTMA G1 6:1	LFH	saRNA-Ext-cLNPs	213.0 ± 3.85	0.217 ± 0.088
DDA B1 6:1	LFH	saRNA-Ext-cLNPs	451.9 ± 42.25	0.438 ± 0.027
DOTAP B1 8:1	LFH	saRNA-Ext-cLNPs	167.3 ± 1.15	0.168 ± 0.033
DOTMA B1 12:1	LFH	saRNA-Ext-cLNPs	174.0 ± 1.19	0.141 ± 0.005
DOTAP F2 4:1	LFH	saRNA-Ext-cLNPs	574.6 ± 1.41	0.371 ± 0.050
DOTMA F2 9:1	LFH	saRNA-Ext-cLNPs	178.2 ± 7.76	0.323 ± 0.041
DOTMA I1 8:1	LFH	saRNA-Ext-cLNPs	185.3 ± 0.45	0.175 ± 0.028
DOTAP I1 8:1	LFH	saRNA-Ext-cLNPs	171.8 ± 0.45	0.208 ± 0.032
DDA F2 12:1	LFH	saRNA-Ext-cLNPs	505.1 ± 16.74	0.404 ± 0.072
DOTAP B1 12:1	Modified Solvent Injection	saRNA-Int-cLNPs	166.4 ± 0.15	0.256 ± 0.030
DOTAP B1 8:1	Modified Solvent Injection	saRNA-Int-cLNPs	151.2 ± 1.62	0.260 ± 0.006
DOTMA B1 12:1	Modified Solvent Injection	saRNA-Int-cLNPs	204.3 ± 3.39	0.293 ± 0.028
DOTAP F1 15:1	Modified Solvent Injection	saRNA-Int-cLNPs	160.8 ± 1.51	0.303 ± 0.021
DOTAP F1 12:1	Modified Solvent Injection	saRNA-Int-cLNPs	187.4 ± 3.51	0.369 ± 0.009
DOTAP F1 8:1	Modified Solvent Injection	saRNA-Int-cLNPs	220.5 ± 8.49	0.436 ± 0.080
DOTMA F1 12:1	Modified Solvent Injection	saRNA-Int-cLNPs	287.8 ± 5.18	0.453 ± 0.005
DDA F2 12:1	Modified Solvent Injection	saRNA-Int-cLNPs	377.3 ± 6.91	0.435 ± 0.029
MC3 H2 8:1	Modified Solvent Injection	saRNA-Int-iLNPs	332.4 ± 4.77	0.255 ± 0.012
DOTAP E1 8:1	Microfluidics	saRNA-Int-cLNPs	76.2 ± 0.53	0.114 ± 0.202
MC3 E2 12:1	Microfluidics	saRNA-Int-iLNPs	46.0 ± 0.43	0.148 ± 0.013
MC3 E2 8:1	Microfluidics	saRNA-Int-iLNPs	49.2 ± 0.73	0.160 ± 0.018
MC3 H2 8:1	Microfluidics	saRNA-Int-iLNPs	55.1 ± 1.38	0.260 ± 0.040

Chapter 7

References

1. Boylston A. The origins of inoculation. *J R Soc Med* (2012) 105:309–313. doi: 10.1258/jrsm.2012.12k044

2. Plotkin SA, Plotkin SL. The development of vaccines: How the past led to the future. *Nat Rev Microbiol* (2011) 9:889–893. doi: 10.1038/nrmicro2668

3. Fraser A, Goldberg E, Acosta CJ, Paul M, Leibovici L. Vaccines for preventing typhoid fever. *Cochrane Database Syst Rev* (2007) doi: 10.1002/14651858.CD001261.pub2

4. Rappuoli R, De Gregorio E, Costantino P. On the mechanisms of conjugate vaccines. *Proc Natl Acad Sci U S A* (2019) 116:14–16. doi: 10.1073/pnas.1819612116

5. vaccines.gov. Vaccine Types. (2020) https://www.vaccines.gov/basics/types [Accessed January 4, 2021]

6. WHO. Immunization coverage. (2019) https://www.who.int/news-room/fact-sheets/detail/immunization-coverage [Accessed January 4, 2021]

7. Younger DS, Younger APJ, Guttmacher S. Childhood Vaccination: Implications for Global and Domestic Public Health. *Neurol Clin* (2016) 34:1035–1047. doi: 10.1016/j.ncl.2016.05.004

8. Bloom K, van den Berg F, Arbuthnot P. Self-amplifying RNA vaccines for infectious diseases. *Gene Ther* (2021) 28:117–129. doi: 10.1038/s41434-020-00204-y

9. Yeh M Te, Smith M, Carlyle S, Konopka-Anstadt JL, Burns CC, Konz J, Andino R, Macadam A. Genetic stabilization of attenuated oral vaccines against poliovirus types 1 and 3. *Nature* (2023) doi: 10.1038/s41586-023-06212-3

10. Duan H, Chen X, Boyington JC, Cheng C, Zhang Y, Jafari AJ, Stephens T, Tsybovsky Y, Kalyuzhniy O, Zhao P, et al. Glycan Masking Focuses Immune Responses to the HIV-1 CD4-Binding Site and Enhances Elicitation of VRC01-Class Precursor Antibodies. *Immunity* (2018) 49:301-311.e5. doi: 10.1016/J.IMMUNI.2018.07.005

11. Shirley JL, de Jong YP, Terhorst C, Herzog RW. Immune Responses to Viral Gene

Therapy Vectors. *Mol Ther* (2020) 28:709–722. doi: 10.1016/j.ymthe.2020.01.001

12. Hobernik D, Bros M. DNA vaccines—How far from clinical use? *Int J Mol Sci* (2018) 19: doi: 10.3390/ijms19113605

13. Mendonça SA, Lorincz R, Boucher P, Curiel DT. Adenoviral vector vaccine platforms in the SARS-CoV-2 pandemic. *npj Vaccines* (2021) 6:97. doi: 10.1038/s41541-021-00356-x

14. Khobragade A, Bhate S, Ramaiah V, Deshpande S, Giri K, Phophle H, Supe P, Godara I, Revanna R, Nagarkar R, et al. Efficacy, safety, and immunogenicity of the DNA SARS-CoV-2 vaccine (ZyCoV-D): the interim efficacy results of a phase 3, randomised, double-blind, placebo-controlled study in India. *Lancet (London, England)* (2022) 399:1313–1321. doi: 10.1016/S0140-6736(22)00151-9

15. Lamb YN. BNT162b2 mRNA COVID-19 Vaccine: First Approval. *Drugs* (2021) 81:495–501. doi: 10.1007/s40265-021-01480-7

16. Baden LR, Sahly HM El, Essink B, Kotloff K, Frey S, Novak R, Diemert D, Spector SA, Rouphael N, Creech CB, et al. Efficacy and Safety of the mRNA-1273 SARS-CoV-2 Vaccine. *N Engl J Med* (2020) 384:403–416. doi: 10.1056/NEJMOA2035389

17. Polack FP, Thomas SJ, Kitchin N, Absalon J, Gurtman A, Lockhart S, Perez JL, Pérez Marc G, Moreira ED, Zerbini C, et al. Safety and Efficacy of the BNT162b2 mRNA Covid-19 Vaccine. *N Engl J Med* (2020) 383:2603–2615. doi: 10.1056/NEJMoa2034577

18. Wolff J, Malone R, Williams P, Chong W, Acsadi G, Jani A, Felgner P. Direct gene transfer into mouse muscle in vivo. *Science* (1990) 247:1465–1468. doi: 10.1126/SCIENCE.1690918

19. Pardi N, Hogan MJ, Porter FW, Weissman D. mRNA vaccines-a new era in vaccinology. *Nat Rev Drug Discov* (2018) 17:261–279. doi: 10.1038/nrd.2017.243

20. Kairuz D, Samudh N, Ely A, Arbuthnot P, Bloom K. Advancing mRNA technologies for therapies and vaccines: An African context. *Front Immunol* (2022) 0:6452. doi: 10.3389/FIMMU.2022.1018961

21. Lou D, Saltzman WM. Synthetic DNA delivery systems. *Nat Biotechnol* (2000) 18:33–

37. doi: 10.1038/71889

22. Pestova T V., Kolupaeva VG, Lomakin IB, Pilipenko E V., Shatsky IN, Agol VI, Hellen CUT. Molecular mechanisms of translation initiation in eukaryotes. *Proc Natl Acad Sci U S A* (2001) 98:7029–7036. doi: 10.1073/PNAS.111145798

23. Strong T, Hampton T, Louro I, Bilbao G, Conry R, Curiel D. Incorporation of beta-globin untranslated regions into a Sindbis virus vector for augmentation of heterologous mRNA expression. *Gene Ther* (1997) 4:624–627. doi: 10.1038/SJ.GT.3300423

24. Holtkamp S, Kreiter S, Selmi A, Simon P, Koslowski M, Huber C, Türeci O, Sahin U. Modification of antigen-encoding RNA increases stability, translational efficacy, and T-cell stimulatory capacity of dendritic cells. *Blood* (2006) 108:4009–4017. doi: 10.1182/BLOOD-2006-04-015024

25. Wilusz CJ, Wormington M, Peltz SW. The cap-to-tail guide to mRNA turnover. *Nat Rev Mol Cell Biol 2001 24* (2001) 2:237–246. doi: 10.1038/35067025

26. Meyer S, Temme C, Wahle E. Messenger RNA turnover in eukaryotes: pathways and enzymes. *Crit Rev Biochem Mol Biol* (2004) 39:197–216. doi: 10.1080/10409230490513991

27. Ross J, Sullivan TD. Half-lives of beta and gamma globin messenger RNAs and of protein synthetic capacity in cultured human reticulocytes. *Blood* (1985) 66:1149–1154. doi: 10.1182/BLOOD.V66.5.1149.1149

28. Gallie D. The cap and poly(A) tail function synergistically to regulate mRNA translational efficiency. *Genes Dev* (1991) 5:2108–2116. doi: 10.1101/GAD.5.11.2108

29. Munroe D, Jacobson A. mRNA poly(A) tail, a 3’ enhancer of translational initiation. *Mol Cell Biol* (1990) 10:3441. doi: 10.1128/MCB.10.7.3441

30. Hahn S. Structure and mechanism of the RNA polymerase II transcription machinery. *Nat Struct Mol Biol* (2004) 11:394–403. doi: 10.1038/nsmb763

31. Doublié S, Tabor S, Long AM, Richardson CC, Ellenberger T. Crystal structure of a bacteriophage T7 DNA replication complex at 2.2 A resolution. *Nature* (1998) 391:251–258. doi: 10.1038/34593

32. Pasquinelli AE, Dahlberg JE, Lund E. Reverse 5’ caps in RNAs made in vitro by phage RNA polymerases. *RNA* (1995) 1:957.

33. Stepinski J, Waddell C, Stolarski R, Darzynkiewicz E, Rhoads RE. Synthesis and properties of mRNAs containing the novel “anti-reverse” cap analogs 7-methyl(3’-O-methyl)GpppG and 7-methyl (3’-deoxy)GpppG. *RNA* (2001) 7:1486. /pmc/articles/PMC1370192/?report=abstract [Accessed July 13, 2021]

34. Ensinger MJ, Martin SA, Paoletti E, Moss B. Modification of the 5’-terminus of mRNA by soluble guanylyl and methyl transferases from vaccinia virus. *Proc Natl Acad Sci U S A* (1975) 72:2525. doi: 10.1073/PNAS.72.7.2525

35. Daffis S, Szretter KJ, Schriewer J, Li J, Youn S, Errett J, Lin TY, Schneller S, Zust R, Dong H, et al. 2’-O methylation of the viral mRNA cap evades host restriction by IFIT family members. *Nature* (2010) 468:452–456. doi: 10.1038/NATURE09489

36. Shuman S. Catalytic activity of vaccinia mRNA capping enzyme subunits coexpressed in Escherichia coli. *J Biol Chem* (1990) 265:11960–11966. doi: 10.1016/S0021-9258(19)38494-7

37. Vaidyanathan S, Azizian KT, Haque AKMA, Henderson JM, Hendel A, Shore S, Antony JS, Hogrefe RI, Kormann MSD, Porteus MH, et al. Uridine Depletion and Chemical Modification Increase Cas9 mRNA Activity and Reduce Immunogenicity without HPLC Purification. *Mol Ther - Nucleic Acids* (2018) 12:530–542. doi: 10.1016/j.omtn.2018.06.010

38. Polack FP, Thomas SJ, Kitchin N, Absalon J, Gurtman A, Lockhart S, Perez JL, Marc GP, Moreira ED, Zerbini C, et al. Safety and Efficacy of the BNT162b2 mRNA Covid-19 Vaccine. *https://doi.org/101056/NEJMoa2034577* (2020) 383:2603–2615. doi: 10.1056/NEJMOA2034577

39. Mockey M, Gonçalves C, Dupuy F, Lemoine F, Pichon C, Midoux P. mRNA transfection of dendritic cells: synergistic effect of ARCA mRNA capping with Poly(A) chains in cis and in trans for a high protein expression level. *Biochem Biophys Res Commun* (2006) 340:1062–1068. doi: 10.1016/J.BBRC.2005.12.105

40. Grier AE, Burleigh S, Sahni J, Clough CA, Cardot V, Choe DC, Krutein MC, Rawlings DJ,

Jensen MC, Scharenberg AM, et al. pEVL: A Linear Plasmid for Generating mRNA IVT Templates With Extended Encoded Poly(A) Sequences. *Mol Ther - Nucleic Acids* (2016) 5:e306. doi: 10.1038/mtna.2016.21

41. Tautz D, Schlötterer. Simple sequences. *Curr Opin Genet Dev* (1994) 4:832–837. doi: 10.1016/0959-437x(94)90067-1

42. Trepotec Z, Geiger J, Plank C, Aneja MK, Rudolph C. Segmented poly(A) tails significantly reduce recombination of plasmid DNA without affecting mRNA translation efficiency or half-life. *RNA* (2019) 25:507–518. doi: 10.1261/RNA.069286.118

43. Pardi N, Hogan MJ, Porter FW, Weissman D. mRNA vaccines — a new era in vaccinology. *Nat Rev Drug Discov 2018 174* (2018) 17:261–279. doi: 10.1038/nrd.2017.243

44. Chen B, Chen Y, Li J, Wang C, Song W, Wen Y, Lin J, Wu Y, Ying T. A Single Dose of Anti-HBsAg Antibody-Encoding mRNA-LNPs Suppressed HBsAg Expression: a Potential Cure of Chronic Hepatitis B Virus Infection. *MBio* (2022) 13:e0161222. doi: 10.1128/MBIO.01612-22

45. Pardi N, Secreto AJ, Shan X, Debonera F, Glover J, Yi Y, Muramatsu H, Ni H, Mui BL, Tam YK, et al. Administration of nucleoside-modified mRNA encoding broadly neutralizing antibody protects humanized mice from HIV-1 challenge. *Nat Commun* (2017) 8:14630. doi: 10.1038/NCOMMS14630

46. Tiwari PM, Vanover D, Lindsay KE, Bawage SS, Kirschman JL, Bhosle S, Lifland AW, Zurla C, Santangelo PJ. Engineered mRNA-expressed antibodies prevent respiratory syncytial virus infection. *Nat Commun* (2018) 9:1–15. doi: 10.1038/s41467-018-06508-3

47. Hyde JL, Chen R, Trobaugh DW, Diamond MS, Weaver SC, Klimstra WB, Wilusz J. The 5′ and 3′ ends of alphavirus RNAs – Non-coding is not non-functional. *Virus Res* (2015) 206:99. doi: 10.1016/J.VIRUSRES.2015.01.016

48. Pietilä M, Hellström K, Ahola T. Alphavirus polymerase and RNA replication. *Virus Res* (2017) 234:44–57. doi: 10.1016/J.VIRUSRES.2017.01.007

49. Pepini T, Pulichino A-M, Carsillo T, Carlson AL, Sari-Sarraf F, Ramsauer K, Debasitis JC, Maruggi G, Otten GR, Geall AJ, et al. Induction of an IFN-Mediated Antiviral Response by a Self-Amplifying RNA Vaccine: Implications for Vaccine Design. *J Immunol* (2017) 198:4012–4024. doi: 10.4049/jimmunol.1601877

50. Lazzaro S, Giovani C, Mangiavacchi S, Magini D, Maione D, Baudner B, Geall A, De Gregorio E, D'Oro U, Buonsanti C. CD8 T-cell priming upon mRNA vaccination is restricted to bone-marrow-derived antigen-presenting cells and may involve antigen transfer from myocytes. *Immunology* (2015) 146:312–326. doi: 10.1111/IMM.12505

51. Iwasaki A, Medzhitov R. Control of adaptive immunity by the innate immune system. *Nat Immunol 2015 164* (2015) 16:343–353. doi: 10.1038/ni.3123

52. Maruggi G, Zhang C, Li J, Ulmer J, Yu D. mRNA as a Transformative Technology for Vaccine Development to Control Infectious Diseases. *Mol Ther* (2019) 27:757–772. doi: 10.1016/J.YMTHE.2019.01.020

53. Vogel AB, Lambert L, Kinnear E, Busse D, Erbar S, Reuter KC, Wicke L, Perkovic M, Beissert T, Haas H, et al. Self-Amplifying RNA Vaccines Give Equivalent Protection against Influenza to mRNA Vaccines but at Much Lower Doses. *Mol Ther* (2018) 26:446–455. doi: 10.1016/j.ymthe.2017.11.017

54. Zhou X, Berglund P, Rhodes G, Parker SE, Jondal M, Liljeström P. Self-replicating Semliki Forest virus RNA as recombinant vaccine. *Vaccine* (1994) 12:1510–1514. doi: 10.1016/0264-410X(94)90074-4

55. Blakney A, Ip S, Geall A. An Update on Self-Amplifying mRNA Vaccine Development. *Vaccines* (2021) 9:1–26. doi: 10.3390/VACCINES9020097

56. Lundstrom K. Self-Amplifying RNA Viruses as RNA Vaccines. *Int J Mol Sci* (2020) 21:1–29. doi: 10.3390/IJMS21145130

57. Magini D, Giovani C, Mangiavacchi S, Maccari S, Cecchi R, Ulmer JB, Gregorio E De, Geall AJ, Brazzoli M, Bertholet S. Self-Amplifying mRNA Vaccines Expressing Multiple Conserved Influenza Antigens Confer Protection against Homologous and Heterosubtypic Viral Challenge. *PLoS One* (2016) 11:e0161193. doi: 10.1371/JOURNAL.PONE.0161193

58. Chahal JS, Khan OF, Cooper CL, McPartlan JS, Tsosie JK, Tilley LD, Sidik SM, Lourido S, Langer R, Bavari S, et al. Dendrimer-RNA nanoparticles generate protective immunity against lethal Ebola, H1N1 influenza, and Toxoplasma gondii challenges with a single dose. *Proc Natl Acad Sci* (2016) 113:E4133–E4142. doi: 10.1073/PNAS.1600299113

59. Erasmus JH, Archer J, Fuerte-Stone J, Khandhar AP, Voigt E, Granger B, Bombardi RG, Govero J, Tan Q, Durnell LA, et al. Intramuscular Delivery of Replicon RNA Encoding ZIKV-117 Human Monoclonal Antibody Protects against Zika Virus Infection. *Mol Ther Methods Clin Dev* (2020) 18:402. doi: 10.1016/J.OMTM.2020.06.011

60. Li Y, Su Z, Zhao W, Zhang X, Momin N, Zhang C, Wittrup KD, Dong Y, Irvine DJ, Weiss R. Multifunctional oncolytic nanoparticles deliver self-replicating IL-12 RNA to eliminate established tumors and prime systemic immunity. *Nat Cancer 2020 19* (2020) 1:882–893. doi: 10.1038/s43018-020-0095-6

61. Li Y, Teague B, Zhang Y, Su Z, Porter E, Dobosh B, Wagner T, Irvine DJ, Weiss R. In vitro evolution of enhanced RNA replicons for immunotherapy. *Sci Reports 2019 91* (2019) 9:1–10. doi: 10.1038/s41598-019-43422-0

62. Blakney AK, McKay PF, Yus BI, Aldon Y, Shattock RJ. Inside out: optimization of lipid nanoparticle formulations for exterior complexation and in vivo delivery of saRNA. *Gene Ther* (2019) 26:363–372. doi: 10.1038/s41434-019-0095-2

63. Perri S, Greer CE, Thudium K, Doe B, Legg H, Liu H, Romero RE, Tang Z, Bin Q, Dubensky TWJ, et al. An alphavirus replicon particle chimera derived from venezuelan equine encephalitis and sindbis viruses is a potent gene-based vaccine delivery vector. *J Virol* (2003) 77:10394–10403. doi: 10.1128/jvi.77.19.10394-10403.2003

64. Buschmann MD, Carrasco MJ, Alishetty S, Paige M, Alameh MG, Weissman D. Nanomaterial Delivery Systems for mRNA Vaccines. *Vaccines* (2021) 9: doi: 10.3390/vaccines9010065

65. Adams D, Gonzalez-Duarte A, O'Riordan WD, Yang C-C, Ueda M, Kristen A V., Tournev I, Schmidt HH, Coelho T, Berk JL, et al. Patisiran, an RNAi Therapeutic, for Hereditary Transthyretin Amyloidosis. *N Engl J Med* (2018) 379:11–21. doi: 10.1056/NEJMOA1716153

66. Bulbake U, Doppalapudi S, Kommineni N, Khan W. Liposomal Formulations in Clinical Use: An Updated Review. *Pharmaceutics* (2017) 9:12. doi: 10.3390/PHARMACEUTICS9020012

67. Hou X, Zaks T, Langer R, Dong Y. Lipid nanoparticles for mRNA delivery. *Nat Rev Mater* (2021) 6:1078–1094. doi: 10.1038/s41578-021-00358-0

68. Kairuz D, Singh P, Smith T, Arbuthnot P, Ely A, Bloom K. "Synthetic mRNA Gene Therapies and Hepatotropic Non-viral Vectors for the Treatment of Chronic HBV Infections.," In: Jurga S, Barciszewski J, editors. Cham: Springer International Publishing (2022). p. 157–179 doi: 10.1007/978-3-031-08415-7_8

69. Crawford R, Dogdas B, Keough E, Haas RM, Wepukhulu W, Krotzer S, Burke PA, Sepp-Lorenzino L, Bagchi A, Howell BJ. Analysis of lipid nanoparticles by Cryo-EM for characterizing siRNA delivery vehicles. *Int J Pharm* (2011) 403:237–244. doi: 10.1016/J.IJPHARM.2010.10.025

70. Kulkarni JA, Darjuan MM, Mercer JE, Chen S, Van Der Meel R, Thewalt JL, Tam YYC, Cullis PR. On the Formation and Morphology of Lipid Nanoparticles Containing Ionizable Cationic Lipids and siRNA. *ACS Nano* (2018) 12:4787–4795. doi: 10.1021/acsnano.8b01516

71. Semple SC, Akinc A, Chen J, Sandhu AP, Mui BL, Cho CK, Sah DWY, Stebbing D, Crosley EJ, Yaworski E, et al. Rational design of cationic lipids for siRNA delivery. *Nat Biotechnol* (2010) 28:172–176. doi: 10.1038/nbt.1602

72. Akinc A, Querbes W, De S, Qin J, Frank-Kamenetsky M, Jayaprakash KN, Jayaraman M, Rajeev KG, Cantley WL, Dorkin JR, et al. Targeted Delivery of RNAi Therapeutics With Endogenous and Exogenous Ligand-Based Mechanisms. *Mol Ther* (2010) 18:1357–1364. doi: 10.1038/MT.2010.85

73. Kwon YJ, Standley SM, Goh SL, Fréchet JMJ. Enhanced antigen presentation and immunostimulation of dendritic cells using acid-degradable cationic nanoparticles. *J Control Release* (2005) 105:199–212. doi: https://doi.org/10.1016/j.jconrel.2005.02.027

74. Li Y, Wang J, Wientjes MG, Au JL-S. Delivery of nanomedicines to extracellular and

intracellular compartments of a solid tumor. *Adv Drug Deliv Rev* (2012) 64:29–39. doi: https://doi.org/10.1016/j.addr.2011.04.006

75. Kelf TA, Sreenivasan VKA, Sun J, Kim EJ, Goldys EM, Zvyagin A V. Non-specific cellular uptake of surface-functionalized quantum dots. *Nanotechnology* (2010) 21:285105. doi: 10.1088/0957-4484/21/28/285105

76. Lajoie P, Nabi IR. "Chapter 3 - Lipid Rafts, Caveolae, and Their Endocytosis.," In: Jeon KWBT-IR of C and MB, editor. *International Review of Cell and Molecular Biology*. Academic Press (2010). p. 135–163 doi: https://doi.org/10.1016/S1937-6448(10)82003-9

77. Pozzi D, Marchini C, Cardarelli F, Salomone F, Coppola S, Montani M, Zabaleta ME, Digman MA, Gratton E, Colapicchioni V, et al. Mechanistic evaluation of the transfection barriers involved in lipid-mediated gene delivery: Interplay between nanostructure and composition. *Biochim Biophys Acta - Biomembr* (2014) 1838:957–967. doi: https://doi.org/10.1016/j.bbamem.2013.11.014

78. Pozzi D, Marchini C, Cardarelli F, Rossetta A, Colapicchioni V, Amici A, Montani M, Motta S, Brocca P, Cantù L, et al. Mechanistic Understanding of Gene Delivery Mediated by Highly Efficient Multicomponent Envelope-Type Nanoparticle Systems. *Mol Pharm* (2013) 10:4654–4665. doi: 10.1021/mp400470p

79. Cardarelli F, Pozzi D, Bifone A, Marchini C, Caracciolo G. Cholesterol-Dependent Macropinocytosis and Endosomal Escape Control the Transfection Efficiency of Lipoplexes in CHO Living Cells. *Mol Pharm* (2012) 9:334–340. doi: 10.1021/mp200374e

80. Blakney AK, McKay PF, Hu K, Samnuan K, Jain N, Brown A, Thomas A, Rogers P, Polra K, Sallah H, et al. Polymeric and lipid nanoparticles for delivery of self-amplifying RNA vaccines. *J Control Release* (2021) 338:201–210. doi: 10.1016/J.JCONREL.2021.08.029

81. Yan W, Chen W, Huang L. Reactive oxygen species play a central role in the activity of cationic liposome based cancer vaccine. *J Control release Off J Control Release Soc* (2008) 130:22–28. doi: 10.1016/j.jconrel.2008.05.005

82. Tanaka T, Legat A, Adam E, Steuve J, Gatot J-S, Vandenbranden M, Ulianov L, Lonez C,

Ruysschaert J-M, Muraille E, et al. DiC14-amidine cationic liposomes stimulate myeloid dendritic cells through Toll-like receptor 4. *Eur J Immunol* (2008) 38:1351–1357. doi: 10.1002/eji.200737998

83. Vangasseri DP, Cui Z, Chen W, Hokey DA, Falo LDJ, Huang L. Immunostimulation of dendritic cells by cationic liposomes. *Mol Membr Biol* (2006) 23:385–395. doi: 10.1080/09687860600790537

84. Kedmi R, Ben-Arie N, Peer D. The systemic toxicity of positively charged lipid nanoparticles and the role of Toll-like receptor 4 in immune activation. *Biomaterials* (2010) 31:6867–6875. doi: 10.1016/j.biomaterials.2010.05.027

85. Miao L, Li L, Huang Y, Delcassian D, Chahal J, Han J, Shi Y, Sadtler K, Gao W, Lin J, et al. Delivery of mRNA vaccines with heterocyclic lipids increases anti-tumor efficacy by STING-mediated immune cell activation. *Nat Biotechnol* (2019) 37:1174–1185. doi: 10.1038/s41587-019-0247-3

86. De Serrano LO, Burkhart DJ. Liposomal vaccine formulations as prophylactic agents: design considerations for modern vaccines. *J Nanobiotechnology* (2017) 15:83. doi: 10.1186/s12951-017-0319-9

87. Liu Y, Hardie J, Zhang X, Rotello VM. Effects of engineered nanoparticles on the innate immune system. *Semin Immunol* (2017) 34:25–32. doi: 10.1016/j.smim.2017.09.011

88. Hassett KJ, Benenato KE, Jacquinet E, Lee A, Woods A, Yuzhakov O, Himansu S, Deterling J, Geilich BM, Ketova T, et al. Optimization of Lipid Nanoparticles for Intramuscular Administration of mRNA Vaccines. *Mol Ther Nucleic Acids* (2019) 15:1–11. doi: 10.1016/j.omtn.2019.01.013

89. Raval N, Maheshwari R, Kalyane D, Youngren-Ortiz SR, Chougule MB, Tekade RK. "Importance of Physicochemical Characterization of Nanoparticles in Pharmaceutical Product Development.," In: Tekade RKBT-BF of DD, editor. *Advances in Pharmaceutical Product Development and Research*. Academic Press (2019). p. 369–400 doi: https://doi.org/10.1016/B978-0-12-817909-3.00010-8

90. Bangham AD, Standish MM, Watkins JC. Diffusion of univalent ions across the lamellae of swollen phospholipids. *J Mol Biol* (1965) 13:238-IN27. doi: 10.1016/S0022-

2836(65)80093-6

91. Gregoriadis G, da Silva H, Florence AT. A procedure for the efficient entrapment of drugs in dehydration-rehydration liposomes (DRVs). *Int J Pharm* (1990) 65:235–242. doi: 10.1016/0378-5173(90)90148-W

92. Olson F, Hunt CA, Szoka FC, Vail WJ, Papahadjopoulos D. Preparation of liposomes of defined size distribution by extrusion through polycarbonate membranes. *BBA - Biomembr* (1979) 557:9–23. doi: 10.1016/0005-2736(79)90085-3

93. Carugo D, Bottaro E, Owen J, Stride E, Nastruzzi C. Liposome production by microfluidics: potential and limiting factors. *Sci Rep* (2016) 6:25876. doi: 10.1038/srep25876

94. Schubert MA, Müller-Goymann CC. Solvent injection as a new approach for manufacturing lipid nanoparticles – evaluation of the method and process parameters. *Eur J Pharm Biopharm* (2003) 55:125–131. doi: https://doi.org/10.1016/S0939-6411(02)00130-3

95. Tóth EL, Holczer EG, Iván K, Fürjes P. Optimized Simulation and Validation of Particle Advection in Asymmetric Staggered Herringbone Type Micromixers. *Micromachines* (2015) 6:136–150. doi: 10.3390/mi6010136

96. Chaudhary N, Weissman D, Whitehead KA. mRNA vaccines for infectious diseases: principles, delivery and clinical translation. *Nat Rev Drug Discov 2021 2011* (2021) 20:817–838. doi: 10.1038/s41573-021-00283-5

97. Geall AJ, Verma A, Otten GR, Shaw CA, Hekele A, Banerjee K, Cu Y, Beard CW, Brito LA, Krucker T, et al. Nonviral delivery of self-amplifying RNA vaccines. *Proc Natl Acad Sci U S A* (2012) 109:14604–14609. doi: 10.1073/pnas.1209367109

98. Anderluzzi G, Lou G, Woods S, Schmidt ST, Gallorini S, Brazzoli M, Johnson R, Roberts CW, O'Hagan DT, Baudner BC, et al. The role of nanoparticle format and route of administration on self-amplifying mRNA vaccine potency. *J Control release Off J Control Release Soc* (2022) 342:388–399. doi: 10.1016/j.jconrel.2021.12.008

99. de Alwis R, Gan ES, Chen S, Leong YS, Tan HC, Zhang SL, Yau C, Low JGH, Kalimuddin S,

Matsuda D, et al. A single dose of self-transcribing and replicating RNA-based SARS-CoV-2 vaccine produces protective adaptive immunity in mice. *Mol Ther* (2021) 29:1970–1983. doi: 10.1016/j.ymthe.2021.04.001

100. McKay PF, Hu K, Blakney AK, Samnuan K, Brown JC, Penn R, Zhou J, Bouton CR, Rogers P, Polra K, et al. Self-amplifying RNA SARS-CoV-2 lipid nanoparticle vaccine candidate induces high neutralizing antibody titers in mice. *Nat Commun* (2020) 11:3523. doi: 10.1038/s41467-020-17409-9

101. Goswami R, O'hagan DT, Adamo R, Baudner BC. Conjugation of Mannans to Enhance the Potency of Liposome Nanoparticles for the Delivery of RNA Vaccines. *Pharmaceutics* (2021) 13:1–14. doi: 10.3390/PHARMACEUTICS13020240

102. Luo F, Zheng L, Hu Y, Liu S, Wang Y, Xiong Z, Hu X, Tan F. Induction of Protective Immunity against Toxoplasma gondii in Mice by Nucleoside Triphosphate Hydrolase-II (NTPase-II) Self-amplifying RNA Vaccine Encapsulated in Lipid Nanoparticle (LNP). *Front Microbiol* (2017) 0:605. doi: 10.3389/FMICB.2017.00605

103. Lou G, Anderluzzi G, Schmidt ST, Woods S, Gallorini S, Brazzoli M, Giusti F, Ferlenghi I, Johnson RN, Roberts CW, et al. Delivery of self-amplifying mRNA vaccines by cationic lipid nanoparticles: The impact of cationic lipid selection. *J Control Release* (2020) 325:370–379. doi: 10.1016/j.jconrel.2020.06.027

104. Blakney AK, McKay PF, Ibarzo Yus B, Hunter JE, Dex EA, Shattock RJ. The Skin You Are In: Design-of-Experiments Optimization of Lipid Nanoparticle Self-Amplifying RNA Formulations in Human Skin Explants. *ACS Nano* (2019) 13:5920–5930. doi: 10.1021/ACSNANO.9B01774/SUPPL_FILE/NN9B01774_SI_001.PDF

105. Anderluzzi G, Lou G, Gallorini S, Brazzoli M, Johnson R, O'Hagan DT, Baudner BC, Perrie Y. Investigating the Impact of Delivery System Design on the Efficacy of Self-Amplifying RNA Vaccines. *Vaccines* (2020) 8:212. doi: 10.3390/vaccines8020212

106. Samnuan K, Blakney AK, McKay PF, Shattock RJ. Design-of-Experiments In Vitro Transcription Yield Optimization of Self-Amplifying RNA. *bioRxiv* (2021)2021.01.08.425833. doi: 10.1101/2021.01.08.425833

107. Trilink BioTechnologies. CleanCap® Reagent AU.

https://www.trilinkbiotech.com/cleancap-reagent-au.html

108. Hennecke M, Kwissa M, Metzger K, Oumard A, Kröger A, Schirmbeck R, Reimann J, Hauser H. Composition and arrangement of genes define the strength of IRES-driven translation in bicistronic mRNAs. *Nucleic Acids Res* (2001) 29:3327–3334. doi: 10.1093/NAR/29.16.3327

109. Hoekstra D, Scherphof G. Effect of fetal calf serum and serum protein fractions on the uptake of liposomal phosphatidylcholine by rat hepatocytes in primary monolayer culture. *Biochim Biophys Acta* (1979) 551:109–121. doi: 10.1016/0005-2736(79)90357-2

110. Chonn A, Semple SC, Cullis PR. Association of blood proteins with large unilamellar liposomes in vivo. Relation to circulation lifetimes. *J Biol Chem* (1992) 267:18759–18765. doi: 10.1016/S0021-9258(19)37026-7

111. Zhang D, Atochina-Vasserman EN, Lu J, Maurya DS, Xiao Q, Liu M, Adamson J, Ona N, Reagan EK, Ni H, et al. The Unexpected Importance of the Primary Structure of the Hydrophobic Part of One-Component Ionizable Amphiphilic Janus Dendrimers in Targeted mRNA Delivery Activity. *J Am Chem Soc* (2022) 144:4746–4753. doi: 10.1021/jacs.2c00273

112. Melo M, Porter E, Zhang Y, Silva M, Li N, Dobosh B, Liguori A, Skog P, Landais E, Menis S, et al. Immunogenicity of RNA Replicons Encoding HIV Env Immunogens Designed for Self-Assembly into Nanoparticles. *Mol Ther* (2019) 27:2080–2090. doi: 10.1016/j.ymthe.2019.08.007

113. Escalona-Rayo O, Zeng Y, Knol RA, Kock TJF, Aschmann D, Slütter B, Kros A. In vitro and in vivo evaluation of clinically-approved ionizable cationic lipids shows divergent results between mRNA transfection and vaccine efficacy. *Biomed Pharmacother* (2023) 165:115065. doi: https://doi.org/10.1016/j.biopha.2023.115065

114. Akinc A, Maier MA, Manoharan M, Fitzgerald K, Jayaraman M, Barros S, Ansell S, Du X, Hope MJ, Madden TD, et al. The Onpattro story and the clinical translation of nanomedicines containing nucleic acid-based drugs. *Nat Nanotechnol* (2019) 14:1084–1087. doi: 10.1038/s41565-019-0591-y

115. Kartje ZJ, Janis HI, Mukhopadhyay S, Gagnon KT. Revisiting T7 RNA polymerase transcription in vitro with the Broccoli RNA aptamer as a simplified real-time fluorescent reporter. *J Biol Chem* (2021) 296: doi: 10.1074/JBC.RA120.014553

116. Henderson JM, Ujita A, Hill E, Yousif-Rosales S, Smith C, Ko N, McReynolds T, Cabral CR, Escamilla-Powers JR, Houston ME. Cap 1 Messenger RNA Synthesis with Co-transcriptional CleanCap® Analog by In Vitro Transcription. *Curr Protoc* (2021) 1:e39. doi: 10.1002/CPZ1.39

117. Ishida T, Harashima H, Kiwada H. Liposome Clearance. *Biosci Rep* (2002) 22:197–224. doi: 10.1023/A:1020134521778

118. Hassett KJ, Higgins J, Woods A, Levy B, Xia Y, Hsiao CJ, Acosta E, Almarsson Ö, Moore MJ, Brito LA. Impact of lipid nanoparticle size on mRNA vaccine immunogenicity. *J Control Release* (2021) 335:237–246. doi: https://doi.org/10.1016/j.jconrel.2021.05.021

119. Hald Albertsen C, Kulkarni JA, Witzigmann D, Lind M, Petersson K, Simonsen JB. The role of lipid components in lipid nanoparticles for vaccines and gene therapy. *Adv Drug Deliv Rev* (2022) 188:114416. doi: 10.1016/j.addr.2022.114416

120. Precision Nanosystems. NanoAssemblr Platform. https://www.precisionnanosystems.com/platform-technologies/product-comparison

121. Abdelwahed W, Degobert G, Stainmesse S, Fessi H. Freeze-drying of nanoparticles: formulation, process and storage considerations. *Adv Drug Deliv Rev* (2006) 58:1688–1713. doi: 10.1016/J.ADDR.2006.09.017

122. Blakney AK, Deletic P, McKay PF, Bouton CR, Ashford M, Shattock RJ, Sabirsh A. Effect of complexing lipids on cellular uptake and expression of messenger RNA in human skin explants. *J Control Release* (2021) 330:1250–1261. doi: https://doi.org/10.1016/j.jconrel.2020.11.033